# Differentiation and activation of tuft cells tunes type 2 immunity in the small intestine

Marija S. Nadjsombati

A dissertation

submitted in partial fulfillment of the

requirements for the degree of

Doctor of Philosophy

University of Washington

2022

Reading Committee:

Jakob von Moltke, Ph.D., Chair

Kevin Urdahl, M.D., Ph.D.

Steven Ziegler, Ph.D.

Program Authorized to Offer Degree:

Immunology

University of Washington

**Abstract**

Differentiation and activation of tuft cells tunes type 2 immunity in the small intestine

Marija S. Nadjsombati

Chair of the Supervisory Committee:

Dr. Jakob von Moltke

Department of Immunology

Type 2 immune responses are elicited by parasitic worm, helminth, infections and are the cause of many allergic diseases. Both helminth infection and allergy are significant global health issues with high prevalence worldwide. Therefore, a better understanding of type 2 immunity will provide novel insights into how we can treat both types of conditions. Type 2 immune responses are most often elicited at barrier tissues like the lung, skin and gut. However, unlike for bacteria, viruses and fungi, our understanding of how the immune system senses the presence of helminths or allergens is much more limited. Tuft cells, a specialized lineage of epithelial cells, have been identified as critical in initiating immune responses to helminths and protists in the small intestine. Tuft cells secrete interleukin 25 (IL-25) and other effector molecules to activate group 2 innate lymphoid cells (ILC2s) in the lamina propria. ILC2s

produce canonical type 2 cytokines to promote a multifaceted immune response. IL-13 in particular signals to epithelial stem cells, biasing their lineage commitment toward tuft and goblet cells, resulting in hyperplasia of both cell types and activation of a feed-forward circuit, which we refer to as the tuft-ILC2 circuit. The identification of a role for tuft cells provided a major advance in our understanding of how type 2 immune responses are initiated in the small intestine. However, the mechanism by which tuft cells sense the presence of helminths or protists in the intestinal lumen remained unclear.

Studying tuft cell activation mechanisms, we identified succinate as the first intestinal tuft cell ligand. We find that administering succinate in the drinking water of mice is sufficient to activate the tuft-ILC2 circuit and elicit a multifaceted type 2 immune response. This response is mediated by binding of succinate to the succinate receptor (SUCNR1) on tuft cells. Yet activation of the tuft-ILC2 circuit by the helminth, *N. brasiliensis,* is SUCNR1-independent. In contrast, detection of *Tritrichomonas* protist colonization requires SUCNR1. These findings uncover a novel paradigm in which the type 2 immune response monitors microbial metabolism in the small intestine. Additionally, they highlight how tuft cell sensing of pathogens or commensals is context specific and likely involves multiple different signaling pathways.

The importance of the tuft-ILC2 circuit has been demonstrated in numerous contexts, but how epithelial progenitors become tuft cells and how the circuit differs between mouse strains remains poorly understood. To address these questions, we characterized the succinate response in C57BL/6J (B6) and Balb/cJ (Balb) mice. Compared to B6, Balb mice have fewer tuft cells at baseline and do not develop tuft cell hyperplasia when treated with succinate. Through

quantitative trait locus mapping we found a single locus on chromosome 9 associated with these phenotypes. Congenic Balb mice carrying the B6 chromosome 9 locus (Balb.Chr9$^{B6/B6}$) have elevated baseline number of tuft cells and develop tuft cell hyperplasia when treated with succinate. Within this chromosome 9 locus is *Pou2af2*, a transcriptional cofactor essential for tuft cell differentiation. There are two isoforms of *Pou2af2*, of which only the long isoform encodes a functional protein. The ratio of long isoform to total *Pou2af2* transcript is significantly decreased in Balb tuft cell progenitors. Finally, we find Balb mice maintain effective activation of the tuft-ILC2 circuit when infected with helminths but do not activate the circuit when colonized with innocuous *Tritrichomonas* protists. In sum, we identify a genetic locus that regulates tuft cell differentiation and the threshold of tuft-ILC2 circuit activation between different strains of mice.

Together, these findings advance our knowledge about how tuft cells sense luminal signals to initiate downstream type 2 immunity and how regulation of tuft cell differentiation can impact these immunological outcomes in the small intestine. These novel insights into tuft cell biology have important implications for our understanding of intestinal homeostasis and inflammation.

**Table of contents**

**Chapter 1: Introduction** ..... 1
1.1 Helminth infection and allergic disease ..... 2
1.2 Initiation of type 2 immune responses ..... 2
1.3 Tuft cells ..... 4
1.4 The tuft-ILC2 circuit ..... 7
1.5 Dissertation objectives and significance ..... 8
1.6 Figures ..... 10

**Chapter 2: Detection of succinate by intestinal tuft cells triggers a type 2 innate immune circuit** ..... 12
2.1 Introduction ..... 13
2.2 Results ..... 16
2.3 Discussion ..... 25
2.4 Material and Methods ..... 29
2.5 Acknowledgments ..... 45
2.6 Figures ..... 46
2.7 Supplemental Figures ..... 56
2.8 Tables ..... 60

**Chapter 3: Genetic mapping reveals *Pou2af2*-dependent tuning of tuft cell differentiation and intestinal type 2 immunity** ..... 61
3.1 Introduction ..... 62
3.2 Results ..... 64
3.3 Discussion ..... 78
3.4 Material and Methods ..... 82
3.5 Acknowledgments ..... 94
3.6 Figures ..... 96
3.7 Supplemental Figures ..... 107
3.8 Tables ..... 113

**Chapter 4: Summary and future directions** ..... 118
4.1 Summary ..... 119
4.2 Conclusions and future directions ..... 121

**References** ..... 126

## List of figures and tables

**Chapter 1:**

Figure 1 ..... 10
Figure 2 ..... 11

**Chapter 2:**

Figure 1 ..... 46
Figure 2 ..... 48
Figure 3 ..... 50
Figure 4 ..... 52
Figure 5 ..... 54
Figure 5 ..... 55

Figure S1 ..... 56
Figure S2 ..... 57
Figure S3 ..... 58
Figure S4 ..... 59

Table 1 ..... 60

**Chapter 3:**

Figure 1 ..... 96
Figure 2 ..... 98
Figure 3 ..... 99
Figure 4 ..... 100
Figure 5 ..... 102
Figure 6 ..... 103
Figure 7 ..... 105

Figure S1 ..... 107
Figure S2 ..... 108
Figure S3 ..... 109
Figure S4 ..... 110
Figure S5 ..... 111
Figure S6 ..... 112
Figure S7 ..... 114

Table 1 ..... 116
Table 2 ..... 117

**Acknowledgments**

I thank my mentor, Jakob, for his support, guidance and enthusiasm throughout my Ph.D. I am extremely grateful to have worked for an advisor who encouraged my research independence, fostered my confidence and supported me every step of the way through graduate school. I will never take for granted the time and energy Jakob poured into every practice talk, grant application and manuscript draft, which all played a critical role in my accomplishments as a graduate student and development as a scientist. He has always been an exemplary role model for me both in science but also just as a compassionate and kind individual in every aspect of life. I will always be deeply appreciative of the mentorship and support Jakob has given me throughout the past five and a half years in his lab.

I thank the members of my committee for their valuable support and feedback throughout the years. I always looked forward to our meetings because I knew I would leave each meeting with new insights and perspectives on my project that would ultimately improve it. I am especially grateful that my committee always put my goals and research interests first. Having such a brilliant and generous committee invested in my success as a scientist was a huge confidence boost and was the best encouragement I could have ever asked for.

I thank every one of the Moltke lab members I was fortunate enough to call colleagues. They are all hard working, brilliant scientists and I have learned more from them than any class could have ever taught me. But even more importantly, it was invaluable to be surrounded by such genuinely nice individuals on a day-to-day basis (especially through a global pandemic). I appreciated the everyday science discussions, but what I appreciate most is that we care about each other's interests, goals and well-being outside of lab. Being in such a welcoming and

supportive environment made me excited to come to lab every morning and made me miss the lab whenever I was away. I know I will miss the lab tremendously, but I can't wait for us to all continue to be colleagues and friends for many years to come.

Finally, I thank my friends and family. My UW Immunology classmates and fellow graduate students were the first friends I made when I moved to Seattle and it's because of them this city started to feel like home. I always was and continue to be impressed by the high level of work, perseverance, and kindness that UW Immunology graduate students exemplify. As time went on, I slowly began to make friends in Seattle outside of science and hanging out with them allowed me to briefly forget about graduate school and explore all the other fun things there are to do, like frisbee and skiing. Finally, I would like to thank my parents, Biljana and Sinisa, and my sister Tamara. I have felt their endless support and love, even from afar. They have always encouraged me to keep going when I was down and have celebrated all my successes, no matter how small, along the way. I could not have gotten here without them and am forever thankful for our family.

# Chapter 1

## Introduction

Parts of this chapter are adapted from the following publication:

Billipp TE*, Nadjsombati MS*, von Moltke J. Tuning tuft cells: new ligands and effector functions reveal tissue-specific function. Current Opinion in Immunology. 2021. 68:98-106.

* Denotes equal contribution

### 1.1 Helminth infection and allergic disease

According to the WHO in 2022, 24% of the world's population is infected by soil-transmitted helminths*(1)*. Allergic diseases such as food allergy, atopic dermatitis and asthma are on the rise in developing countries*(2)*. Although seemingly very different, type 2 immune responses are both elicited by helminth infection and are the cause of allergic diseases.

The type 2 immune response is characterized by the differentiation of $CD4^+$ T helper 2 (Th2) cells and the production of type 2 cytokines; IL-4, IL-5, IL-9 and IL-13*(3)*. These cytokines go on to elicit a multifaceted type 2 immune response which includes, B cell class switching to IgE, recruitment of eosinophils, mast cells and basophils, and release of histamine and other inflammatory mediators. A hallmark of type 2 immune responses is tissue remodeling, which often includes mucus overproduction, muscle contraction and vasodilation. Together this coordinated immune response can be effective at expelling helminth infection. However, when inappropriately activated against innocuous antigens, this response can cause debilitating or even life-threatening allergic disease*(4)*. While the immune components that make up the type 2 immune response are well defined, much less is understood about when and how these responses are initiated. A better understanding of how type 2 immunity is initiated will allow us to better treat helminth infection and prevent development of allergy.

### 1.2 Initiation of type 2 immune responses

The initiation of type 1 or type 17 immune responses often relies on innate immune recognition of pathogens by pattern recognition receptors such as toll like receptors or retinoic acid-inducible gene-I (RIG-I)-like receptors*(5, 6)*. These receptors detect pathogen-associated

molecular patterns to trigger well defined signaling mechanisms that lead to the initiation of appropriate anti-viral, anti-bacterial or anti-fungal immunity. In contrast, no such ligand-receptor pairs have been as well characterized for the initiation of type 2 immune responses. Instead, it is appreciated that type 2 immune responses are initiated by the alarmin cytokines, IL-25, IL-33, and TSLP*(7–9)*. These cytokines are expressed by a variety of non-immune cells such as epithelial, endothelial and stromal cells, primarily at barrier surfaces. When released, these cytokines can act on a wide variety of immune cells to induce many aspects of a type 2 immune response including cell proliferation, Th2 differentiation and type 2 cytokine production

Among the cells that respond to TSLP, IL-133 and IL-25 are group 2 innate lymphoid cells (ILC2s). First identified in 2010, ILC2s are defined by their expression of GATA3+ and lack of a TCR*(10–12)*. Without a TCR, ILC2s instead serve as signaling hubs integrating multiple tissue derived signals*(13)*. ILC2s are strongly activated by IL-25, IL-33 and TSLP. They can also respond to lipid mediators such as leukotrienes as well as neuropeptides such as neuromedin U*(14–16)*. Once activated, ILC2s secrete IL-5, IL-9 and IL-13 to rapidly and effectively initiate type 2 immune responses. ILC2s are primarily found in non-lymphoid tissues and are uniquely poised to respond to tissue-specific cues based on where they are found*(17)*. For example, ILC2s in the lung express high levels of ST2, the IL-33 receptor, and this signaling axis is key in allergic airway disease. In contrast, in the intestine, ILC2s express high levels of the IL-25 receptor, IL-17RB. Even before the role of ILC2s was appreciated, studies had demonstrated an important role of IL-25 for anti-helminth immunity in the small intestine*(18)*. However, the cellular source of IL-25 remained elusive until 2016 when three separate groups identified tuft cells, a unique and rare epithelial cell type, as the sole source of IL-25*(19–21)*.

### 1.3 Tuft cells

Tuft cells are rare chemosensory epithelial cells that are activated by apical environmental cues and transmit signals to neighboring epithelial cells and the underlying tissue. They can be found in most mucosal barriers of mice and humans, including those of the upper airways, stomach, biliary tree, intestines, and urethra*(22)*. There are also tuft cells in the medullary thymic epithelium*(23, 24)*. Within the literature, tuft cells have been given different names in different tissues—microvillus cells in the olfactory epithelium, solitary chemosensory cells in the respiratory epithelium, brush cells in the trachea, tuft cells in the gastrointestinal tract—but share a common transcriptional and developmental identity driven by the transcription factor POU2F3 and here will all be referred to as tuft cells*(21, 25–27)*. Tuft cells in all tissues are defined by an apical "tuft" of long microvilli and share a transcriptional signature that includes genes also required for taste transduction (*Trpm5, Plcb2, Gnat3*) and genes associated with effector functions (*Alox5, Chat, Il25, Ptgs1*)*(28, 29)*.

*Tuft cell differentiation*

The ontogeny of tuft cells is perhaps best understood in the small intestine (SI), where they are one of five post-mitotic lineages of epithelial cells that comprise the SI lining. SI epithelial cells are replenished every 4-5 days from a pool of intestinal stem cells (ISCs) that reside in the crypts of the SI*(30)*. ISCs are self-renewing and divide into progenitor cells called transit amplifying cells *(31)*(**Figure 1**). These transit amplifying cells are highly proliferative and integrate complex environmental cues that influence their differentiation into each of the five epithelial cell types. Within this transit amplifying zone, cells that receive Notch ligand signals

turn on the transcription factor Hairy/E(spl) (HES) and go on to fully differentiate into absorptive enterocytes, which comprise the majority of mature intestinal epithelial cells. HES promotes enterocyte differentiation by repressing atonal homolog 1 (ATOH1), which is the transcription factor required for Paneth, goblet and enteroendocrine cell differentiation. Paneth cells reside at the base of the crypt and provide critical support factors to ISCs as well as produce antimicrobial peptides. Goblet cells secrete mucus. Enteroendocrine cells secrete various hormones and can sometimes form synapses with neurons. Each of these lineages requires ATOH1 but has unique downstream transcription factor requirements. SPDEF and GFI1 are both required for goblet and Paneth cell differentiation. Paneth cells also require SOX9. Enteroendocrine cells are dependent on NEUROG3.

The cell intrinsic signals that direct tuft cell differentiation remain poorly understood, although the transcription factor POU2F3 is absolutely necessary for tuft cell differentiation and dispensable for all other epithelial lineages*(21)*. Recent literature has described that in the SI, there can be ATOH1-dependent and -independent tuft cell differentiation. It is not well understood whether these two subsets are functionally distinct*(32–35)*. Beyond ATOH1, small intestinal tuft cells are the only epithelial cells that express the transcription factor GFI1$\beta$, but its functional significance is yet to be determined*(33)*.

The homeostatic cues that direct tuft cell differentiation are unknown, but in mice free of specific pathogens including *Tritrichomonas* protists, tuft cells are rare (~1% of the epithelium). On the other hand, in mice infected with helminths or colonized with *Tritrichomonas* protists, interleukin 13 (IL-13) signaling through IL-4RA and STAT6 in epithelial progenitors is necessary and sufficient to induce a 5-10 fold increase in tuft cell frequency

(hyperplasia)*(19–21, 36)*. In mice lacking ATOH1, IL-13 can still induce tuft cell hyperplasia suggesting these STAT6-driven tuft cells can be ATOH1-independent*(35)*. Furthermore, there is some evidence that ATOH1-independent IL-13 induced tuft cells rely on SOX4 for differentiation but more work is needed to fully understand the interplay between ATOH1, STAT6 and SOX4 in both homeostatic and type 2 inflammatory contexts*(37)*.

Even less is known about the transcriptional networks needed to generate tuft cells in other tissues beyond a requirement for POU2F3. Furthermore, robust IL-13 induced tuft cell hyperplasia that occurs in the SI has not been observed in other tissues. Tuft cell expansion is documented in the nasal cavity of humans with chronic rhinosinusitis, in human serrated colorectal polyps and in cases of non-small cell lung cancer*(38–40)*. In mice, tuft cell expansion has been observed in the trachea in response to aeroallergen exposure and tuft cells appear in the distal lung after influenza-induced damage*(41, 42)*. However, in both of these models, tuft cell differentiation was independent of IL-13, indicating that there are many different, tissue and context specific ways to generate tuft cells.

*Tuft cell chemosensing*

The taste chemosensing pathway expressed in tuft cells was identified in the 1990s, well before tuft cell function was understood*(43)*. Canonically, in taste cells this pathway is activated by G protein-coupled taste receptors (TAS1R, TAS3R, and the TAS2R family) signaling through GNAT3 (G Protein Subunit Alpha Transducin 3), PLCB2 (Phospholipase C Beta 2) and ITPR3 (Inositol 1,4,5-Trisphosphate Receptor Type 3)*(44)*. The resulting $Ca^{2+}$ flux opens the membrane cation channel TRPM5 (Transient Receptor Potential Cation Channel Subfamily M Member 5),

which depolarizes the cell and drives release of ATP to activate adjacent neurons. The core transcriptional signature shared by tuft cells from at least 5 tissues includes *Gnat3*, *Plcb2* and *Trpm5(29).* All effector functions of tuft cells described to date rely on signaling through TRPM5, although requirement of the other signaling components like the g-alpha subunit can vary based on context*(45)*.

**1.4 The tuft-ILC2 circuit in the small intestine**

Although tuft cells were discovered more than 60 years ago, it wasn't until the last ten years that studies uncovered their contributions to innate immunity at barrier tissues. An immune function for tuft cells was first described in the airways, where they sense bacterial ligands and regulate secretion of antimicrobial peptides and mast cell degranulation via neuronal stimulation*(46, 47)*. Airway tuft cells also mediate evasion of noxious substances via transient breathing cessation*(48, 49)*. New roles for tuft cells in regulating innate immunity in tissues such as the urethra, upper airways and gallbladder are being discovered frequently and have been summarized elsewhere*(45, 50–52)*. Here we focus on the role of tuft cells in initiating type 2 immune responses in the small intestine.

An immune role for intestinal tuft cells was first described in 2016 when three studies were published describing a role for tuft cells in the initiation of innate type 2 immune responses in the SI*(19–21)*. SI tuft cells detect the presence of helminths and *Tritrichomonas* protists using a signaling pathway related to taste transduction in the tongue*(20)*. Once activated, tuft cells produce the cytokine interleukin 25 (IL-25) and, in some contexts, lipid-derived cysteinyl leukotrienes (cysLTs) to directly activate group 2 innate lymphoid cells (ILC2s)

in the SI lamina propria (SILP)*(19–21, 53)*. ILC2s in turn produce the canonical type 2 cytokines IL-5, -9, and -13, which collectively regulate hallmarks of type 2 immunity, including eosinophilia, hyperresponsivity of smooth muscle, and mucus overproduction. Meanwhile, the IL-13-induced tuft cell hyperplasia establishes a feed-forward tuft-ILC2 circuit (**Figure 2**). Tuft-ILC2 circuit activation can promote helminth clearance, but the function of tuft cell hyperplasia during *Tritrichomonas* colonization remains unclear as these protists are acquired from parents post-partum and persist for the life of the mouse*(19–21)*.

### 1.5 Dissertation objectives and significance

The identification of tuft cells as a key cellular players in the initiation of type 2 immune responses provided a major advance in our understanding of this process. However, the mechanism by which tuft cells are able to sense the presence of helminths or protists remained unclear. Therefore, we sought to ask what are the ligand/receptor pairs that tuft cells use to sense luminal organisms? Through RNA sequencing and genetic knockout mouse models we identified succinate as a ligand for intestinal tuft cells. Binding of succinate to the succinate receptor (SUCNR1) on tuft cells is sufficient to induce a multi-faceted type 2 immune response, making it one of the only innate type 2 immune ligands identified to date. Moreover, we found that sensing of *N. brasiliensis* is SUCNR1-independent, while detection of the *Tritrichomonas* requires SUCNR1. These findings uncover a novel paradigm in which the type 2 immune response monitors microbial metabolism in the SI. These findings are described in Chapter 2.

While studying succinate activation of the tuft-ILC2 circuit, we observed that succinate responses vary among different strains of inbred mice. This observation led us to exploit

differences between inbred mouse strains to identify a novel mechanism that regulates tuft cell differentiation and sets a threshold for tuft-ILC2 circuit activation. Quantitative trait loci mapping revealed a single locus on chromosome 9 (chr9) associated with variations in succinate responsiveness. This chr9 locus includes *Pou2af2*, a transcriptional cofactor essential for tuft cell development*(54)*. We found that epithelial progenitors in Balb mice, the non-responsive strain, expressed less of the functional full-length *Pou2af2* isoform. Examining the consequences of *Pou2af2* isoform usage on type 2 immune responses in the intestine, we found that Balb mice maintain responsiveness to helminth pathogens while ignoring commensal *Tritrichomonas* protists. In sum, we propose that differential *Pou2af2* isoform usage regulates tuft cell frequency at homeostasis and tunes the sensitivity and kinetics of tuft cell-mediated responses to distinct immune stimuli. This work is presented in Chapter 3.

Collectively, these findings advance our knowledge about how tuft cells sense luminal signals to initiate a type 2 immunity and how regulation of tuft cell differentiation can impact these immune responses in the small intestine. These novel insights into tuft cell biology have important implications for our understanding for intestinal immunity and could help inform how we design therapies to treat helminth infections and allergies. Beyond type 2 immune responses, there is a growing body of literature demonstrating a role for tuft cells in a variety of disease settings and physiological responses, from the airways to the gallbladder. The more we understand about the signaling mechanism regulating tuft cell activation and differentiation, the better we can inform the design of therapies that tune the immunologic tone of diverse mucosal tissues.

## 1.6 Figures

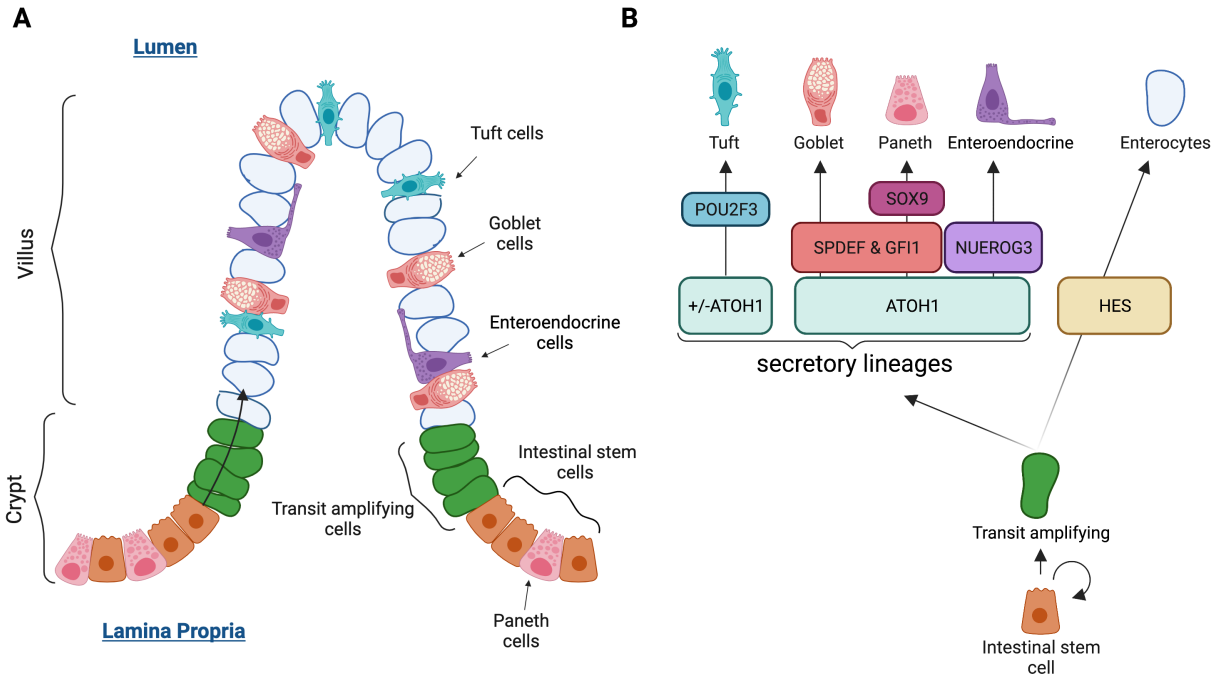


**Figure 1. Small intestinal epithelium.**

**(A)** The epithelium is comprised of crypts and villi*(31)*. Within the crypts are intestinal stem cells (ISCs) and transit amplifying cells that give rise to all 5 lineages of post-mitotic epithelial cells. As they differentiate, these cells move up the villi and are eventually sloughed off from the tip of the villus. Paneth cells on the other hand reside in the base of the crypt for up to two months, where they secrete antimicrobial peptides, and provide niche supporting signals to ISCs. (**B**) Transcription factors required for the differentiation of each epithelial cell lineage.

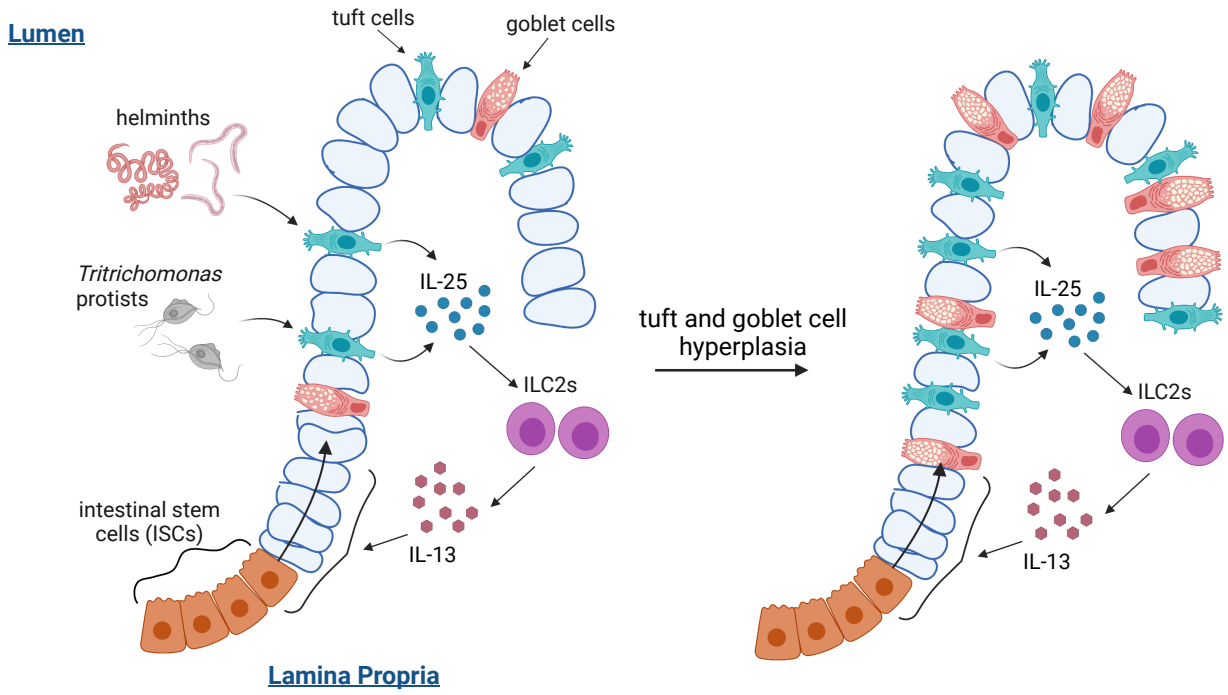


**Figure 2. Tuft-ILC2 circuit**

In the small intestine, tuft cells, can stimulate a type 2 immune response during helminth infection or *Tritrichomonas* protist colonization by activating group 2 innate lymphoid cells (ILC2s) via secretion of IL-25*(19–21)*. IL-25 induces IL-13 secretion from neighboring ILC2s. IL-13 in turn signals in epithelial stem cells, biasing their lineage commitment to increase the frequency of tuft cells in the intestinal epithelium leading to more IL-25 and a feed-forward loop that initiates the type 2 response. This signaling cascade results in smooth muscle contractions and mucus overproduction, leading to worm clearance.

## Chapter 2

Detection of succinate by intestinal tuft cells triggers a type 2 innate immune circuit

This chapter is adapted from the following publication:

Nadjsombati MS***,** McGinty JW*, Lyons-Cohen MR, Jaffe JB, DiPeso L, Schneider C, Miller CN, Pollack JL, Nagana Gowda GA, Fontana MF, Erle DJ, Anderson MS, Locksley RM, Raftery D, von Moltke J. Detection of succinate by intestinal tuft cells triggers a type 2 innate immune circuit. Immunity. 2018. 49:33-41.

* Denotes equal contribution

## 2.1 Introduction

Innate immune sensing is the critical first step to initiating a rapid, appropriate, and effective immune response against microbes. Many receptor-ligand pairs have been discovered for the recognition of conserved ligands derived from viruses, bacteria, and fungi*(5)*. However, much less is understood about how the immune response is alerted to the presence of helminths and allergens.

Our understanding of this process was greatly advanced in 2016 when three groups identified tuft cells as the sole producers of the cytokine IL-25, a signal critical for worm clearance from the small intestine (SI)*(19–21)*. These studies demonstrated that during helminth infection or protist colonization in the SI, tuft cell derived IL-25 activates ILC2s in the lamina propria. Intestinal ILC2s highly express the IL-25 receptor, IL17RB, and upon activation produce the canonical type 2 cytokines IL-5, -9, and -13. These cytokines drive classic manifestations of type 2 immunity, including eosinophilia and hyperresponsivity of smooth muscle. IL-13 in particular signals to intestinal stem cells, biasing their lineage commitment toward tuft and goblet cells, resulting in hyperplasia of both cell types and activation of a feed-forward circuit, referred to as the tuft-ILC2 circuit.

Tuft cells are a rare population of intestinal epithelial cells in specific-pathogen-free mice*(21)*. However, the intestinal flora of mice in many research vivariums include flagellated Tritrichomonas protists*(55, 56)*. These Tritrichomonas protists can activate the tuft-ILC2 circuit and induce tuft cell hyperplasia*(20)*. Furthermore, the tuft-ILC2 circuit is even more potently activated during infection with helminths, including the hookworm *Nippostrongylus brasiliensis (N. brasiliensis)*, the round worm*, Heligmosomoides polygyrus,* and the nematode, *Trichinella*

*spiralis(19–21)*. These infections lead to a 5 - 10 fold increase in the number of tuft cells, and in the case of *N. brasiliensis* this tuft-ILC2 response in necessary for efficient worm clearance*(21)*. A major outstanding question from these findings was how exactly are tuft cells sensing the presence of these luminal protists and helminths?

Some clues as to how this could be happening could be found by examining the transcriptional profiles of tuft cells. In 2008, Bezencon et al performed gene microarray on tuft cells, confirming that tuft cells express many components of the taste transduction pathway*(28, 43)*. In taste cells, this signaling pathway begins with ligand binding to surface-expressed G-protein coupled taste receptors, which signal through the alpha subunit called, a-gustducin (Gnat3). Gustducin activates phospholipase C beta 2 (PLCB2), leading to the release of intracellular $Ca^{2+}$ stores and sodium influx via the calcium-gated membrane channel TRPM5 (transient receptor potential cation channel subfamily M member 5). In taste cells, this cell depolarization leads to release of neuromediators and propagation of taste sensation*(57)*. Studies of tuft cells in the airway demonstrated that tuft cells express a subset of taste receptors and can regulate smooth muscle contraction in response to bitter ligands or bacterial quorum-sensing molecules*(48–50)*. In the intestinal epithelium, tuft cells are the only TRPM5 expressing cells and express many components of this signaling pathway including GNAT3 and PLCB2*(28)*. Howitt et al, demonstrated that in the intestine, tuft cell sensing of tritrichomonads requires TRPM5 and GNAT3*(20)*. Therefore, we and others hypothesized that tuft cell sensing relied on receptor ligand pairs that signal through this chemosensing pathway.

Here, we found that sensing of the microbial metabolite succinate by tuft cells was sufficient to induce a type 2 immune response and that succinate receptor-deficient mice failed

to detect *Tritrichomonas* protist colonization. These findings identify the first intestinal tuft cell ligand.

## 2.2 Results

### mRNA sequencing identifies a transcriptional tuft cell signature

While it was known that tuft cells exist in a variety of different tissues, no studies had yet compared the transcriptional profiles of these various populations. Therefore, we performed mRNA sequencing on tuft cells sorted from the gallbladder, SI, colon, trachea, and thymus of Flare25 reporter mice. We also sorted non-tuft epithelial cells from the SI as controls. Principle component analysis of these data revealed that the tissue of origin drove the majority of transcriptional differences, with thymic tuft cells separating furthest from all other populations (Figure 1A). Intestinal tuft cells from both the SI and colon were closest to each other and to the non-tuft control group. These trends could be visualized by hierarchical clustering of differentially expressed genes among tuft cell subsets showing clear tissue specific patterns (Figure 1B). Although clear differences emerged, there was a subset of genes shared by tuft cell across tissues, but not expressed by non-tuft SI epithelium, which we defined as the tuft cell gene signature (Figure 1C, Table 1). This signature includes the master transcription factor of tuft cells, *Pou2f3*, as well as other markers previously attributed to tuft cells in various tissues such as *Dclk1, Ptgs1, Alox5* and *Chat(21, 28)*.

Also within this signature are several genes associated with the TRPM5-depenedent chemosensing pathway, consistent with previous studies. These genes include *Trpm5*, *Plcb2*, and *Gnat3* (Figure 1D-F). However, the tuft cell gene signature contains no canonical taste receptors. Instead, we found only a handful of canonical taste receptors are expressed by tuft cells in some tissues like in the trachea and thymus. Intriguingly, no taste receptors were expressed by SI tuft cells. We therefore hypothesized different GPCRs could be upstream of the

TRPM5-dependent chemosensing pathway in SI tuft cells. Based on previous work, we knew tuft cell activation by tritrichomonads in the SI is TRPM5-dependent, and TRPM5 activation is $Ca^{2+}$ dependent; therefore, we began our search by looking for GPCRs that induce $Ca^{2+}$ flux, are surface expressed and are restricted to tuft cells within the SI epithelium. Two metabolite receptors matched these criteria, FFAR3 and SUCNR1. FFAR3 is the receptor for the short-chain fatty acids (SCFAs) propionate and butyrate and has been implicated in sensing these bacterial metabolites in the intestine*(58)*. SUCNR1 is the extracellular receptor for the citric acid cycle intermediate succinate and is best characterized in the kidney, where it helps to regulate blood pressure*(59)*. In our RNA sequencing data set, we find *Ffar3* expression is highest in tuft cells from the intestinal tract, SI, colon and gallbladder. *Sucnr1* is most highly expressed by tuft cells in the SI and trachea. To validate the SI results, we performed quantitative PCR (qPCR) on sorted tuft cells and non-tuft epithelial cells. This confirmed *Ffar3* and *Sucnr1* were enriched in SI tuft cells. We also measured expression of other SCFA receptors but did not detect expression of *Ffar1* and *Ffar2* in either tuft cells or non-tuft epithelium, whereas both populations expressed equal amounts of *Ffar4*. Therefore, SUCNR1 and FFAR3 particularly warranted further analysis as candidate receptors upstream of TRPM5-dependent tuft cell signaling.

**Succinate is sufficient to induce a type 2 immune response in the small intestine**

To test whether tuft cells can detect luminal SCFA and/or succinate, we added 150 mM sodium succinate, propionate, acetate, or butyrate or 300 mM NaCl (to match sodium molarity) to the drinking water of mice for 7 days and quantified tuft cell hyperplasia in the SI. Succinate,

but not SCFAs or NaCl, was sufficient to induce a >5-fold increase in tuft cells (Figures 2A and 2B). Although tuft cell hyperplasia was detectable throughout the SI, it was most pronounced in the distal segment (last 10 cm) (Figure 2C). There was no change in tuft cell frequency in the cecum or colon of succinate treated mice (Figure S1A). Over a range of concentrations, 150mM succinate in the drinking water induced the most robust tuft cell hyperplasia. Concentrations of 75 and 300 mM both elicited less tuft cell hyperplasia, the latter of which was most likely due to reduced water consumption at such high sodium concentrations (Figure 2D). To understand the kinetics of this succinate response, we performed a time course and found that tuft cell hyperplasia peaked around days 7 and 8 (Figure 2E). We noted a downward trend in tuft cell numbers at later time points, perhaps because of regulatory feedback mechanisms, but tuft cell frequency remained well above background throughout the time course. Unless otherwise noted, we performed further experiments by analyzing the distal SI after 7 days of 150 mM succinate administration.

Next, we looked for other measures of innate type 2 immunity in the SI. In addition to tuft cell hyperplasia, mice treated with succinate also had elevated numbers of goblet cells, and goblet cell size was increased indicating more mucus production (Figures 2F- 2H). Within the mesenteric lymph nodes (MLN) of succinate treated mice there was an accumulation of ILC2s and eosinophils (Figures 2I–2J and Figures S2B–S2D), all indicative of an ongoing type 2 immune response. As mentioned previously, type 2 immune responses are essential for timely expulsion of intestinal helminths such as *Nippostrongylus brasiliensis*. Mice treated with succinate prior to and during *N. brasiliensis* infection had accelerated worm clearance, further demonstrating that succinate is sufficient to induce a bona fide intestinal type 2 immune response (Figure 2K).

Finally, because commensal bacteria both produce and consume succinate, it was possible that succinate treatment in the drinking water activated type 2 immune responses indirectly by altering the composition of the intestinal microbiome*(60, 61)*; however, germ-free mice treated with succinate readily developed tuft cell hyperplasia. Together, our data demonstrate that succinate is an innate immune ligand that is sufficient to induce a multifactorial innate type 2 immune response in the small intestine.

**Succinate signals via the tuft-ILC2 circuit**

Previous publications defined an innate tuft-ILC2 circuit where tuft cell derived IL-25 activates ILC2s, which subsequently produce IL-13*(19–21)*. IL-13 acts on epithelial stem cells to drive differentiation of more tuft and goblet cells, resulting in hyperplasia of both cell types. To determine whether succinate-driven tuft cell hyperplasia similarly required the tuft-ILC2 circuit, we tested mice deficient in various components of this circuit (Figure 3A). Consistent with previous findings, succinate-induced tuft cell hyperplasia was completely dependent on IL-4 receptor alpha (*Il4ra*), necessary for IL-13 signaling (Figures 3B and 3C)*(19)*. In *Rag1*$^{-/-}$ mice which lack adoptive lymphocytes, tuft cell hyperplasia was largely intact. However, *Il2rg*$^{-/-}$ mice, which lack both innate and adaptive lymphocytes, completely failed to induce tuft cell hyperplasia in response to succinate, indicating that ILC2s are the dominant source of IL-13 in this succinate induced system.

IL-25 potently activates ILC2s in the intestinal lamina propria and was necessary for tuft cell hyperplasia following succinate treatment. IL-33, another ILC2-activating cytokine that signals through ST2, was not required for this response. Tuft cells are the exclusive source of IL-

25*(19)*. In line with the lack of response in *Il-25*$^{-/-}$ mice, tuft cells were required for type 2 immune activation following succinate treatment as goblet cell hyperplasia and hypertrophy were absent in tuft-cell-deficient *Pou2f3*$^{-/-}$ mice (Figures 3D-3F). TRPM5, a key signaling component of the tuft cell chemosensory pathway, was required for tuft cell hyperplasia, as well as ILC2 and eosinophil accumulation in the MLNs of succinate-treated mice (Figures 3B, 3C, 3G and 3H). Furthermore, rapid succinate-induced IL-13 production (measured with the Smart13 reporter) was seen in ILC2s from the mLN and lamina propria in wild-type mice but was completely absent in *Trpm5*$^{-/-}$ mice (Figures 3I-3L). Finally, as expected, the response to succinate administration was completely dependent on succinate receptor, SUCNR1 (Figure 3B and 3C).

To further confirm that succinate sensing occurs in tuft cells and is amplified through the tuft-ILC2 circuit, we stimulated sort-purified lamina propria ILC2s and analyzed IL-13 production after succinate stimulation. As expected, recombinant IL-25 activated ILC2s to produce IL-13, but succinate had no effect, confirming that ILC2s do not directly sense succinate (Figure S2A and S2B). We generated intestinal epithelial organoids, which contain only epithelial cells, and treated them with recombinant IL-13 (rIL-13) or succinate. rIL-13 induced tuft cell hyperplasia, as previously demonstrated*(19)*, but succinate again had no effect, indicating that succinate signaling in epithelial cells is not sufficient to induce tuft cell hyperplasia (Figure S2C). Together, these results strongly support a model in which tuft cells sense succinate through SUCNR1 to activate the feed-forward tuft-ILC2 circuit and drive intestinal type 2 immunity.

### *N. brasiliensis* and a Tritrichomonads secrete succinate

Given the link between tuft cells and the type 2 immune response to microbes, we hypothesized that succinate sensing is a mechanism for monitoring microbial metabolism in the intestinal lumen. Unlike land vertebrates, which principally generate lactic acid under anaerobic conditions, the anaerobic metabolites of helminths, protists, and bacteria are far more diverse and include hydrogen, ethanol, acetate, propionate, lactate, and other metabolites*(62)*. Various organisms, including bacteria, some protists (e.g., *Tritrichomonas fetus*) and some helminths, use fumarate as a terminal electron acceptor during fermentation, resulting in production and release of succinate*(62, 63)*. A previous study reported that *N. brasiliensis* does indeed secrete succinate, but this has not been further investigated*(64)*. Therefore, we wondered whether succinate sensing by tuft cells might contribute to the immune response to *N. brasiliensis*. We analyzed *N. brasiliensis* excretory-secretory product (NES) by using nuclear magnetic resonance (NMR) and indeed found succinate as well as acetate, propionate, and lactate were all produced at detectable levels (Figure 4A). Furthermore, succinate and NES induced $Ca^{2+}$ in mouse embryonic fibroblasts transduced with *Sucnr1*, but not in non-transduced control cells (Figures 4B and 4C). Thus, *N. brasiliensis* can secrete succinate and this is capable of triggering SUCNR1 signaling *in vitro*.

Similar to helminths, *Tritrichomonas* protists also activate the innate tuft-ILC2 circuit in the SI and can be found in the microflora of many research vivariums. In the University of Washington vivarium, we identified a mouse colony that harbored abundant protists (>100 million/ cecum) with *Tritrichomonas*-like morphology (Figure S3A). Internal transcribed spacer (ITS) sequencing identified this colony as containing a previously undescribed tritrichomonad

with >97% and >86% homology to the ITS of *T. musculis* and *T. muri*s, respectively (Figure S3B). We refer to this University of Washington isolate as *T. rainier*. Like *N. brasiliensis*, *T. rainier* secreted succinate upon anaerobic culture (Figure 4D).

**Sensing of *T. rainier*, but not *N. brasiliensis*, requires *Sucnr1***

Previously published results demonstrated that immune sensing of tritrichomonads requires TRPM5 and GNAT3*(20)*. We tested the requirement of these signaling components in the sensing of *N. brasiliensis*. We found both worm clearance and tuft cell hyperplasia following *N. brasiliensis* infection are TRPM5 dependent, with both significantly delayed in *Trpm5*$^{-/-}$ mice compared to wild-type (Figures 4E and 4F). By contrast, tuft cell hyperplasia developed normally in *N. brasiliensis*-infected *Gnat3*$^{-/-}$ mice, suggesting distinct sensing mechanisms for helminths and protists upstream of TRPM5 (Figure 4G). Given that both *N. brasiliensis* and *T. rainier* could secrete succinate *in vitro*, next we sought to test the requirement of SUCNR1. Like in *Gnat3*$^{-/-}$ mice, the immune response to *N. brasiliensis* in *Sucnr1*$^{-/-}$ mice was equivalent to wild-type with no delay in worm clearance (Figures 4H and 4I). In contrast, the immune response to *T. rainier* was completely absent in *Sucnr1*$^{-/-}$ mice, with no evidence of tuft cell hyperplasia or MLN infiltrates in *Sucnr1*$^{-/-}$ mice despite equivalent colonization with *T. rainier* (Figures 4J–4M and Figures S3C). In sum, tuft cells sense *T. rainier* via SUCNR1, but SUCNR1 signaling is redundant or perhaps absent during *N. brasiliensis* infection.

One possible hypothesis for the lack of phenotype in *N. brasiliensis* infected *Sucnr1*$^{-/-}$ mice is that there are multiple redundant receptors that sense helminth infection. We had generated *Ffar3*$^{-/-}$ mice and *Gprc5c*$^{-/-}$ mice in the lab. As discussed above, FFAR3 is a GPCR

expressed by SI tuft cells that detects the SCFAs, propionate and acetate. GPRC5C is an orphan GPCR that is very highly expressed by SI tuft cells. One publication suggested a potential role of GPRC5C in pH sensing but no ligand has been defined to date*(65)*. We made both *Ffar3*$^{-/-}$*;Sucnr1*$^{-/-}$ or *Gprc5c*$^{-/-}$*;Sucnr1*$^{-/-}$ double knockout mice and tested their type 2 immune response to *N. brasiliensis* infection. We found no decrease in tuft cell hyperplasia in either the proximal or distal SI, and no delay in worm clearance by day 7 (Figures S4A-S4C). These data do not exclude the possibility that yet another GPCR on tuft cells may be responsible for tuft cell sensing of helminth infection. An alternative hypothesis is that tuft cells sense helminth activity, perhaps through mechanosensing or barrier disruption, rather than a secreted ligand. Ultimately, more work is needed to identify mechanisms of tuft cell sensing of helminth infection.

**Bacterial succinate production can activate the tuft-ILC2 circuit**

Commensal bacteria both consume and produce succinate as a metabolite*(60, 61)*. In a healthy microbiome the ratio of succinate producers and consumers is balanced, such that there is little free succinate. Perhaps succinate sensing by tuft cells is a mechanism of monitoring for bacterial dysbiosis. The low frequency of tuft cells in *Tritrichomonas*-free SPF mice suggests that bacterial succinate is not sensed at homeostasis, but this could change in states of dysbiosis, especially if bacterial species that secrete succinate are expanded. Indeed, Lei et al. demonstrated that induction of bacterial dysbiosis with the antibiotic Streptomycin or a laxative, PEG3350, causes SUCNR1-dependent tuft cell hyperplasia localized to the distal SI, presumably by increasing the abundance of succinate-secreting bacteria*(66)*. However, when

we repeated these experiments with mice bred in the University of Washington vivarium or purchased from Charles River laboratories, we saw no Streptomycin-induced tuft cell hyperplasia (Figures 5A-5B). One explanation for this discrepancy is that the University of Washington and Charles River microbiomes do not contain the same Streptomycin resistant succinate-producing species as the mice used in the previous publication. This suggests that effects of Streptomycin depend on the composition of the microbiome and do not always result in activation of the tuft-ILC2 circuit.

However, to demonstrate sensing of bacterial succinate directly, we performed a mono-colonization experiment in germ-free mice with a succinate-producing commensal bacterial species, *Bacteroides ovatus (B. ovatus)* or a *B. ovatus* mutant in which succinate secretion is reduced ~50%. We find mice colonized with *B. ovatus*, but not the *B. ovatus* mutant, develop tuft cell hyperplasia in the distal SI (Figure 5C). We confirmed that bacterial burden was equivalent in colonized mice (Figure 5D). Taken together, a model emerges in which tuft cells sense succinate to monitor microbial metabolism in the distal SI, with elevated succinate levels indicating a dysbiosis. In response, tuft cells activate the tuft-ILC2 circuit and associated immune response.

## 2.3 Discussion

Since the identification of a role for tuft cells in type 2 immunity, the mechanisms of immune sensing by intestinal tuft cells have been of great interest. In this study, we found that succinate is an intestinal tuft cell ligand, as two other groups also recently reported*(66, 67)*. We demonstrate that succinate alone is sufficient to drive a multifaceted intestinal type 2 immune response (Figure 2). Further, this response is dependent on tuft cell chemosensing through SUCNR1 and TRPM5, and production of IL-25 ultimately leading to ILC2 activation (Figure 3). Finally, we demonstrate Tritrichomonad sensing is dependent on SUCNR1 but succinate sensing is dispensable for the response to *N. brasiliensis* (Figure 4).

Succinate is an intermediate of the mammalian TCA cycle, where it is contained within mitochondria and therefore is not found in large quantities extracellularly. Interestingly, all previous studies linking succinate to immune responses have characterized this molecule as an enhancer of type 1 immunity*(68–71)*. Signaling through SUCNR1 on dendritic cells and macrophages or intracellular sensing of succinate all potentiate classical type 1 inflammatory pathways. In the intestine, however, sensing of succinate seems to be wired differently, leading to a type 2 immune response.

Helminths, protists, and both commensal and pathogenic bacteria have diverse metabolic strategies, some of which include the secretion of succinate as a byproduct of metabolism*(62)*. Indeed, Schneider et al, and our own studies both confirmed that Tritrichomonas protists produce succinate*(29, 67)*. Schneider et al, observed that Tritrichomonad protist numbers expand dramatically in the cecum around the time of weaning, which correlated with an increase in tuft cell numbers*(67)*. The authors went on to show that

Tritrichomonads need fermentable fiber to persist in the lumen and therefore their expansion in numbers corresponds to when the mouse transitions from a milk to chow diet at weaning. Intriguingly, tritrichomonads are not cleared or even reduced in number by a type 2 immune response suggesting that they can tolerate detection via succinate. In parallel, colonization by Tritrichomonas does not seem to negatively impact the host in any way raising the question of why does the immune response sense these organisms in the first place?

In addition to protists, many bacteria can produce or consume bacteria as part of their metabolism. Lei et al. observed SUCNR1-dependent tuft cell hyperplasia in the very distal SI following treatment of mice with the antibiotic Streptomycin or laxative PEG3350, without the presence of protists or helminths*(66)*. This suggests that during microbial dysbiosis bacterial derived succinate is capable of activating the tuft-ILC2 circuit in the SI. However, we hypothesize this sensing would only occur if the dysbiosis skewed the ratio of succinate producing to consuming bacteria towards the consumers, thereby increasing the local concentrations above some threshold to trigger tuft cell activation. Thus, this dysbiosis induced tuft cell hyperplasia is microbiome dependent. Indeed, when we treated mice bred in the University of Washington vivarium or Charles River laboratories with Streptomycin, we did not observe any tuft cell hyperplasia (Figure 5). These results establish a paradigm in which succinate sensing by tuft cells drives an innate type 2 immune response to protist colonization or bacterial dysbiosis.

In contrast, succinate sensing in not required for detection of helminth infection. *N brasiliensis* can secrete succinate when cultured *in vitro*, yet we and others did not observe a significant defect in tuft cell hyperplasia and worm clearance 7–8 days after *N. brasiliensis*

infection in *Sucnr1*$^{-/-}$ mice (Figures 4A, 4H and 4I). We also tested whether combination knockouts of *Sucnr1*$^{-/-}$ and *Ffar3*$^{-/-}$ or *Gprc5c*$^{-/-}$ would abrogate tuft cell sensing of *N. brasiliensis*, but in both cases there was no effect (Figure S4). We must therefore conclude that either tuft cells do not sense helminth-derived succinate or sensing is redundant. Further studies are needed to identify one or more additional sensors that signal upstream of TRPM5 during helminth infection.

Finally, we must also consider the possibility that tuft cells detect endogenous or dietary succinate, although our data suggest that it is difficult to globally increase the concentration of succinate in the intestinal lumen, most likely because of rapid uptake of succinate by the intestinal epithelium*(61, 72)*. Accordingly, even 75 mM succinate in drinking water, was insufficient to induce maximal tuft cell hyperplasia (Figure 2D). We favor the model that microbes that gain access to the intestinal epithelium are uniquely able to deliver succinate locally at levels that are high enough to activate SUCNR1 in tuft cells. Whether succinate released from dying epithelial cells can similarly activate tuft cells remains to be determined.

Regardless of its physiological source, succinate is an unusual innate immune ligand. Most innate immune ligands characterized thus far are unique microbe associated molecules that are integral to the survival or structure of the virus, bacteria or fungi, making them difficult to evolve away from. In contrast, succinate is one of many metabolites that could be used as a terminal electron acceptor in anaerobic metabolism. Given how diverse the metabolism of bacteria and protists is, it seems plausible that if succinate sensing posed a serious threat to the survival of an organism, it could evolve away from succinate secretion. Yet protists and bacteria do not. One hypothesis is that this type 2 inflamed environment may benefit some microbes,

potentially through increased availability of mucus, which some microbes can use as a source of nutrients and energy. Another hypothesis is that in some way the type 2 response to succinate benefits the host during times of microbial dysbiosis by shifting the antimicrobial profile of the lumen in an effort to restore homeostasis. This may be hard to model or observe in specific pathogen-free conditions, but may be more important in natural environments where microbial shifts can leave the host vulnerable to opportunistic pathogens. More work is required to understand the context in which succinate sensing is most important.

In sum, we have defined a paradigm in which metabolite sensing by tuft cells drives an innate type 2 immune response. This finding has important implications for our understanding of intestinal immunity and homeostasis and suggests novel strategies for therapeutic intervention.

## 2.4 Materials and Methods

### Experimental Animals

Mice aged 6 weeks and older were used for all experiments. Mice were age-matched within each experiment, but pooled results include both male and female mice of varying ages. C57BL/6J mice were bred in house or purchased from Jackson Laboratories or where specified, purchased from Charles River Laboratories. B6.*Rag1*$^{-/-}$ (B6.129S7-Rag1$^{tm1Mom}$/J), B6.Il2rg$^{-/-}$ (B6.129S4-Il12rg$^{tm1Wjhl}$/J), and B6.*Trpm5*$^{-/-}$ (B6.129P2-Trpm5$^{tm1Dgen}$/J) mice were purchased from Jackson Laboratories. B6.*Il25*$^{Flare25/Flare25}$ and B6.*Il13*$^{Smart13/Smart13}$ mice were generated as previously described*(19, 73)*. *Il25*$^{-/-}$ mice were generated as previously described*(18)*, generously provided by A. McKenzie, and backcrossed at least 8 generations to C57BL/6J. IL4ra$^{-/-}$ mice were generated as previously described*(74)*, generously provided by F. Brombacher, and backcrossed at least 8 generations to C57BL/6J. B6.*Pou2f3*$^{-/-}$ (Pou2f3 tm1.1(KOMP)Vlcg, Project ID #VG18280) were generously provided by M. Anderson. B6.*Gnat3*$^{-/-}$ mice were generated by pronuclear injection of Cas9 mRNA and two sgRNA (Guide 1: GCTTCAGGAGGATGCTGAGCGGG, Guide 2: CTCCAGTTCTTTGGACCTTCTGG) into fertilized C57BL/6J zygotes at the Gladstone Institutes (San Francisco, CA). B6.*Sucnr1*$^{-/-}$ mice were generated by pronuclear injection of Cas9 mRNA and two sgRNA (Guide 1: CGATTGCATAAAATGCAGAGAGG; Guide 2: AGAGTTATGCCAATGATAAGGGG) into fertilized C57BL/6J zygotes at the Gene Targeting Facility of the Cancer Research Laboratory at UC Berkeley (Berkeley, CA). Founder *Gnat3* and *Sucnr1* mice were genotyped by Sanger sequencing and founders carrying mutations were backcrossed once to C57BL/6J before intercrossing to generate homozygous mutant mice. All mice not purchased from Jackson Laboratories, Charles River laboratories or newly generated were

rederived into the University of Washington vivarium. Lewis rats were purchased from Envigo (LEW/SsNHsd). Except mice noted below, all mice and rats were maintained in specific pathogen-free conditions at the University of Washington and were confirmed to be tritrichomonas-free by qPCR. Germ free mice were housed and treated in the University of Washington Gnotobiotic Animal Core. All experimental procedures (with exceptions noted below) were approved by the Institutional Animal Care and Use Committee at the University of Washington. B6.*Il25*$^{Flare25/Flare25}$ mice used to sort cells for mRNA sequencing and B6.*Gnat3*$^{-/-}$ mice were maintained in specific pathogen-free conditions at the University of California, San Francisco and experimental procedures were approved by the Institutional Animal Care and Use Committee at the University of California, San Francisco. B6.*Il25*$^{Flare25/Flare25}$ were retrospectively found to be colonized with a tritrichomonad of unknown identity.

**Germ Free Mice**

C57BL/6J mice were raised under standard germ-free conditions in the University of Washington Gnotobiotic Animal Core. For succinate administration, mice were transferred to hermetically-sealed positive pressure isocages as described*(75)* and given autoclaved drinking water supplemented with 150 mM sodium succinate hexahydrate ad libitum for 7 days. For mono-colonization experiments mice were transferred to hermetically-sealed positive pressure isocages and administered roughly 6 x 10^7 bacterial cfu/mouse in 200ul media by oral gavage. Media used to grow bacteria and used to gavage ice for the media control group is LYHBHI Media prepared as described*(76)*. Mice received either *Bacteroides ovatus* (ATCC 8486) or *Bacteroides ovatus* △*yjjPB* generously provided to us by the Baldridge lab (Washington

University). Mice were euthanized and tissues harvested 7 days after colonization. Bacterial burden was measured by qPCR of cecal content.

**Cell culture and transduction**

Immortalized C57BL/6J mouse embryonic fibroblasts (MEFs; kindly provided by Dr. D. Stetson) and HEK293T were cultured in DMEM supplemented with 10% fetal calf serum (VWR), L-glutamine, penicillin/streptomycin, sodium pyruvate, HEPES and β-mercaptoethanol. For lentiviral transduction, the ORF for mouse *Sucnr1* was obtained directly from prepared cDNA from sorted small intestinal tuft cells (described above). After sequencing verification, *mSucnr1* was cloned into the pRRL-MND-MCS-2A-Puro lentiviral vector downstream of an MND promoter as previously described*(77)*. VSV-G pseudotyped, self-inactivating lentivirus was prepared by transfecting HEK293T cells with 1.5 µg pVSV-G, 3 µg psPAX-2, and 6 µg pRRL lentiviral vector, and viral supernatant collected and filtered before use. MEFs were incubated with viral supernatant overnight, and media was replaced with fresh culture media. Puromycin (5ug $mL^{-1}$) selection was added 72 hours post transduction and continued for 7 days.

**Short Chain Fatty Acid and Succinate Administration**

Mice were provided with sodium succinate hexahydrate (Alfa Aesar), sodium propionate (Arcos Organics), sodium acetate trihydrate (Fisher Chemical), or sodium butyrate (Alfa Aesar) ad libitum in drinking water. Unless otherwise noted, mice were treated for 7 days with 150 mM agonist, except NaCl, which was given at 300 mM to match sodium molarity with succinate treatment.

**Mouse Infection/Colonization**

Infectious third-stage *N. brasiliensis* larvae (L3) were raised and maintained as described*(73)*. Mice were infected subcutaneously at the base of the tail with 500 *N. brasiliensis* L3 and were euthanized at the indicated time points to collect tissues for staining or to count worm burden. Worm burden was enumerated across the entire small intestine. Wild-type mice naturally colonized with *T. rainier* were used as a source of protists for colonization studies. *T. rainier* colonization status was determined by microscopy and confirmed by qPCR and ITS sequencing. To transfer *T. rainier* to naïve mice, cecal contents of colonized mice were isolated and washed in PBS, filtered through a 70 μm strainer, and spun down. Contents were washed a second time in PBS and total protists enumerated using a hemocytometer. Mice received a single oral gavage of 20-30 x $10^6$ protists in a volume of 150 μl PBS. After 7 days mice were sacrificed for analysis. Successful colonization was again determined by microscopy and confirmed by qPCR.

**Streptomycin treatment**

Streptomycin treatment was administered as described*(66)*. Briefly, mice received 20mg Streptomycin in 200μl water by oral gavage daily for 5 days. 2 days after the final Streptomycin dose, distal SI was harvested for analysis.

**Tissue fixation and staining**

For tuft cell staining, intestinal tissues were flushed with PBS and fixed in 4% paraformaldehyde for 4 h at 4° C. Tissues were washed with PBS and incubated in 30% (w/v) sucrose overnight at

4° C. Small intestine and colon samples were then coiled into "Swiss rolls" and embedded in Optimal Cutting Temperature Compound (Tissue-Tek) and sectioned at 8 μm on a Microm HM550 cryostat (Thermo Scientific). Immunofluorescent staining was performed in Tris/NaCl blocking buffer (0.1 M Tris-HCL, 0.15 M NaCl, 5μg $ml^{-1}$ TSA blocking reagents (Perkin Elmer), pH 7.5) as follows: 1 h 5% goat serum, 1 h primary antibody (αDCLK1, Abcam ab31704), 40 min goat anti-rabbit IgG F(ab')2-AF594 secondary antibody (Life Technologies) and mounted with Vectashield plus DAPI (Vector Laboratories). Tuft cell frequency was calculated using ImageJ software to manually quantify DCLK1+ cells per millimeter of crypt-villus axis. Four 10x images were analyzed for each replicate and at least 30 total villi were counted.

For goblet cell staining, tissues were flushed with PBS, fixed in 10% buffered formalin at 4° C for 3 h, coiled into "Swiss rolls" and returned to formalin. After 24 h tissues were moved to 70% ethanol for storage. Tissue processing, paraffin embedding, sectioning, and staining were performed by the Pathology Research Services Laboratory at the University of Washington. Periodic acid Schiff (PAS) or Alcian blue staining was used to identify goblet cells. Goblet cell frequency was calculated as described above for tuft cells. Hypertrophy was quantified using ImageJ software to measure the area of at least 80 goblet cells for each biological replicate. Brightfield and fluorescent images were acquired on an Axio Observer.A1 inverted microscope (Zeiss).

**Single-cell tissue preparation**

For single cell epithelial preparations from small intestines, gall bladder, and colon, tissues were flushed with PBS, opened, and rinsed with PBS to remove intestinal contents. Intestinal tissue

was cut into 2-5 cm pieces and incubated rocking at 37° C in 15 mL HBSS ($Ca^{+2}$/$Mg^{+2}$-free) supplemented with 5mM dithiothreitol (DTT, Sigma-Aldrich), 5% fetal calf serum (FCS, VWR), and 10mM HEPES (Gibco). Tissues were vortexed vigorously and supernatant was discarded. Tissues were then incubated rocking at 37° C in 15 mL HBSS ($Ca^{+2}$/$Mg^{+2}$-free) supplemented with 5mM EDTA (Invitrogen), 5% FCS, and 10mM HEPES. Tissues were vortexed thoroughly and released epithelial cells were passed through a 70 μm filter. Tissues were then incubated in fresh EDTA/HBSS solution for 15 minutes, vortexed, and filtered. Supernatants were pooled and washed once before staining for flow cytometry.

For lamina propria preparations small intestinal tissue was processed as above to remove the epithelial fraction. Tissues were then rinsed in 20 mL HBSS (with $Ca^{+2}$/$Mg^{+2}$) supplemented with 5% FCS and 10mM HEPES, shaking at 37° C for 20 minutes. Supernatants were discarded and tissues were incubated in 5 mL HBSS (with $Ca^{+2}$/$Mg^{+2}$) supplemented with 3% FCS, 10mM HEPES, 30 μg $mL^{-1}$ DNase I (Sigma Aldrich), and 0.1 Wunsch $mL^{-1}$ Liberase TM (Sigma Aldrich), shaking at 37° C for 30 minutes. Tissues were vortexed and cells were passed through a 70 μm filter and washed. The resulting pellet was resuspended in 40% Percoll (Sigma Aldrich), centrifuged for 5 minutes at 1500 rpm, and supernatant discarded. Pelleted cells were then washed and stained for flow cytometry.

For mesenteric lymph node preparations, MLN were harvested into RPMI + 5% FBS on ice. Tissues were incubated 30 minutes at 37° C in 5 mL RPMI supplemented with 2 mg $mL^{-1}$ collagenase VIII (Sigma-Aldrich) and 7.5 μg $mL^{-1}$ DNase I (Sigma-Aldrich). Digested MLN were passed through a 70 μM filter and remaining tissue was mashed through filter. Cells were washed once and stained for flow cytometry.

For tracheal epithelium, the trachea was dissected from mice, stored in DMEM + 5% FBS and cleaned of stroma using a dissecting microscope. Tissue was cut into 6 pieces and incubated at room temperature in 16U $mL^{-1}$ Dispase (Corning) in DPBS without $Ca^{2+}$/$Mg^{2+}$. Incubation was monitored carefully and stopped by transfer into DMEM + 5% FBS when epithelium began to lift away from stroma (23-28 minutes). Epithelium was then peeled off under a dissecting microscope and collected in DMEM + 5% FBS on ice. Harvested epithelium was digested in 0.5% Trypsin + EDTA for 20 minutes at 37° C. After digest, cells were vortexed briefly and trypsin was quenched with DMEM + 5% FBS. Cells were washed once and stained for flow cytometry.

For thymic epithelium, thymi were isolated, cleaned of fat and transferred to DMEM + 2% FBS on ice. Thymi were minced with a razor blade and tissue pieces were moved with a glass Pasteur pipette to 15 ml tubes and vortexed briefly in 10 ml of media. Fragments were allowed to settle before removing the media and replacing it with 4 ml of digestion media containing 2% FBS, 100 $\mu g\ mL^{-1}$ DNase I (Roche), and 100 $\mu g\ mL^{-1}$ Liberase TM (Sigma-Aldrich) in DMEM. Tubes were moved to a 37° C water bath and fragments were triturated through a glass Pasteur pipette at 0 min and 6 min to mechanically aid digestion. At 12 min, tubes were spun briefly to pellet undigested fragments and the supernatant was moved to 20 ml of 0.5% BSA (Sigma-Aldrich), 2 mM EDTA (TekNova), in PBS (MACS buffer) on ice to stop the enzymatic digestion. This was repeated twice for a total of three 12 min digestion cycles, or until there were no remaining tissue fragments. The single cell suspension was then pelleted and washed once in MACS Buffer. Density-gradient centrifugation using a three-layer Percoll gradient (GE Healthcare) with specific gravities of 1.115, 1.065, and 1.0 was used to enrich for stromal cells.

Cells isolated from the Percoll-light fraction, between the 1.065 and 1.0 layers, were then washed and resuspended for staining.

**Flow cytometry and cell sorting**

Single cell suspensions were prepared as described and stained in DPBS + 3% FBS with antibodies to surface markers for 20 min at 4° C, followed by DAPI (Roche) for dead cell exclusion. Samples were FSC-A/SSC-A gated to exclude debris, SSC-H/SSC-W gated to select single cells and gated to exclude $DAPI^+$ dead cells. Samples were run on an LSR II (BD Biosciences) or Aurora (Cytek) and analyzed with FlowJo 10 (Tree Star). For cell sorting, single cell suspensions were prepared and stained as described and sorted into $CD45^{lo}$ $IL25(RFP)^+$ $EpCAM^+$ and $CD45^{lo}$ $IL25(RFP^-)$ $EpCAM^+$ populations using a MoFlo XDP (Beckman Coulter) or an Aria II (BD Biosciences).

**RNA sequencing & analysis**

Single cell suspensions of epithelial cells from gall bladder, small intestine, colon, thymus, and trachea were generated as described above from *Il25*$^{Flare25/Flare25}$ reporter mice. $CD45^{lo}$ $RFP^+$ $EpCAM^+$ tuft cells were sorted from all tissues and $CD45^{lo}RFP^-EpCAM^+$ cells were also sorted from the small intestine. With the exception of tracheal tuft cells, which were pooled from four mice for each replicate, each biological replicate represents one mouse. Four biological replicates were collected for each sample. Average sorted cells for each sample were as follows: $SI\_RFP^+$: 35,250; $SI\_RFP^-$: 55,000; Colon: 14,775; Gall: 2287, Thymus: 1612; Trachea: 255.

Cells were sorted directly into lysis buffer from the Dynabead mRNA Direct Purification Kit (ThermoFisher) and mRNA was isolated according to the manufacturer's protocol. Amplified cDNA was prepared using the NuGen Ovation RNA-Seq system V2 kit, according to the manufacturer's protocol (NuGen Technologies). Sequencing libraries were generated using the Nextera XT library preparation kit with multiplexing primers, according to manufacturer's protocol (Illumina). Library fragment size distributions were assessed using the Bioanalyzer 2100 and the DNA high-sensitivity chip (Agilent Technologies). Library sequence quality was assessed by sequencing single-end 50 base pair reads using the Illumina MiSeq platform and were pooled for high-throughput sequencing on the Illumina HiSeq 4000 by using equal numbers of uniquely mapped reads (Illumina). Twelve samples per lane were multiplexed to ensure adequate depth of coverage. Sequencing yielded a median read depth of 89.2 million reads per sample. The analytic pipeline included de-multiplexing raw sequencing results, trimming adapter sequences, and aligning to the reference genome. Sequence alignment and splice junction estimation was performed using the STAR software program. For differential expression testing, the genomic alignments were restricted to those that map uniquely to the set of known Ensembl IDs (including all protein coding mRNAs and other coding and noncoding RNAs). STAR aggregated mappings on a per-gene basis were used as raw input for normalization by DESeq2 software. Replicates failing quality control at any stage were discarded. Resulting datasets were deposited in the GEO database (GSE114067).

To determine the tuft cell signature, any genes with a mean normalized read count <300 in any tuft cell subset were removed from analysis. Next, genes were ranked based on log2 fold change between the mean expression level in all tuft samples and the mean expression level in

all non-tuft samples, with a cutoff of 4. GO Term and KEGG pathway analysis was performed using the Database for Annotation, Visualization, and Integrated Discovery*(78, 79)*. Visualization of taste receptor expression was generated using Morpheus (https://software.broadinstitute.org/morpheus/).

**Quantitative RT-PCR**

For tuft cell qPCR, $CD45^{lo}RFP^{+}EpCAM^{+}$ and $CD45^{lo}RFP^{-}EPCAM^{+}$ populations from small intestinal epithelium of *Il25*$^{Flare25/Flare25}$ mice were sorted into Buffer RLT (Qiagen) using an Aria (BD Biosciences). To validate *Gnat3*$^{-/-}$ mice, $CD45^{lo}EpCAM^{+}$ epithelial cells from the small intestine were sorted into Buffer RLT (Qiagen). RNA was isolated using the Micro Plus RNeasy kit (Qiagen) and reverse transcribed using SuperScript Vilo Master Mix (Life Technologies). For tritrichomonas quantification, total DNA was isolated from cecal contents using the QIAmp Fast DNA Stool Mini Kit (Qiagen). Cecal DNA or cDNA were used as template for quantitative PCR with Power SYBR Green reagent on a StepOnePlus cycler (Applied Biosystems). For mouse cells, transcripts were normalized to *Rps17* (40S ribosomal protein S17) expression. For cecal DNA, transcripts were normalized to bacterial 16s rRNA.

**Nuclear Magnetic Resonance Quantification of SCFA and Succinate**

NMR analyses were made using a Bruker AVANCE III 800 MHz equipped with a 5 mm HCN cryoprobe suitable for $^{1}H$ inverse detection with Z-gradients at 298 K. Samples were prepared to contain 50 µM TSP (3-(trimethylsilyl) propionic-2,2,3,3-$d_4$ acid sodium salt) for quantitative and chemical shift reference. One-dimensional $^{1}H$ NMR spectra were obtained using the CPMG

(Carr-Purcell-Meiboom-Gill) pulse sequence that included residual water signal suppression from a pre-saturation pulse during the relaxation delay. For each spectrum, 32k data points were acquired using a spectral width of 9615 Hz. The raw data were processed using a spectral size of 32k points and by multiplying with an exponential window function equivalent to a line broadening of 0.3 Hz. The resulting spectra were phase and baseline corrected and referenced with respect to the internal TSP signal. Bruker Topspin version 3.5pl6 software package was used for NMR data acquisition and processing. Assignment of peaks was made based on $^{1}$H NMR chemical shifts and spin-spin couplings obtained from the spectra of standard compounds under similar experimental conditions at 800 MHz. Chenomx NMR Suite Professional Software package (version 5.1; Chenomx Inc., Edmonton, Alberta, Canada) was used to quantitate metabolites. This software allows fitting spectral lines using the standard metabolite library for 800 MHz $^{1}$H NMR spectra and the determination of concentrations. Peak fitting with reference to the internal TSP signal enabled the determination of absolute concentrations for the short chain fatty acids and other organic acids. All NMR experiments were performed in conjunction with the Northwest Metabolomics Research Center at the University of Washington.

**Preparation of *N. brasiliensis* excretory-secretory product (NES)**

Infectious third-stage *N. brasiliensis* larvae (L3) were raised and maintained as described above. Lewis rats were infected subcutaneously with 2000 *N. brasiliensis* L3. Mature (L5) worms were collected from the entire small intestine 7 days post infection. Worms were washed 10 times in Wash Solution I (PBS with 200U ml$^{-1}$ Pen-Strep), allowing worms to settle by gravity between each wash. Worms were allowed to equilibrate in Wash Solution II (RPMI 1640 with 200U ml$^{-1}$

Pen-Strep) for 1 hour at room temperature, before being transferred to a tissue culture flask in NES culturing media (RPMI 1640, with 100U $ml^{-1}$ Pen-Strep, 2mM L-Glutamine and 1% glucose) and cultured at 37° C. Supernatant was collected at 24 and 48 hours and filtered prior to use as NES. For NMR analysis, phosphate buffer prepared in deuterated water (0.1M; pH =7.4) containing TSP (3-(trimethylsilyl) propionic-2,2,3,3-$d_4$ acid sodium salt) was added to NES to achieve a final concentration of 50uM TSP.

***Tritrichomonas* culture**

Culture of *T. rainier* was performed as described*(80)*. Briefly, cecums of *T. rainier* colonized mice were flushed with PBS, passed through the 70 um cell strainers and centrifuged at 1000 rpm for 5 min. To enrich for tritrichomonads a 40/80% percoll gradient centrifugation step was performed at 1000 g for 15 min with brakes off. Tritrichomonads were collected at the interphase and the tritrichomonad containing fraction was washed with PBS and resuspended in tritrichomonad culture medium. Tritrichomonad culture medium was modified from the method described by (Saeki et al., 1983). To prepare medium, cecums of mice were harvested and homogenized in PBS with 25 volumes of PBS per gram cecum. In order to get homogeneous suspension, the cecal extract was stirred at 4°C for 6 h and then centrifuged at 3500rpm for 10 min and the supernatant was filtered. The filtered cecal extract was used to resuspend the BBL Trichosel™ Broth (BD Biosciences) and titrated to pH 7 with NaOH. The medium was then autoclaved for 10 minutes. After cooling media was supplemented with 10% heat-inactivated horse serum and the following antibiotics; amphotericin B (5ug/mL), ampicillin (100ug/mL), chloramphenicol (100ug/mL), gentamicin (50ug/mL), kanomycin (100ug/mL), streptomycin

(100ug/mL), vanomycin (5ug/mL). The enriched tritrichomonads were resuspended in culture medium at 2 x $10^6$ protists per mL and cultured under anaerobic conditions for 24h. Media was collected and centrifuged 1750 rpm for 10 min. Supernatant was filter (0.22um PVDF filter). For NMR analysis, phosphate buffer prepared in deuterated water (0.1M; pH =7.4) containing TSP (3-(trimethylsilyl) propionic-2,2,3,3-$d_4$ acid sodium salt) was added to tritrichomonad conditioned media to achieve a final concentration of 50uM TSP.

***Tritrichomonas* sequencing**

Internal transcribed spacer (ITS) sequencing of the tritrichomonad identified in the University of Washington vivarium was performed as previously described*(55)*. Briefly, DNA was isolated from the cecal contents of colonized mice using the QIAmp Fast DNA Stool Mini Kit (Qiagen) and the ITS region was PCR-amplified using pan-parabasalid primers (Forward: AATACGTCCCCTGCCCTTTGT Reverse: TCCTCCGCTTAATGAGATGC). The resulting PCR product was sequenced by Sanger Sequencing (Genewiz). A BLASTn search identified the sequence as novel but closely related to both murine and human tritrichomonads. Alignment with the ITS sequences of *T. muris* (Accession: AY886843.1) and *T. musculis* (Accession: KX000922.1) showed >97% and >86% sequence identify, respectively. For clarity, we refer to this novel isolate as *Tritrichomonas rainier*, although its precise taxonomic relationship to *T. muris* and *T. musculis* remains to be determined. The ITS sequence for *T. rainier* is available in GenBank (Accession #: MH370486).

**Organoid Culture**

Small intestinal crypt-derived organoids were grown as described*(81)*, replacing recombinant R-spondin with supernatants from R-spondin expressing L-cells and replacing recombinant Noggin with supernatants from Noggin expressing cells. Crypts were harvested from the small intestine of naive B6.*Il25*$^{Flare25/Flare25}$ mice and plated on day 0. On day 1 and day 4, media were replaced and organoids were treated with 20 ng ml$^{-1}$ recombinant IL-13 or 10mM sodium succinate. On day 7 organoids were harvested and resuspended in Accutase (Corning). Organoids were sheared with a 28G insulin syringe, incubated for 1 h at room temperature, washed, and then stained for flow cytometry as described above.

**Calcium imaging**

Mouse embryonic fibroblasts were plated 7 x $10^4$ cells/well in 24-well plates coated with poly-D-lysine. After overnight incubation, cells were washed with assay buffer (1X HBSS with $Ca^{2+}$/$Mg^{2+}$, 10mM HEPES, pH 7.4). Cells were incubated for 1 hr at 37°C in assay buffer supplemented with 2.5 mM Fluo-4AM (Invitrogen) and 0.05% pluronic-F127 (Invitrogen). Cells were washed twice with assay buffer and incubated in assay buffer with 1mM probenecid (Biotium) for 30 minutes at 37° C prior to imaging. Cells were maintained at 37° C with 5% $CO_2$ throughout imaging. While imaging, sodium succinate was added to assay buffer at a final concentration of 150uM or 100ul NES or NES culturing media was added to 250ul assay buffer. Following addition of test agonist, ionomycin was added at a final concentration of 1ug mL$^{-1}$. Fluorescence images were collected at 1.44 frames per second with a 40X extra-long working distance objective on a Nikon TiE Inverted Widefield Fluorescence Nikon microscope and

analyzed with NIS Elements AR 3.2 software. For data presentation, fluorescence/background ($R/R_0$) was quantified over time. More than 50 cells were analyzed per replicate.

**ILC2 Stimulation Assay**

Small intestinal lamina propria ILC2s were isolated from Smart13 reporter mice and sorted as described. Sorted cells were plated at 4000-5000 cells per well in a 96 well plate and incubated overnight in 10 ng/mL IL-7 (R&D Systems) and basal media composed of high glucose DMEM supplemented with non-essential amino acids, 10% FBS, 100 mg/mL streptomycin/penicillin, 10mM HEPES, 1mM sodium pyruvate, 100μM 2-mercaptoethanol, and 2mM L-glutamine. The next morning media was replaced with fresh media and 10 ng/mL IL-7 and cells were stimulated with the indicated agonist. After a six-hour incubation at 37 °C, cells were stained with 1 μl/well of PE-conjugated anti-hCD4 for 20 minutes at 4 °C. Cells were washed, resuspended in DAPI, and analyzed on an LSRII (BD Biosciences).

**Quantification and Statistical Analysis**

All experiments were performed using randomly assigned mice without investigator blinding. Statistical details of experiments can be found in the figure legends. All data points and "n" values reflect biological replicates (i.e. mice), except in 4C where they represent technical replicates. No data were excluded. Statistical analysis was performed as noted in figure legends using Prism 7 (GraphPad) software. Holm-Sidak was used to correct for multiple comparisons. Graphs show mean + SEM.

## Data and Software Availability

RNA-Seq data are available at the NCBI GEO under accession number GSE114067. The ITS sequence for *T. rainier* is available in GenBank under accession number MH370486.

**2.5 Acknowledgements**

We thank staff at the University of Washington Gnotobiotic Core for assistance with germ free mouse experiments, Z. Wang for experimental assistance, N. Arpaia for guidance on NMR analysis of intestinal samples, D. Hailey and the Garvey Cell Imaging Lab in the Institute for Stem & Cell Regenerative Medicine for microscopy support, K. Smith for reagents and advice, and M. Fontana for critical reading and editing of the manuscript. JWM is supported by the University of Washington Immunology Training Grant (T32 AI106677). JVM is a Damon Runyon–Dale Frey Breakthrough Scientist and a Searle Scholar. This work was supported by NIH 1DP2 OD024087 (JVM) and the University of Washington. mRNA sequencing was supported by NIH R01 AI26918 (RML) and the SABRE Center at UC San Francisco.

**Author contributions**

MSN and JWM designed and performed experiments, analyzed data, and wrote the paper with JVM. MRLC, JBJ, and LP assisted with experiments at the University of Washington. CNM and CS assisted with cell isolations for RNA sequencing at UC San Francisco. GANG performed NMR analysis, with supervision by DR. JLP performed bioinformatics analysis of mRNA sequencing data, with supervision by DJE. MSA and RML acquired funding and provided resources for mRNA sequencing. JVM conceived of and supervised the study, performed experiments, analyzed data, and wrote the paper with MSN and JWM. All experiments besides RNA sequencing and *Gnat3*$^{-/-}$ infection were initiated at the University of Washington.

## 2.6 Figures

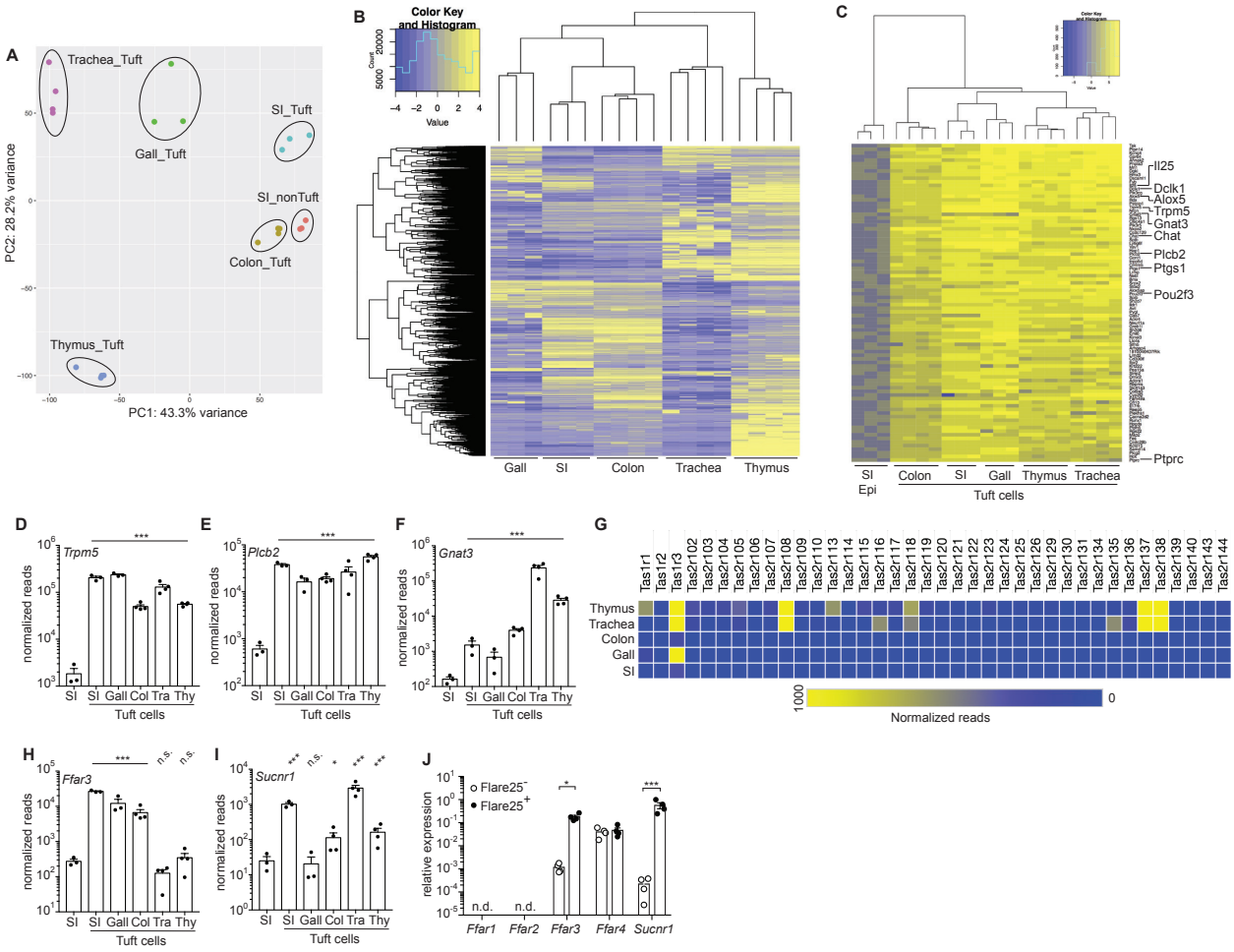


**Figure 1. RNA-Seq identifies a transcriptional tuft cell signature and a tissue-specific chemosensory receptor repertoire**

**(A-I)** Tuft cells (CD45$^{lo}$ EPCAM$^{+}$ Flare25$^{+}$) were sorted from small intestine (SI), gall bladder (Gall), colon (Col), trachea (Tra), and thymus (Thy) of naïve B6.*Il25*$^{Flare25/Flare25}$ mice for mRNA sequencing. Non-tuft epithelial cells of the small intestine (SI Epi; CD45$^{lo}$ EPCAM$^{+}$ Flare25$^{-}$) were sorted as a negative control. **(A)** Principal component analysis of gene expression. **(B)** Hierarchical clustering of differentially expressed genes (fold change > 8; FDR < 0.01) among tuft cell subsets. **(C)** Ranked list of a tuft cell transcriptional signature ($Log_2$ fold-change >4 in all

tuft cells relative to SI Epi). **(D-F)** Normalized read count of indicated genes. **G)** Heat map of normalized read count of all taste receptors. **(H-I)** Normalized read count of indicated genes. **(J)** Indicated genes analyzed by RT-qPCR in small intestinal tuft cells (Flare25$^{+}$) and non-tuft epithelial cells (Flare25$^{-}$). A-I: biological replicates from one mRNA sequencing experiment. J: biological replicates pooled from three experiments. In A-I *, FDR < .05; ***, FDR < .001 by statistical analysis in RNAseq pipeline. In J *, $p < 0.05$; ***, $p < 0.001$ by multiple *t*-tests. n.s., not significant; n.d., not detectable. Graphs show mean + SEM.

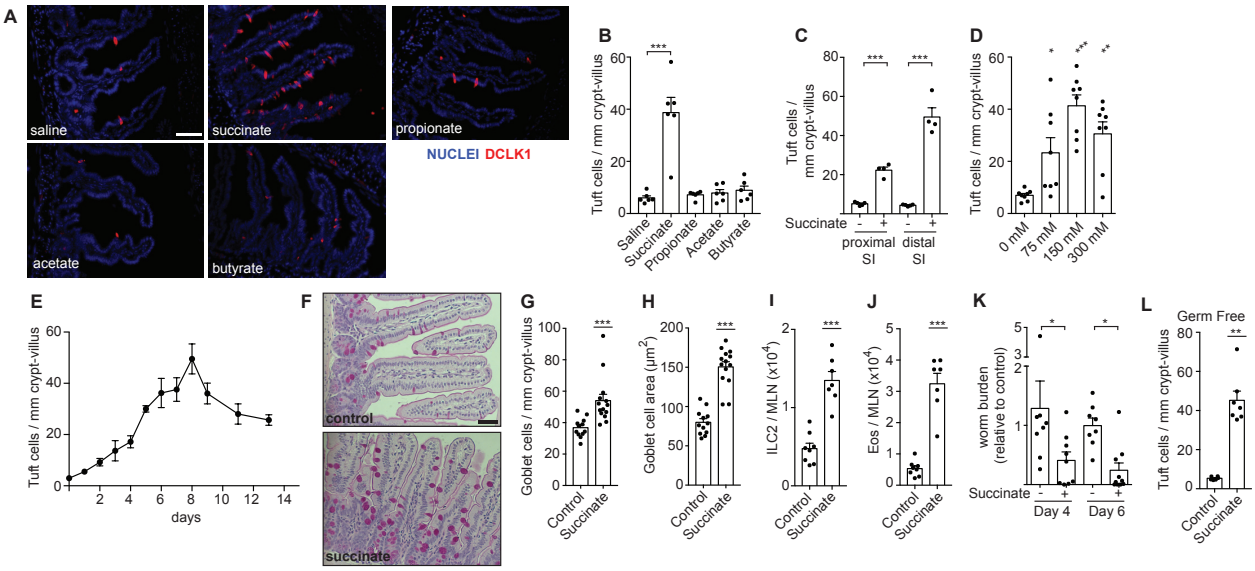


**Figure 2. Succinate is sufficient to induce a type 2 immune response in the small intestine**

**(A-J)** Unless otherwise indicated, wild-type mice were given 150 mM succinate or control water for 7 d. **(A)** Representative images and **(B)** quantification of tuft cells in the distal (last 10 cm) SI. DCLK1 marks tuft cells. Scale bar = 50 μm. **(C)** Tuft cell quantification in the proximal (first 10 cm) or distal SI. **(D-E)** Tuft cell quantification in the distal SI at indicated **(D)** succinate concentrations and **(E)** timepoints. **(F)** Representative images of middle SI stained with periodic acid-Schiff to visualize goblet cells. Scale bar = 50 μm. **(G-H)** Quantification of goblet cell **(G)** numbers and **(H)** hypertrophy. **(I-J)** Absolute numbers of **(I)** ILC2s and **(J)** eosinophils quantified in MLN. **(K)** Worm burden in mice that received succinate treatment or water control 7 days prior to and during infection with *N. brasiliensis*. Worm burden represented as relative to median of control within each experiment. **(L)** Tuft cell quantification in distal SI of germ-free mice. In B-D, G-L each symbol represents an individual mouse from three or more pooled experiments. In E, each symbol represents the average of 3-9 mice from three experiments. *, p

< 0.05; **, p < 0.01; ***, p < 0.001 by one-way ANOVA with comparison to control (B, D), by Mann-Whitney (G-J, L), or by multiple *t*-test (C, K). Graphs depict mean + SEM.

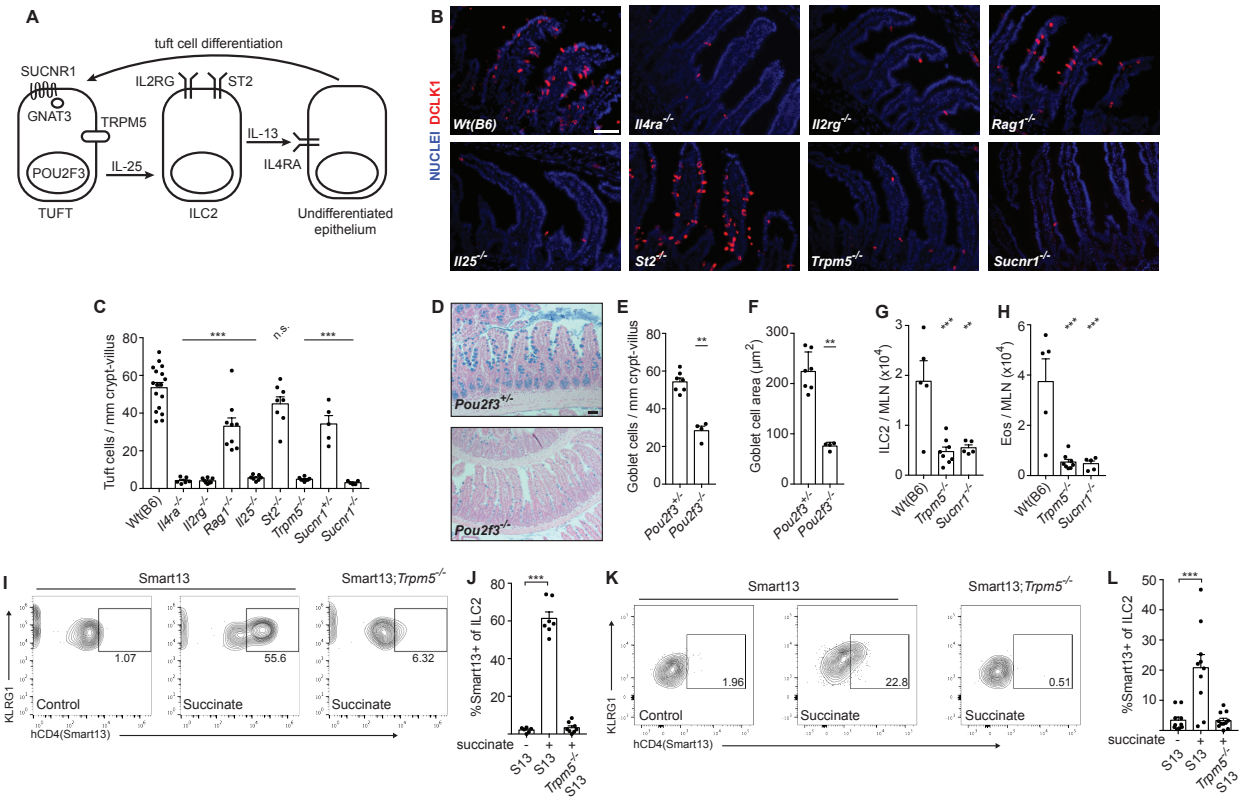


**Figure 3. Succinate signals via the tuft cell-ILC2 circuit in a TRPM5 and SUCNR1-dependent manner**

**(A)** Schematic of cells and proteins in the tuft-ILC2 circuit. **(B-J** Mice of indicated genotypes were given 150 mM succinate for 7 d. **(B)** Representative images and **(C)** quantification of distal SI. DCLK1 marks tuft cells. Scale bar = 50 μm. **(D)** Representative images of middle (10-20 cm from cecum) SI stained with Alcian blue to visualize goblet cells. Scale bar = 100 μm. **(E-F)** Quantification of goblet cell **(E)** numbers and **(F)** hypertrophy in D. **(G-J)** MLN analyzed by flow cytometry to quantify **(G)** ILC2s, **(H)** eosinophils, and **(I-J)** IL-13 production by ILC2s. Smart13: IL-13 reporter. **(K-L)** Lamina propria cells from mice of indicated genotypes given 150 mM succinate for 36 hours and analyzed as in I-J. In C-H, J-L each symbol represents one mouse from at least two pooled independent experiments. *, $p < 0.05$; **, $p < 0.01$; ***, $p < 0.001$ by

one-way ANOVA (C, G-H, J, L) with comparison to Wt (B6) or untreated Smart13 control, or by Mann-Whitney (E-F). n.s., not significant. Graphs depict mean + SEM.

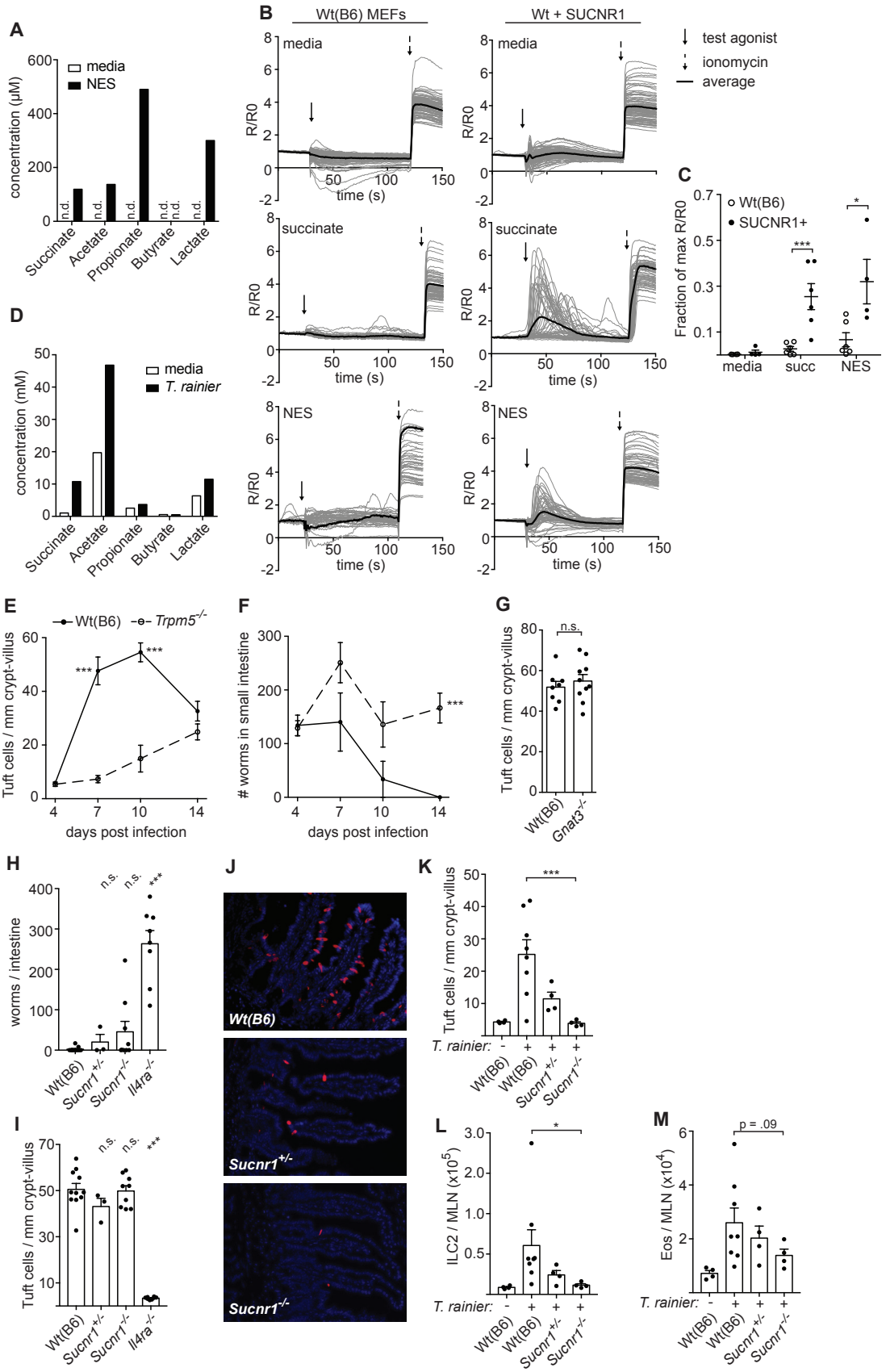
A
media
NES
concentration (μM)
Succinate
Acetate
Propionate
Butyrate
Lactate
B
Wt(B6) MEFs
Wt + SUCNR1
media
succinate
NES
R/R0
time (s)
test agonist
ionomycin
average
C
Wt(B6)
SUCNR1+
Fraction of max R/R0
media
succ
NES
D
media
T. rainier
concentration (mM)
E
Wt(B6)
Trpm5-/-
Tuft cells / mm crypt-villus
days post infection
F
# worms in small intestine
G
n.s.
Wt(B6)
Gnat3-/-
H
worms / intestine
Wt(B6)
Sucnr1+/-
Sucnr1-/-
Il4ra-/-
I
J
Wt(B6)
Sucnr1+/-
Sucnr1-/-
K
T. rainier:
L
ILC2 / MLN (x10^5)
M
Eos / MLN (x10^4)
p = .09

**Figure 4. Immune sensing of *T. rainier* but not *N. brasiliensis* requires SUCNR1**

**(A)** Concentration of indicated molecules measured in *N. brasiliensis* excretory-secretory product (NES) or media control by NMR. **(B)** Representative calcium fluxes in wild-type (B6) or SUCNR1-transduced MEFs treated as indicated. **(C)** Quantification of B. **(D)** Concentrations of indicated molecules measured in *T. rainier* conditioned media or media alone by NMR. **(E-I)** Mice of indicated genotypes were infected with *N. brasiliensis.* **(E)** Tuft cell quantification in the distal (last 10 cm) small intestine (SI), and **(F)** total worm burden at indicated times. **(G)** Tuft cell quantification in the distal SI 7 d post infection. **(H)** Tuft cell quantification in the distal SI and **(I)** total worm burden 8 d post infection. **(J-M)** Mice of indicated genotypes were colonized with *T. rainier* for 7 d or left untreated. **(J)** Representative images of distal SI. DCLK1 marks tuft cells. Scale bar = 50 µm. **(K)** Quantification of tuft cells in J. **(L-M)** MLN analyzed by flow cytometry to quantify **(L)** ILC2s and **(M)** eosinophils. A-B, D show representative data from at least two independent experiments. In C, each symbol represents one technical replicate. In G-I, K-M each symbol represents one mouse from at least two pooled experiments. In E-F each symbol represents the average of 3-10 mice from three pooled experiments. *, $p < 0.05$; **, $p < 0.01$; ***, $p < 0.001$ by one-way ANOVA (H-I, K-M) with comparison to Wt(B6) control, by Mann-Whitney (G), or using multiple *t*-tests (C, E, F). n.s., not significant. Graphs depict mean + SEM.

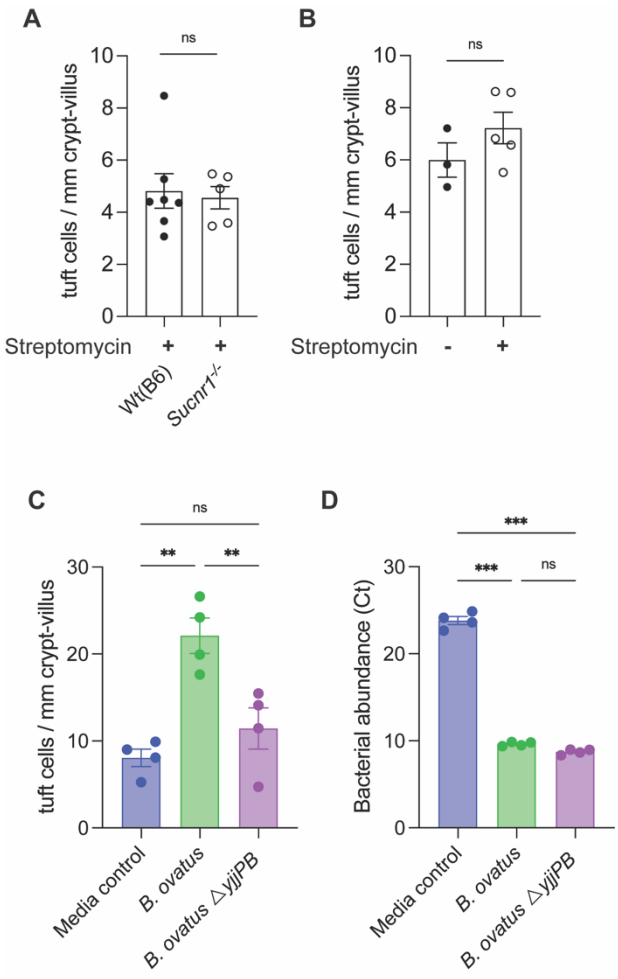


**Figure 5. Bacterial succinate can activate tuft-ILC2 circuit**

**(A)** Tuft cell quantification in the distal SI of streptomycin treated mice, bred in University of Washington vivarium. **(B)** Tuft cell quantification in the distal SI of B6 mice purchased from Charles River laboratories, with or without streptomycin treatment. (**C and D**) Germ-free B6 mice were mono-colonized with wild-type *B. ovatus* or *B. ovatus* ΔyjjPB mutant. (C) Tuft cell quantification in the distal 5cm of the SI. (D) Bacterial load in the cecal content quantified by 16S qPCR. In A-D each symbol represents one mouse from at (A) two pooled or (B-D) one experiment. *, $p < 0.05$; **, $p < 0.01$; ***, $p < 0.001$ by Mann-Whitney (A-B) or one-way ANOVA (C-D). n.s., not significant. Graphs depict mean +/- SEM.

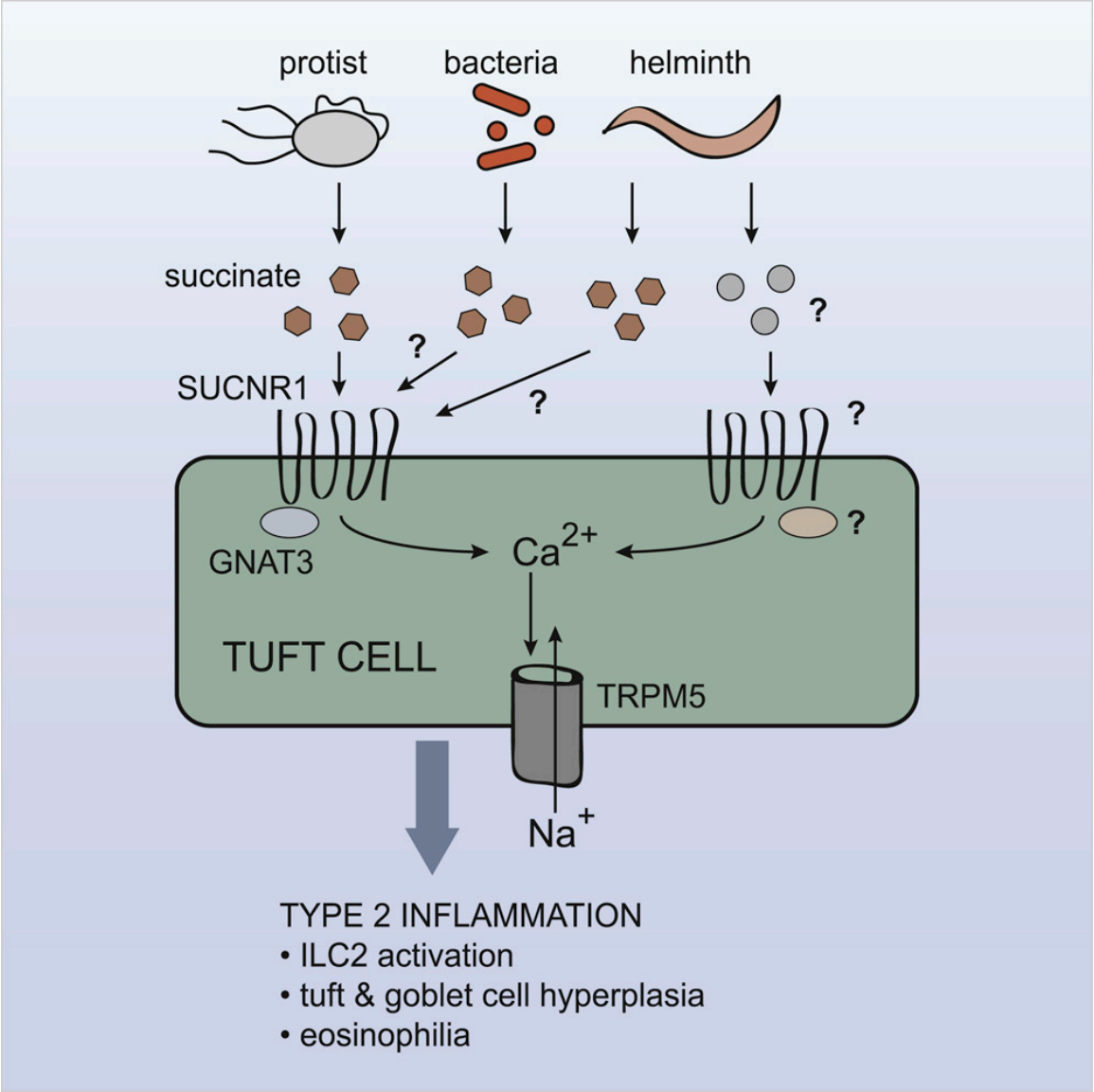


**Figure 6. Proposed model for activation of intestinal tuft cells by succinate.** Tritrichomonad protists that colonize the cecum and distal small intestine secrete succinate as a metabolite. This signals through the receptor SUCNR1, expressed on tuft cells, resulting in an intracellular calcium flux, opening of the TRPM5 cation channel, and release of mediators that initiate a type 2 immune response.

## 2.7 Supplemental Figures

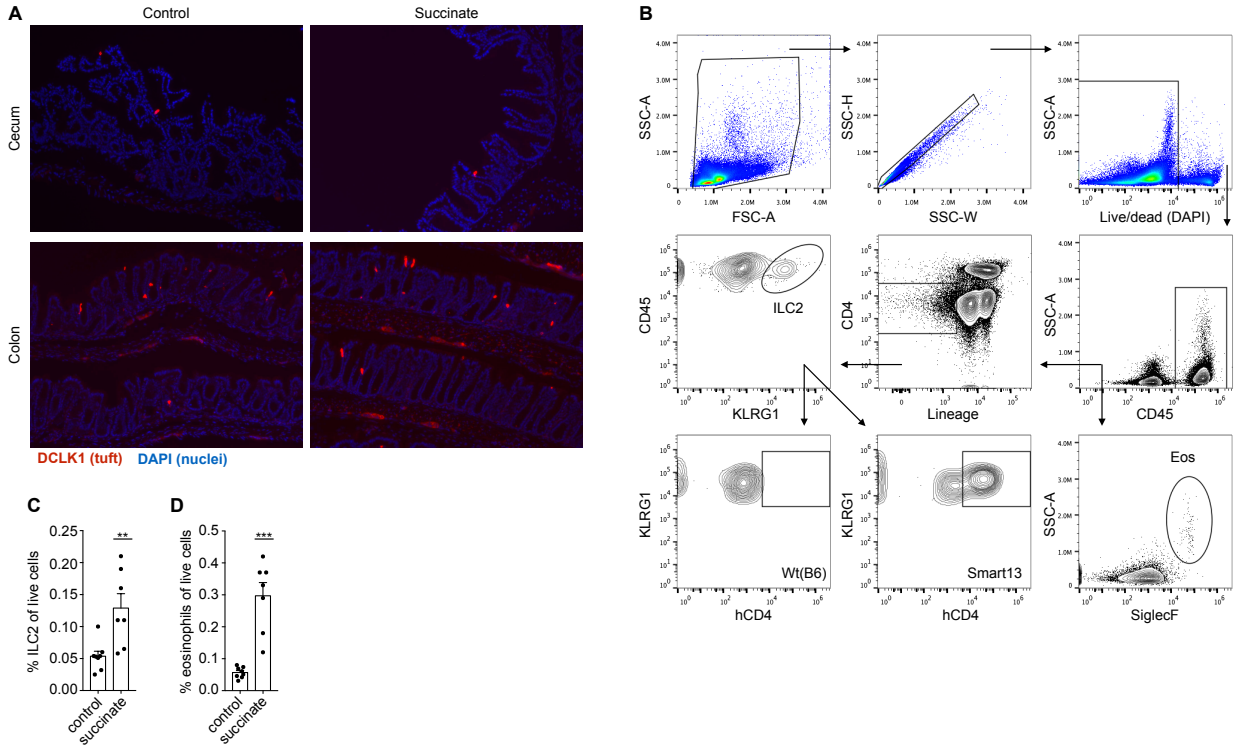


**Figure S1. Related to Figure 2**

**(A)** Indicated tissues from control or succinate-treated (150 mM; 7 days) wild-type mice were stained for tuft cells (anti-DCLK1; red) and nuclei (DAPI; blue). **(B)** Gating strategy for identification of ILC2s and eosinophils in the mesenteric lymph nodes (MLN). IL-13 production was assessed by staining for human CD4 in Smart13 reporter mice. **(C-D)** MLN from control or succinate-treated (150 mM; 7 days) wild-type mice were analyzed by flow cytometry to assess the frequency of ILC2s **(C)** and eosinophils **(D)** among all live cells. Data in A-B are representative of at least three experiments. Data in C-D are pooled from two experiments and bar graphs depict mean + SEM. Each symbol represents an individual mouse.**, $p < 0.01$; ***, $p < 0.001$ by Mann-Whitney.

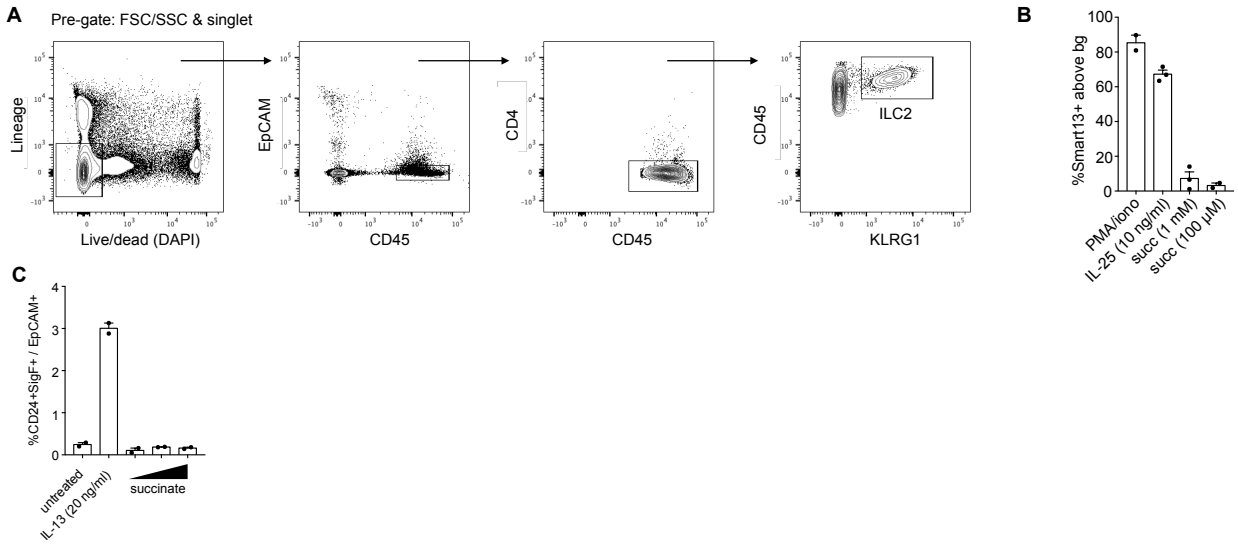


**Figure S2. Related to Figure 3**

**(A)** Gating strategy to identify ILC2s in the lamina propria of the small intestine. **(B)** ILC2s were stimulated in vitro as indicated for 6 hours and IL-13 production was quantified by flow cytometry using Smart13 reporter expression. **(C)** Epithelial organoids from murine small intestine were cultured for 7 days under indicated conditions. Succinate concentrations = 100 µM, 1mM, and 10 mM. Tuft cell frequency (CD24+SigF+EpCAM+ cells) was quantified by flow cytometry. Data are representative of one (B) or two (A, C) experiments. Bar graphs depict mean + SEM. Each symbol represents a technical replicate (B-C).

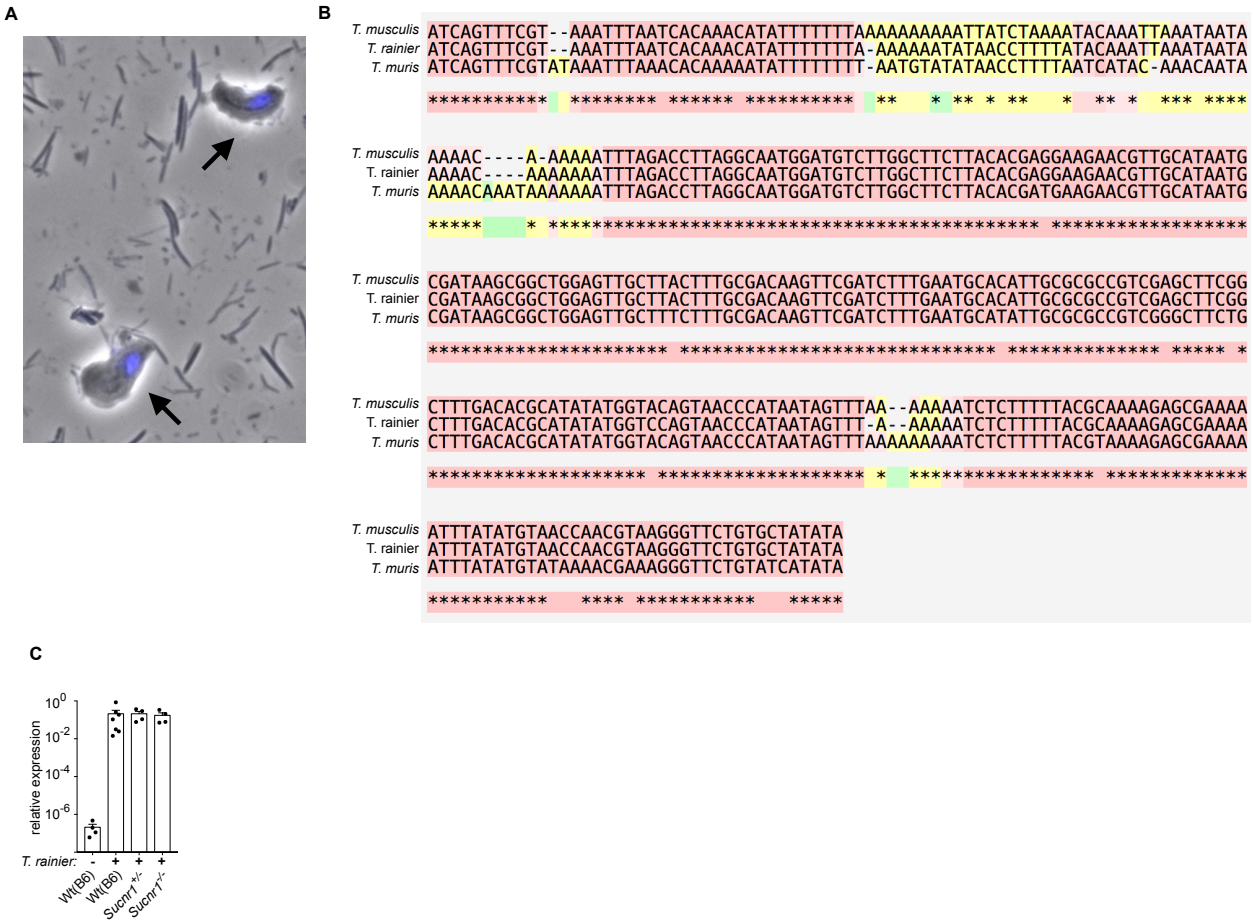


**Figure S3. Related to Figure 4**

**(A)** Representative images of *T. rainier* (arrows) with DAPI (blue) staining of nuclei. **(B)** Alignment of internal transcribed spacer sequence of *T. rainier* with published sequences for *T. muris* and *T. musculis*. **(C)** *Tritrichomonas* colonization of indicated mice was quantified by qPCR using DNA generated from cecal contents. Data are representative of three (B) or two (A) experiments or pooled (C) from two experiments. Bar graphs depict mean + SEM. Each symbol represents an individual mouse.

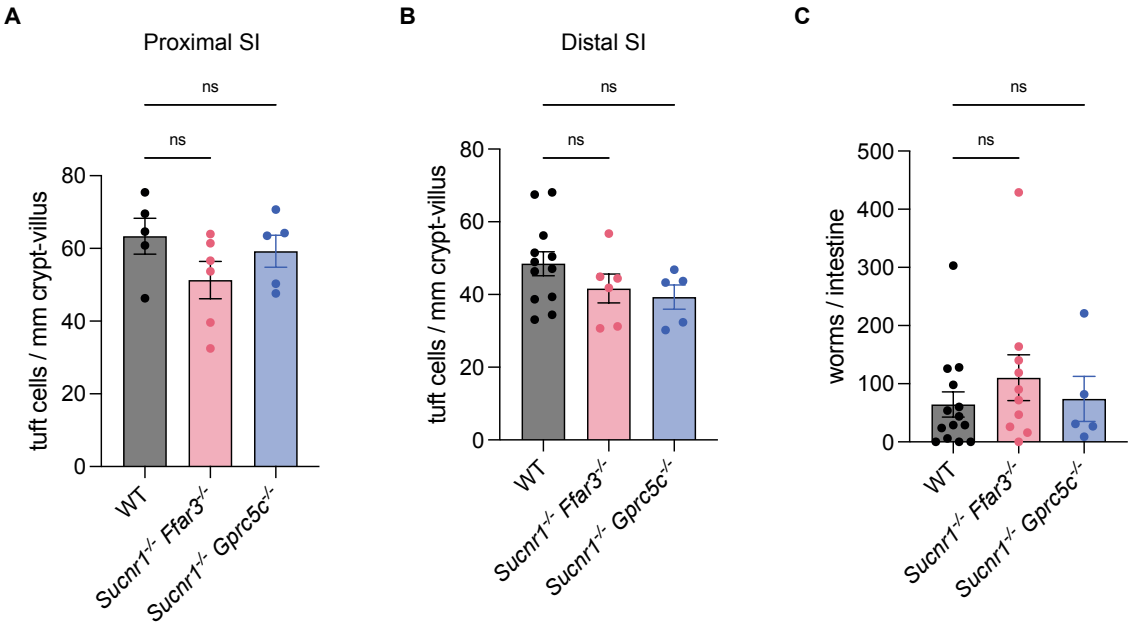


**Figure S4. Related to Figure 4**

(**A** to **C**) Mice of indicated genotypes were infected with *N. brasiliensis.* Tuft cell quantification in the (**A**) proximal SI (first 10cm) or (**B**) distal SI (last 10 cm) and **(C)** total worm burden 7 days post infection. Data are pooled from two or more experiments. Bar graphs depict mean +/- SEM. Each symbol represents an individual mouse.

| Genes | | |
|---|---|---|
| *Tek* | *Srpx2* | *Runx1* |
| *Ptpn14* | *Stox2* | *Hpgds* |
| *Kcnq4* | *Alox5ap* | *Ptpn6* |
| *Gpr64* | *Pou2f3* | *Rgs22* |
| *Ahnak2* | *Spib* | *Map2* |
| *Pnpla3* | *Sh2d7* | *Fes* |
| *Mn1* | *Ildr1* | *Ccdc28b* |
| *Dgki* | *Avil* | *Kctd15* |
| *Hmx3* | *Pygl* | *Samd14* |
| *Dscaml1* | *Gas7* | *Plcg2* |
| *Fyb* | *Ackr4* | *Hck* |
| *Il25* | *Neurl1a* | *Ptprc* |
| *Dclk1* | *Greb1l* | *Gfi1b* |
| *Pik3cg* | *Sh2d6* | *Il17rb* |
| *Alox5* | *Eml6* | *Reep5* |
| *Rdx* | *Kirrel3* | *Plekhs1* |
| *Pstpip1* | *Ltc4s* | *Cacna2d2* |
| *Trpm5* | *Slfn5* | *Cmtm5* |
| *Nrgn* | *Arhgap4* | *Ptgs1* |
| *Gnat3* | *1810046K07Rik* | *Lrmp* |
| *Rgs13* | *Limd2* | *Nebl* |
| *Clec4a1* | *Cd300lf* | *Bmx* |
| *Pik3r5* | *Itpr2* | |
| *Nxpe2* | *Krt222* | |
| *Ccdc129* | *Pea15a* | |
| *Chat* | *Strip2* | |
| *Sptb* | *Dmxl2* | |
| *Ly6g6f* | *Adora1* | |
| *Vav1* | *Rbpms* | |
| *Hap1* | *Slc41a3* | |
| *Plcb2* | *Col9a3* | |
| *Gcnt1* | *Cyp2f2* | |
| *Inpp5d* | *Fam49a* | |

**Table 1. The transcriptional tuft cell signature (Related to Figure 1C)**

# Chapter 3

Genetic mapping reveals *Pou2af2*-dependent tuning of tuft cell differentiation and intestinal type 2 immunity

This chapter is adapted from the following publication:

Marija S. Nadjsombati, Natalie Niepoth, Lily M. Webeck, Elizabeth A. Kennedy, Danielle L. Jones, Megan T. Baldridge, Andres Bendesky, Jakob von Moltke. Genetic mapping reveals *Pou2af2*-dependent tuning of tuft cell differentiation and intestinal type 2 immunity. Biorxiv. 2022. https://doi.org/10.1101/2022.10.19.512785

## 3.1 Introduction

Dynamic regulation of the small intestinal epithelium facilitates both nutrient absorption and immune defense. During helminth infection or colonization with certain protists, epithelial tuft cells initiate type 2 immunity by activating group 2 innate lymphoid cells (ILC2s) in a feed-forward circuit that results in extensive epithelial remodeling*(19–21)*. However, how epithelial progenitors become tuft cells remains poorly understood.

The identification of succinate as an intestinal tuft cell ligand provided a new opportunity to study the kinetics and regulation of the tuft-ILC2 circuit in a controlled way*(29, 66, 67)*. Helminth infection extensively activates the tuft-ILC2 circuit, but these model organisms come with their own caveats that can introduce complex variables. For instance, the complicated life cycle of *Nippostrongylus brasiliensis (Nb)*, which first traffics through the skin, blood stream and lungs before migrating to the small intestine (SI), means the timing of when worms arrive in the SI can vary mouse to mouse, experiment to experiment*(82)*. With succinate, we have the opportunity to activate the tuft-ILC2 circuit precisely and acutely in order to study the dynamics of tuft cell activation and hyperplasia.

Since the identification of the tuft-ILC2 circuit, the majority of studies have been conducted using mice on a C57BL/6J background given the abundance and availability of genetic knockouts on this background. However, studying different inbred strains of mice has provided insight into mechanisms of type 2 immunity. In particular, seminal studies using *Leishmania major* infection established the notion that $CD4^+$ T helper cell responses in Balb/cJ (Balb) mice are type 2 biased, while C57BL/6J (B6) mice are type 1 biased*(83, 84)*. Such biases have similarly been noted in the SI, where Balb mice clear some helminth infections, such as

*Heligmosomoides polygyrus* (*Hp)* and *Strongyloides ratti*, more efficiently than B6 mice*(85, 86)*. There are many proposed mechanisms for these differences, including intestinal microbiota composition, regulatory T cell function, and strength of T helper 2 cell (Th2) activation*(85, 87, 88)*. Some studies have used genetic mapping to identify loci associated with strain-specific immune responses, but no single gene is responsible for the observed phenotypes*(89, 90)*. Likely these differences arise from a complex network of genetic and environmental differences all contributing to the phenotypic outcomes. Whether tuft cells and the innate SI tuft-ILC2 circuit are differentially regulated across mouse strains has not been examined.

Given the historical paradigm that Balb mice are more type 2 skewed, at least in terms of adaptive immune response, we set out to address how the tuft-ILC2 circuit is regulated in Balb mice. We find that Balb mice have fewer tuft cells than B6 mice in many tissues and fail to activate the tuft-ILC2 circuit following succinate treatment in the SI. These differences are determined by a single genetic locus that regulates tuft cell differentiation and tunes the sensitivity and kinetics of innate type 2 immunity in the SI. Taken together, we exploited differences between inbred mouse strains to identify a novel mechanism that regulates tuft cell differentiation and sets a threshold for tuft-ILC2 circuit activation.

## 3.2 Results

### Balb mice have fewer intestinal tuft cells and do not respond to succinate

Given that Balb mice have been described as "type 2 skewed", but nearly all tuft cell studies have been performed in B6 mice, we set out to compare tuft cell frequency and function between B6 and Balb mice. Balb mice were previously reported to have fewer tuft cells than B6 in the distal SI*(91)*, and we found this discrepancy extended throughout the intestinal tract (Figures 1A, 1B and S1A). Balb mice also had a trend towards fewer tuft cells in the trachea, but equivalent frequencies of tuft cells in the thymus by flow cytometry (Figures 1A-C).

Next, we tested the tuft-ILC2 circuit in Balb mice. As previously described*(29, 66, 67)*, B6 mice given 150mM sodium succinate in the drinking water for 7 days developed robust tuft cell hyperplasia in the distal SI (Figure 1D). Balb mice given succinate drinking water failed to induce tuft cell hyperplasia, even if succinate was administered for longer (14 days) or at a higher dose (250mM for 7 days). We tested whether the defect in succinate-induced hyperplasia in Balb mice was microbiome dependent by cross-fostering Balb and B6 litters. At adulthood, Balb mice raised by a B6 dam still failed to develop tuft cell hyperplasia following succinate administration (Figure 1E). In fact, even after succinate administration, the tuft cell frequency in Balb mice raised by B6 dams remained below the baseline B6 level. Conversely, B6 mice developed hyperplasia regardless of dam. We therefore conclude that the microbiome is not responsible for the homeostatic and induced frequency of tuft cells in B6 and Balb mice.

To test whether responses to succinate are restored when the starting tuft cell number in Balb mice is elevated, we 'primed' the tuft-ILC2 circuit of Balb mice by giving recombinant IL-25 (rIL-25) to directly induce IL-13 release from ILC2s and increase tuft cell frequency (Figure

1F). When rIL-25 treatment was followed by a week of regular drinking water, tuft cell frequency returned towards baseline. However, mice pre-treated with rIL-25 and then given succinate for 7 days readily developed tuft cell hyperplasia. Similar results were achieved if IL-4 complex (IL-4c), which recapitulates the signaling effects of IL-13 on stem cells, was administered to increase tuft cell frequency prior to succinate administration (Figure 1G).

Although we have never noted sex-dependent differences in tuft cell frequency or succinate responsiveness in B6 mice (data not shown), some male Balb mice given IL-4c still failed to respond to succinate (Figure S1B). The effect of sex on tuft cells themselves is unknown, but studies of airway ILC2s have demonstrated androgen-dependent reductions in ILC2 activation*(92–96)*. We hypothesize that SILP ILC2s are similarly impacted, but that this is only revealed in "sensitized" contexts where ILC2s are weakly activated. Nonetheless, these priming experiments demonstrate that the tuft-ILC2 circuit is intact but hyporesponsive in Balb mice.

**ILC2s are abundant and functional in Balb mice**

The tuft-ILC2 circuit contains three cellular components: mature tuft cells, ILC2s, and epithelial stem cells. To determine which component accounts for the Balb defect, we began by assessing the number, phenotype and cytokine production of ILC2s. Compared to B6 mice, unmanipulated Balb mice actually had more ILC2s ($CD45^+$, $Lin^-$, $GATA3^+$) in the distal SILP (Figures 2A and B and S2A). The expression of the IL-25 receptor subunit IL-17RB was equivalent between the two strains, while CD44 and KLRG1, markers of lymphocyte activation, were both reduced on Balb ILC2s (Figures 2C-E). We previously noted similarly-reduced KLRG1 expression

on SILP ILC2s from unmanipulated *Tritrichomonas*-free B6.*Il25*$^{-/-}$ and B6.*Trpm5*$^{-/-}$ mice, suggesting tonic signaling from tuft cells to ILC2s in the absence of known tuft cell ligands *(53)*. Therefore, by analogy to these mice, the low frequency of tuft cells in Balb mice likely leads to loss of tonic signaling and accounts for the lower KLRG1 expression. As before, and consistent with studies in the lung *(96)*, we noted sex-dependent differences in KLRG1, but in all cases the Balb ILC2s had lower KLRG1 expression than sex-matched B6 ILC2s (Figure 2E). Male ILC2s in the SILP have higher expression of KLRG1, yet develop less robust tuft cell hyperplasia in some assays (Figures 1G and S1B). While counterintuitive, both findings are consistent with studies in the lung, where male ILC2s have higher KLRG1 on a population level, yet are less activated following stimulation*(92, 96)*. Finally, there was no difference in the number of GATA3$^{+}$ Th2 cells or eosinophils in the SILP of Balb and B6 mice (Figures S2A-C).

To test the functional capacity of Balb ILC2s, we sorted ILC2s from the SILP of unmanipulated mice and cultured them with rIL-25 with or without leukotriene $C_4$ ($LTC_4$). B6 and Balb ILC2s made moderate but equivalent amounts of IL-5 and IL-13 following 6 hours of rIL-25 treatment (Figures 2F and S2D). Cytokine production was greatly enhanced by the addition of $LTC_4$, but IL-13 and IL-5 secretion was still equivalent between the two strains. Additionally, B6 and Balb ILC2s had equivalent expression of the proliferation marker Ki67 two days post stimulation (Figure S2E). No sex differences were observed in this assay. Overall, compared to B6, Balb ILC2s are more abundant and equally capable of responding to tuft cell signals in the SILP. The failure of Balb mice to activate the tuft-ILC2 circuit in response to succinate is therefore likely ILC2-independent.

**The Balb tuft cell defect is epithelium intrinsic**

Next, we used organoids to determine whether the Balb tuft cell defect was epithelium intrinsic or required signals from surrounding stromal or immune cells. Organoid cultures contain only epithelial cells and recapitulate epithelial differentiation, including IL-13-induced tuft cell hyperplasia*(19–21)*. Tuft cell frequency was significantly lower in untreated Balb organoids compared to B6 organoids after both 1 and 4 weeks in culture, demonstrating that the tuft cell defect is epithelium intrinsic and stably maintained *ex vivo* (Figures 3A, 3B and S3A). Recombinant IL-13 (rIL-13) induced tuft cell hyperplasia in organoids from both strains; however, Balb organoids had a lower frequency of tuft cells when compared to B6 organoids, particularly when cultured 4 weeks before rIL-13 treatment (Figure 3C). Given that Balb organoids started from a lower baseline, the fold increase in tuft cells induced by rIL-13 was greater in Balb organoids, suggesting their defect predominantly impacts IL-13-independent tuft cell differentiation (Figure S3B).

To assess if the Balb defect is specific to tuft cells, we used qPCR to quantify all secretory cell lineages in organoids after 2 weeks in culture. Untreated Balb organoids had significantly lower expression of the tuft cell gene *Pou2f3,* and a strong trend toward less *Dclk1* (Figure 3D). Expression of the goblet cell genes *Spdef* and *Muc2*, the Paneth cell marker *Lyz1* and the enteroendocrine cell marker *Chga* was equivalent between Balb and B6 organoids (Figure 3D). Using this transcriptional measure, there was no difference between rIL-13 treated Balb and B6 organoids for any gene, including tuft cell markers (Figure 3E). The discrepancies with Figure 3C suggest post-transcriptional regulation of tuft cell differentiation, but also further support the conclusion that the Balb defect predominantly impacts homeostatic tuft cell differentiation.

Together, these data demonstrate a tuft cell-specific and epithelium-intrinsic reduction in Balb mice.

**Differential tuft cell frequency between B6 and Balb mice is genetically regulated**

We next hypothesized that the Balb and B6 differences in tuft cell frequency and succinate responsiveness are determined by genetic differences between the two strains. To test heritability of succinate responsiveness, we generated Balb x B6 $F_1$ and $F_2$ mice and measured tuft cell frequency after succinate treatment. In this context we again noted reduced succinate responses in male mice (Figures S4A and S4B), so we assessed succinate response rates using female $F_1$ and $F_2$ mice. $F_1$ mice all developed tuft cell hyperplasia when treated with succinate, but there were both responsive and nonresponsive mice in the $F_2$ generation (Figure 4A). Using a cutoff of 13 tuft cells/mm crypt villus, which is just above the B6 baseline, 80% of $F_2$ female mice responded to succinate. The frequency of succinate responsive $F_1$ and $F_2$ mice is therefore consistent with a single recessive locus determining tuft cell differences between Balb and B6 mice.

Combining high-density single nucleotide polymorphism (SNP) genotyping with phenotypes of $F_2$ mice is a powerful technique for identification of quantitative trait loci (QTL) that explain phenotypic variation. We therefore employed low-coverage whole genome sequencing coupled to imputation to genotype B6 x Balb F2 mice *(97)*. In brief, Tn5 transposase was used to randomly insert DNA tags into genomic DNA from 84 B6 x Balb $F_2$ mice, here analyzing both male and female mice. Tag-adjacent genomic sequences were obtained by next-generation sequencing and assigned to B6 and Balb genomes to provide whole-genome

genotyping at higher resolution than traditional SNP-based arrays. We then combined these genotypes with the succinate-induced tuft cell frequency of each $F_2$ mouse and performed QTL mapping. We detected a dominant QTL on chromosome 9 (Chr9), with a peak at 50,857,809 bp and 1.5 LOD support interval from 45.49 Mb to 53.03 Mb (Figures 4B and 4C). Sex was a significant additive covariate, but the Chr9 locus was dominant in both sexes (Figures S4C). An effect plot at the peak QTL location revealed a clear gene dosage dependent response to succinate (Figure 4D), and the Chr9 locus explained 53% of the variance in succinate response in this 84-mouse $F_2$ cohort. Thus, a single locus accounts for a majority of the difference in succinate-induced tuft cells between B6 and Balb mice.

To begin fine mapping and to generate congenic mice in which only the Chr9 locus is B6-derived, we initiated a series of backcrosses. B6 x Balb $F_1$ mice were crossed to wild-type Balb mice and resulting offspring were again crossed to wild-type Balb mice for 6 to 8 generations. In each generation, we used low-coverage whole genome sequencing coupled to imputation to look for crossover events that reduced the size of the Chr9 locus and to identify mice that had lost B6 DNA in other regions (a process sometimes called speed congenics). This process generated 4 strains of congenic mice carrying distinct B6-derived portions of the Chr9 QTL and homozygous for Balb DNA at all other locations (Figure 4E).

Congenic strains 2-4 had B6-equivalent levels of tuft cells in the distal SI at baseline and developed tuft cell hyperplasia when succinate treated (Figures 4F and 4H). Tuft cell frequency was also increased in proximal SI, colon, and trachea of Strain 3 mice compared to Balb (Figures S4D-F). Strain 1 had Balb-equivalent levels of tuft cells at baseline and did not develop tuft cell hyperplasia after succinate treatment (Figures 4F-H). Strain 1 contains B6 sequence from 33-

50Mb, indicating the relevant locus in not within this region. Instead, the locus controlling baseline tuft cell number and succinate responsiveness is in the 50-67Mb region shared by Strains 2, 3, and 4. In sum, the 50-67 Mb region of Chr9 explains most of the differential succinate sensing in B6 and Balb mice, and when placed in a Balb genome restores B6 levels of homeostatic tuft cells and succinate responsiveness in the distal SI.

**RNA sequencing identifies *1810046K07Rik / Pou2af2* as a gene of interest**

Genetic variation within species often shapes traits by either changing the expression of genes or the amino acid sequence of the proteins they encode. To discover the gene(s) mediating the difference, we systematically compared the congenic interval (Chr9:50-67 Mb) in B6 and Balb mice. We found that the interval contains ~3170 genetic variants that distinguish B6 and Balb genomes. Many of these variants are in intergenic regions or associated with genes that are not expressed in the SI epithelium, but even focusing on the 1.5 LOD confidence interval and on variants predicted to alter protein sequence, it was difficult to identify candidates for further investigation.

To assess gene expression and leverage the congenic strains, we sequenced the mRNA of tuft cells ($CD45^-$ $EPCAM^+$ $SigF^+$ $CD24^+$) sorted from the distal SI of B6, Balb, and congenic Strain 3 mice and identified differentially expressed genes (DEGs; log2FC > 1, FDR < .05) (Figures S5A-C). Hierarchical clustering of all DEGs revealed 3 expression modules (Figures 5A). Within each module, we looked for genes that were part of the SI tuft cell signature and/or located in the Chr9 locus *(29)* (Table 1). Module 1 was comprised of genes more highly expressed in Balb and congenic than B6. One gene, *Hebp1*, was a tuft cell signature gene, but is not located on

Chr9. *Gm7293,* encoded at 51.5 Mb on Chr9 was also in this module. Module 2 contained a subset of 31 genes enriched selectively in Balb samples. Many of these genes were Paneth cell related, such as lysozyme and defensins, and likely represented low-level contamination by $CD24^{+}$ Paneth cells, which is amplified in Balb samples due to the rarity of tuft cells in these mice. None of these genes are located on Chr9. Module 3 contained genes more highly expressed by B6 tuft cells compared to congenic or Balb. There were several tuft cell signature genes within this module, including *Sucnr1* (Figure 5B). *Sucnr1* is encoded on Chr3, is unlikely to directly impact tuft cell differentiation, and was not upregulated in congenic Strain 3 tuft cells, so it does not explain baseline differences in tuft cell frequency. Reduced *Sucnr1* expression could, however, contribute to the failure of Balb mice to sense succinate, yet the effect of the Chr9 locus in Strain 3 mice was enough to restore succinate sensing despite Balb-equivalent *Sucnr1* expression (Figure 4H).

To focus on transcriptional regulation revealed by the congenic mice, we performed a pair-wise comparison between Balb and Strain 3, but identified only 5 DEGs, and none are encoded on Chr9 (Figure 5C). Since genome-wide DEG analysis did not identify any candidate genes, we specifically compared genes from the Chr9 locus (50-67Mb) in B6 and Balb mice (Figure 5D). *Gm7293* again appeared as highly upregulated in Balb mice, while *1810046K07Rik* was the top downregulated gene. *1810046K07Rik* also stood out as the only tuft cell signature gene that was downregulated in Balb mice but rescued in Strain 3 congenic mice, while *Gm7293* expression was unchanged between Balb and Strain 3 (Figures 5E-5G).

*1810046K07Rik* and another gene, *Colca2*, were recently found to encode co-factors required for the function of POU2F3*(54)*. These genes, and the proteins they encode, were

respectively renamed *Pou2af2/*OCA-T1 and *Pou2af3/*OCA-T2 and are located in a gene cluster together with *Pou2af1/*OCA-B. OCA-B is a co-factor for POU2F1 and POU2F2, transcription factors closely related to POU2F3*(98)*. This gene cluster is located at 51.2 Mb on Chr9, very close to the QTL peak (50.8 Mb).

**Differential *Pou2af2* isoform expression in intestinal crypts**

*Pou2af2*$^{-/-}$ mice were reported to lack tuft cells in the SI and trachea, but have normal tuft cell numbers in the thymus, a distribution similar to our findings in Balb mice*(54)*. *Pou2af3*$^{-/-}$ mice have not yet been generated, but *Pou2af3* expression is low or undetectable in RNA sequencing of SI tuft cells, and it is not included in the SI tuft cell signature*(29)*. We therefore focused our attention on identifying a mechanism by which *Pou2af2* might regulate differential tuft cell phenotypes in B6 and Balb mice.

Because *Pou2af2* is currently annotated with two transcriptional start sites, we used 5' Rapid Amplification of cDNA Ends (RACE) for unbiased amplification of *Pou2af2* transcripts. Since the few mature tuft cells that emerge in Balb mice may not represent events that occur during differentiation, we used RNA from distal SI crypts to capture tuft cell progenitor cells. A primer designed to capture all annotated isoforms produced ~550bp and ~450bp bands in B6 samples. Balb samples lacked the 550bp band, but contained the 450bp band and a faint ~100bp band (Figure 6A). Cloning and sequencing of these bands revealed that the 100bp band resulted from non-specific amplification of 18S RNA and the 550bp band corresponded to the full-length *Pou2af2* isoform (Figure 6B). The 450bp band present in both Balb and B6 samples, however, corresponded to an isoform not listed in the current *Mus musculus* genome release

(GRCm39) and did not appear to use either of the annotated transcriptional start sites. This isoform begins 26bp downstream of the annotated transcription start site in exon 2 of the full-length isoform. The first available translation start site in this isoform gives rise to a truncated protein that lacks a 20 amino acid N-terminal motif shared by OCA-T1, OCA-T2, and OCA-B, and required for binding to their target transcription factors (i.e. POU2F3 or POU2F1/2)*(54, 99)*. We did not find evidence that any of the other annotated isoforms were expressed in SI crypts.

The results of the 5' RACE allowed us to design qPCR primers to quantify the abundance of the full-length transcript only and of all transcripts combined. No primers could be designed for just the short isoform, as it shares 100% homology with the full-length isoform. Due to the lack of tuft cells in Balb mice, Balb SI crypts had significantly lower expression of *Pou2f3* and both isoforms of *Pou2af2* than B6 crypts (Figures 6C and 6D). Within each sample, however, the portion of total *Pou2af2* transcript accounted for by full-length transcript is also significantly lower in Balb crypts compared to B6 (Figure 6D). Crypts from congenic strain 1 phenocopy Balb crypts with about 10% of total *Pou2af2* transcript being the full-length isoform. Congenic strains 2,3 and 4 express 70-80% full-length isoform, similar to B6 (Figure 6D).

We also used qPCR to analyze *Pou2af3* expression and isoform usage. *Pou2af3* has a full-length and a short isoform that each contain unique portions, allowing us to design isoform-specific primers. As with *Pou2af2,* the short isoform of *Pou2af3* lacks the POU2F3 binding domain. As expected, SI crypt expression of *Pou2af3* is lower than *Pou2af2* regardless of strain and lower in Balb and Strain 1 than B6 and Strain 2-4 (Figure S6A). The full-length isoform in particular was nearly undetectable in all mice. Nonetheless, Balb and Strain 1 had a decreased ratio of full-length to total *Pou2af3* and increased ratio of short isoform to total *Pou2af3*

compared to B6, Strain 2, 3 and 4 (Figures S6B and S6C). Finally, as in the organoids, there was no difference in expression of genes for other lineages of epithelial cells between B6 and Balb crypts, confirming that the Balb defect is tuft cell specific (Figure S6D).

To understand if the differences between B6 and Balb mice were generalizable, we examined baseline tuft cells and succinate sensing in additional strains of mice. Succinate responsiveness was highly variable in Swiss Webster mice, an outbred strain, suggesting genetic diversity can lead to diverse succinate responses (Figure S6E). Testing inbred strains, we found FVB/NJ and C3H/HeJ strains had very low numbers of tuft cells at baseline and did not develop tuft cell hyperplasia following succinate treatment, phenocopying Balb (Figure 6E). On the other hand, 129S1/SvImJ mice had close to B6 levels of tuft cells at baseline and upon succinate treatment developed tuft cell hyperplasia in the distal SI. We measured *Pou2af2* isoform expression in distal SI crypts from these strains. The ratio of full-length isoform to total *Pou2af2* expression corresponded with baseline tuft cell number and succinate phenotype, with 129S1/SvImJ mice having a high ratio, similar to B6, and FVB/NJ and C3H/HeJ mice having a low ratio, similar to Balb (Figure 6F). Although total *Pou2af3* expression was again lower than *Pou2af2*, the ratio of short and long isoforms followed the same trend as *Pou2af2*. (Figure S6F). It appears, therefore, that *Pou2af2* and *Pou2af3* are somehow coregulated, but given the higher expression of *Pou2af2* and the similarities between *Pou2af2*$^{-/-}$ and Balb mice, we propose that the production of fewer mature tuft cells in Balb and Strain 1 mice results from a lack of functional OCA-T1 expression and therefore a failure to induce POU2F3-dependent gene transcription.

**Analysis of genetic variants in *Pou2af2* locus**

Analysis of genetic variants in the *Pou2af2* locus revealed 11 single nucleotide polymorphisms (SNPs) that distinguish B6 and Balb mice, several of which may be of interest (Figure 6B). First is rs29595736, located in exon 2 of the full-length isoform and just upstream of the transcriptional start site of the short isoform (Figure S6G). This SNP is actually annotated as a splice acceptor variant, but that is based on annotation of an isoform that we did not detect in epithelial crypts. Instead, rs29595736 leads to an arginine (B6) to glycine (Balb) transition at amino acid 6 of full-length OCA-T1, which is just outside the POU2F3 binding site. Although we cannot rule out a change in protein function due to this SNP, its positioning just upstream of a transcriptional start site is more interesting from the perspective of isoform abundance. That said, 129S1/SvImJ mice, which phenocopy B6 mice, carry the Balb allele of rs29595736. Three other SNPs of interest are rs336266049, rs29736233, and rs37184010 (Figure 6B, marked in red). These SNPs are all intronic, but they correlate with the tuft cell phenotypes of inbred strains; B6 and 129S1/SvImJ encode the same nucleotide, while Balb, FVB/NJ and C3H/HeJ all encode a different nucleotide. More work is needed to understand whether these and/or more distal SNPs impact isoform expression or tuft cell differentiation.

**Tuft cell abundance tunes sensitivity and kinetics of the tuft-ILC2 circuit**

To understand the physiologic impact of low baseline tuft cell frequency and the role of *Pou2af2*, we used protists and helminths to activate the tuft-ILC2 circuit. While acute administration of succinate failed to activate the tuft-ILC2 circuit in Balb mice, *Tritrichomonas* protists chronically colonize mice from weaning and are perhaps more immunostimulatory than

succinate alone. Nonetheless, adult Balb mice colonized with *Tritrichomonas* from birth failed to induce tuft cell hyperplasia. Responses in congenic Strain 3 mice were more variable, with only some mice developing hyperplasia despite elevated baseline tuft cell frequency in all mice. The lower expression of *Sucnr1* (Figure 5B) and an unexplained ~60% lower protist burden (Figure 7B) in Strain 3 mice likely kept them at or below the threshold for tuft-ILC2 circuit activation.

Next, we infected Balb and B6 mice with the helminth *Nippostrongylus brasiliensis* (*Nb*), an acute infection model that strongly activates the tuft-ILC2 circuit and is cleared within 7-8 days in B6 mice. Over the course of infection, Balb mice developed tuft cell hyperplasia, but with delayed kinetics compared to B6 (Figures 7C and S7A). Balb mice had 50% higher worm burden on day 5 post infection, but complete worm clearance was not delayed (Figure 7D). Therefore, although Balb mice start with fewer tuft cells, tuft-ILC2 circuit activation reaches a threshold required for *Nb* clearance and/or other mechanisms, such as a stronger adaptive Th2 responses, compensate for innate defects in Balb mice.

*Heligmosomoides polygyrus* (*Hp*) provides a model of long-term SI helminth infection, with clearance taking 6 weeks or more *(100)*. As mentioned previously, Balb mice clear *Hp* infection more rapidly than B6, likely due to a stronger adaptive type 2 immune response *(86, 101, 102)*, but the differences during early infection have not been well characterized. We wondered whether Strain 3 mice could benefit from both enhanced B6-like innate responses and a stronger Balb-like Th2 response. During primary infection, all three strains had equivalent tuft cell hyperplasia by day 12, with Strain 3 mice trending towards having more tuft cells compared to both B6 and Balb (Figure 7E). However, worm fecundity (eggs laid per worm),

worm burden, and total fecal egg counts trended lower in both B6 and Strain 3 mice, suggesting an earlier onset of protective immunity (Figures 7F, 7G and S7B). To test immune memory, we infected mice with *Hp* for 14 days, cleared infection with pyrantel pamoate, waited 28 days, and then challenged the mice with a secondary *Hp* infection. On Day 14 of challenge infection, Balb and Strain 3 mice had fewer worms in the intestine compared to B6 (Figure 7F). Together these data demonstrate that innate tuft-ILC2 responses are delayed or even absent in Balb mice, but that once adaptive immunity is engaged, tuft cell hyperplasia can develop and contribute to enhanced worm restriction and clearance. Congenic mice demonstrate both early B6-like and late Balb-like restriction.

In addition to sensing helminths and protists, intestinal tuft cells are the reservoir for murine norovirus strain CR6 and previous work has demonstrated that norovirus burden is regulated by type 2 signaling*(103)*. Accordingly, unmanipulated B6 mice had ~2-fold higher CR6 burdens than Balb. Treatment with succinate to mimic protist colonization increased ileal CR6 titers ~5-fold in B6 mice but had no effect on titers in Balb mice (Fig. 7I). The two strains had similar norovirus titers in the colon regardless of succinate treatment (fig. S7D). In sum, baseline tuft cell frequency helps determine the sensitivity and kinetics of the innate tuft-ILC2 circuit. Balb mice maintain functional responses to helminth infection while ignoring *Tritrichomonas* colonization and lowering their norovirus burden.

### 3.3 Discussion

Since the identification of the tuft-ILC2 circuit, numerous studies have uncovered ligands, receptors, and effector molecules that regulate this circuit. Much less progress has been made towards understanding cell intrinsic pathways by which epithelial stem cells commit to a tuft cell lineage, and how this process regulates tuft-ILC2 circuit activation. Here we identified differential *Pou2af2* isoform usage as a mechanism that establishes the baseline frequency of tuft cells in multiple tissues and tunes the sensitivity and kinetics of innate type 2 immunity in the SI.

We found that while unmanipulated Balb mice had fewer tuft cells at mucosal sites throughout the body, the B6 sequence from 50-67Mb on Chr9 was sufficient to restore tuft cell numbers to a B6 level in the SI and trachea (Figures 4F-G and Figures S4D and F). Further, congenic mice carrying this interval develop hyperplasia when treated with succinate or, in some cases, when colonized with *Tritrichomonas* (Figures 4H and 7A).

At 51.2 Mb on Chr9, adjacent to the QTL peak at 50.8 Mb, is *Pou2af2,* which was recently shown to encode a POU2F3 co-factor (OCA-T1), and to be necessary for tuft cell differentiation in the SI *(54)*. We found two isoforms of *Pou2af2* expressed in distal SI crypts, a full-length isoform and a shorter isoform, which lacks the POU2F3 interaction domain (Figures 6A-B). Balb and Strain 1 SI crypts express significantly less of the functional full-length *Pou2af2* isoform compared to B6 or Strain 2-4 SI crypts (Figure 6D), leading us to propose that *Pou2af2* isoform usage determines the number of tuft cells at baseline in the SI. What exactly determines isoform transcription is unknown as of now. There are several SNPs of interest within the *Pou2af2* locus, but transcription may be regulated by distal enhancers. The apparent

co-regulation of *Pou2af2* and *Pou2af3* transcription in particular suggests a broader regulatory mechanism that may be revealed by analysis of 3D genome structure.

Interestingly, the entire region of mouse Chr9 from 26.7 to 54 Mb is syntenic with human Chr11, suggesting that the shared function and regulation of genes in this region is evolutionarily conserved. In addition to the *Pou2af* gene cluster, *Pou2f3* is located at 43Mb on mouse Chr9 and 120Mb on human Chr11. Intriguingly, *Pou2f3* has been linked to several human cancers, including small cell lung cancer and colon cancer*(39, 40)*. Particularly relevant to our findings, SNPs in or near *Pou2af2* have also been linked to colon cancer and tuft cell abundance through genome-wide association studies and *in silico* analysis*(104, 105)*. Further studies are needed to fully reveal the role of tuft cells and regulation of these genes in the context of human cancers and immunity. Other tuft cell signature genes in this syntenic region include *Nrgn* and *Dscaml1*, and further analysis may identify additional genes or regulatory elements that regulate tuft cell differentiation and function.

The identification of OCA-T1 (*Pou2af2*) and OCA-T2 (*Pou2af3*) as POU2F3 co-factors advanced our understanding of tuft cell differentiation. Here we add isoform usage as another layer of regulation. Together, these findings suggest interesting avenues for further study. In particular, how do OCA-T1, OCA-T2, and POU2F3 interact with each other and with other transcription factors thought to play a role in SI tuft cell differentiation, such as GFI1b, SOX4 and ATOH1*(32–34, 37)*? In cell lines derived from human tuft-cell-like variants of small-cell lung cancer, deletion of *Pou2af2* results in decreased *Pou2f3* expression and vice versa, suggesting the two genes may impact each other's expression*(39, 54)*. Whether this relationship is present in non-malignant tuft cells in human or mouse still needs to be elucidated. Lastly, our results

from organoids, helminth infection, and succinate stimulation after rIL-25 priming suggest that unlike homeostatic differentiation, the response of Balb progenitors to IL-13 is similar to B6. How *Pou2af2* and *Pou2af3* are regulated in this context remains unknown.

*Pou2af2* isoform usage determines the baseline number of tuft cells, and this tunes the sensitivity and kinetics of the tuft-ILC2 circuit. During helminth infection, tuft cells secrete cysLTs, which potently activate ILC2s when paired with IL-25*(53)*. However, tuft cells do not produce cysLTs when stimulated with succinate*(53)*. Furthermore, the tuft cell deficit in Balb mice is more pronounced in the distal SI, where succinate sensing occurs, than in the proximal SI where helminths predominantly reside (Figure 1B). Ultimately, the integration of baseline tuft cell frequency and strength of signal sets the threshold for tuft-ILC2 circuit activation. Balb mice have few tuft cells but can perhaps overcome this defect with IL-25 and cysLT synergy downstream of helminth sensing (Figures 7C and E). B6 mice likely rely on a higher baseline tuft cell frequency to sense the weaker, cysLT-independent, succinate signal. As a result, while adaptive immune responses in Balb mice are indeed skewed towards type 2 immunity, their innate type 2 immune response is attenuated, particularly in the distal SI. Rather than representing a defect, however, the lower baseline tuft cell frequency in Balb mice may be adaptive. Balb mice maintain functional responses to helminth pathogens while not expending the energy to remodel their epithelium in response to commensal protists. To date, no detrimental effects have been demonstrated in mice that fail to sense Tritrichomonads.

The link between tuft cells and immunity extends beyond helminth infection and protist colonization. In addition to expanding the niche for norovirus, acutely activating the tuft-ILC2 circuit results in worse outcomes for West Nile Virus infection in mice *(103, 106)*. Distal SI tuft

cells can also sense bacterial-derived succinate, and in mice, giving succinate to increase tuft cell frequency reduces inflammation in models of ileitis*(35, 66)*. Perhaps relatedly, in Crohn's disease, tuft cell frequency is lowest in areas of highest inflammation. Beyond the intestine, tracheal tuft cells sense bacterial ligands and regulate breathing, mucociliary clearance, and neuroinflammation *(49, 107, 108)*. In the gallbladder, tuft cells prevent inflammation, perhaps by inducing mucus production and smooth muscle contraction*(51, 52)*. Our data indicate that the Chr9 locus impacts baseline tuft cell frequency in multiple tissues, including the trachea. We expect that *Pou2af2* isoform usage, and associated tuft cell abundance, would influence tuft cell-mediated immune responses in these other contexts as well.

## 3.4 Methods

### Experimental Animals

Mice aged 6 weeks and older were used for all experiments. Mice were age-matched within each experiment. Pooled results include both male and female mice of varying ages unless otherwise indicated. C57BL/6J (B6), and Balb/cJ (Balb) mice were bred in house or purchased from Jackson Laboratories. C3H/HeJ, FVB/NJ, 129S1/SvImJ and Swiss Webster mice were purchased from Jackson Laboratories. Congenic mice were generated and bred in house as described below. All mice were maintained in specific pathogen-free conditions at the University of Washington and were confirmed to be free of *Tritrichomonas* by microscopy and qPCR, unless specifically colonized for experimental purposes. All procedures were conducted within University of Washington IACUC guidelines under approved protocols.

### Quantitative trait locus mapping

We performed quantitative trait locus (QTL) mapping of succinate-induced tuft cell frequency using an F2 intercross between B6 and Balb. We generated Tn5-tagmented whole-genome sequencing libraries for 84 F2 hybrids and sequenced the samples to a depth of ~0.05x in a NextSeq 500/550 (75 cycles). Adapters were trimmed using Trimmomatic v0.36 *(109)*, and reads were aligned to the mm10 reference genome using BWA-MEM.

To impute genotypes, we generated a panel of SNPs between B6 and Balb using sequence variation data from the Mouse Genomes Project *(110)*. SNPs that passed the following thresholds were included in the panel: MQ >= 60, DP between 40 and 140, GQ >= 60, and QUAL > 200. We genotyped each individual at all qualifying variant positions and conducted

genotype imputation using Ancestry-HMM v0.94*(111)*. Genome-wide genotype probabilities from Ancestry-HMM were used to perform QTL analysis of succinate-induced tuft cell frequency using R/qtl. The code and results for this analysis are included as Data File S1.

**Congenic strain generation**

We generated four congenic strains through six to eight generations of backcrossing to Balb to fine map the QTL on chromosome 9. Each generation, libraries were generated, sequenced, and aligned as described above. Genotypes were imputed using Ancestry-HMM v0.94. In each cohort, individuals were prioritized for continued backcrossing if recombination occurred within the congenic interval on chromosome 9. At a minimum, individuals chosen for breeding retained B6 ancestry in the chr9 locus and contained a high proportion of Balb ancestry outside the chr9 locus. Because we were unsuccessful at designing a method in which we could quantify succinate-driven tuft cell hyperplasia without euthanasia of the mouse, we selected breeders based only on their genotype and then phenotyped siblings with the same Chr9 genotypes for succinate responsiveness. After 6-8 generations of backcrossing, each congenic genome was homozygous for Balb DNA at all locations except the Chr9 locus, where they were homozygous for B6 DNA.

**Succinate Treatment**

For succinate experiments mice were given 150mM or 250mM sodium succinate hexahydrate (Thermo) ad libitum in drinking water for the indicated amount of time.

### *In vivo* recombinant cytokine administration

IL-4 complexes were generated by incubating 2 µg mouse rIL-4 (R&D Systems) with 10 µg LEAF purified anti-mouse IL4 antibody (clone 11B11, Biolegend) per mouse for 30 min at room temperature. rIL-4 complex or 500ng rIL-25 were given for 3 consecutive days intraperitoneally in 200 ul PBS.

### Mouse Infection and Treatments

*H*. *polygyrus* and *N. brasiliensis* larvae were raised and maintained as previously described *(112, 113)*. Mice were infected by oral gavage with 200 *H*. *polygyrus* L3 or subcutaneously with 500 *N. brasiliensis* L3 and euthanized at the indicated time points to collect tissues for staining and/or to count worm burden. Worm burden was enumerated across the entire small intestine using a dissection microscope.

### *H. polygyrus* worm fecundity

Adapted from a previously described method *(114)*, 12 female worms were isolated from the proximal 5cm of the small intestine per mouse and individually cultured in 200ul plain RPMI 1640 with 200 U/mL penicillin and 200 µg/mL streptomycin in 96-well plates at 37°C. After 24 hours, eggs were counted, and eggs/worm were calculated.

### *H. polygyrus* fecal egg count

For fecal egg burdens, 2 to 3 fecal pellets were collected and weighed at time of euthanasia. Pellets were softened in PBS, homogenized with electric pestle, and transferred to 5mL $H_20$ saturated with NaCl and eggs were counted using a McMaster's Slide.

### Protist colonization

For protist colonization experiments, breeding pairs were colonized with *Tritrichomonas musculis* as previously described *(29)*. Pups from colonized breeding pairs were analyzed. Protist colonization was quantified by collecting and weighing cecal content at time of euthanasia, diluting in PBS and counting protists using a hemocytometer.

### Generation of murine norovirus stock

Stocks of murine norovirus (MNoV) strain CR6 were generated from molecular clones as previously described *(115)*, except for a modified virus concentration protocol. Briefly, plasmids encoding the viral genomes were transfected into 293T cells to generate infectious virus, which was subsequently passaged on BV2 cells. After two passages, BV2 cultures were frozen and thawed to liberate virions. Virus was concentrated by centrifugation in a 100,000 MWCO ultrafiltration unit (Vivaspin, Sartorius). Titers of virus stocks were determined by plaque assay on BV2 cells*(116)*.

### MNoV infections, sample collection and quantification

Mice received either 150mM sodium succinate or 300mM sodium chloride in the drinking water for 7 days prior to infection with CR6 and continued to receive treatment water until time of harvest. 6-week-old mice were orally inoculated with $10^6$ PFU of CR6 in a volume of 25µl. 7 days post Cr6 infection tissues and stool were harvested into 2-ml tubes (Sarstedt) with 1-mm-

diameter zirconia/silica beads (Biospec). Samples were frozen and stored at -80C until RNA extraction. As previously described *(117)*, RNA from tissues was isolated using TRI Reagent with a Direct-zol-96 RNA kit (Zymo Research) according to the manufacturer's protocol. 5µl of RNA was used for cDNA synthesis with the ImPromII reverse transcriptase system (Promega). MNoV TaqMan assays were performed, using a standard curve for determination of absolute viral genome copies, as described previously *(118)*. qPCR for housekeeping gene *Rps29* was performed as previously described *(119)*. All samples were analyzed with technical duplicates.

**Intestinal tissue fixation and staining**

Intestinal tissues were flushed with PBS and fixed in 4% paraformaldehyde for 4 hours at 4°C. Tissues were washed with PBS and incubated in 30% (w/v) sucrose overnight at 4°C. Samples were then coiled into "Swiss rolls" and embedded in Optimal Cutting Temperature Compound (Tissue-Tek) and sectioned at 8 µm on a CM1950 cryostat (Leica). Immunofluorescent staining was performed in PBS with 1% BSA at room temperature (RT) as follows: 1 h 5% goat serum, 1 h primary antibody (αDCLK1, Abcam ab31704), 40 min goat anti-rabbit IgG F(ab')2-AF594 secondary antibody (Invitrogen) and mounted with Vectashield plus DAPI (Vector Laboratories). Images were acquired with an Axio Observer A1 (Zeiss) microscope with a 10X A Plan objective. Tuft cell frequency was calculated using ImageJ software to manually quantify $DCLK1^+$ cells per millimeter of crypt-villus axis. Four 10x images of the Swiss roll were analyzed for each replicate and at least 25 total villi were counted.

**Tracheal tuft cell staining and quantification**

Tracheas were harvested and connective tissue was removed. Tracheas were opened longitudinally and washed 5 times in 5% FBS/10mM DTT/0.05% Tween-20/HBSS, vortexing for 5

seconds, to remove mucus. Tracheas were stretched out by pinning to SylGard-coated well of 6 well plate and fixed for 1 hr on ice in Cytofix/Cytoperm buffer (BD Biosciences). Immunofluorescent staining was performed in PBS with 0.25% Triton X-100 at 4°C as follows: 24 h 10% goat serum, 24 to 36 h primary antibody (αDCLK1, Abcam ab31704), 2 h goat anti-rabbit IgG F(ab')2-AF488 secondary antibody (Invitrogen), 15 min DAPI (1:1000), and mounted with Vectashield (Vector Laboratories). Images were acquired with a Nikon eclipse Ti microscope using a CSU-W1 spinning disc confocal with a Plan Apo λ 20X objective. 5 images were collected per sample and tuft cells were quantified using QuPath cell detection software.

**Intestinal single-cell tissue preparation**

For single cell epithelial preparations from small intestines or cecum, tissues were flushed with PBS, Peyer's patches removed, opened longitudinally, and rinsed with PBS to remove intestinal contents and mucus. Intestinal tissue was cut into 2-5 cm pieces and cecum was cut into 5-6 strips. Tissues were incubated rocking at 37°C for 10 min in 10ml HBSS ($Ca^{+2}$/$Mg^{+2}$-free) supplemented with 3mM EDTA and 1mM HEPES. Tissues were vortexed thoroughly and released epithelial cells were passed through a 70 μm filter. Tissues were then incubated in fresh EDTA/HBSS solution and incubation, vortexing and filtering was repeated for a total of 3 rounds. Supernatants were pooled and washed once before staining for flow cytometry.

For lamina propria preparations, small intestinal tissue was processed as above to remove the epithelial fraction. Tissues were then incubated in 10ml RPMI 1640 supplemented with 20% FCS, 1mM HEPES, 0.05 mg/ml DNase I (Sigma Aldrich), and 1 mg/mL Collagenase A (Sigma

Aldrich), shaking at 37°C for 30 minutes. Tissues were vortexed and cells were passed through a 100 μm filter, then a 40 μm filter. Cells were then washed and stained for flow cytometry.

**Thymus single-cell tissue preparation**

For thymus epithelial preparations, protocol was adapted from previously described procedure*(23)*. Briefly, thymi cleaned of fat were minced with a razor blade. Tissue was incubated in 37°C water bath for 12 min in 4 ml of digestion medium containing 2% FBS, 100 μ/ml DNase I (Sigma Aldrich) and 100 μ/ml liberase TM (Sigma Aldrich) in DMEM. At 12 min, tubes were spun briefly to pellet undigested fragments and the supernatant was moved to 20 ml of 0.5% BSA, 2 mM EDTA in PBS on ice. The DNAse/Liberase digestion was repeated twice for a total of three 12-min digestion cycles. The single-cell suspension was pooled, pelleted and resuspended in 50% Percoll (Sigma Aldrich), underlaid with 90% Percoll, and centrifuged at 2,000 rpm for 15 min at 20°C. The 50/90 interphase of the Percoll gradient was collected, washed, and stained for flow cytometry as described below.

**Organoid Culture**

Small intestinal crypt-derived organoids were grown as described with modifications described below*(81)*. Briefly, distal small intestine was isolated and villi manually scraped off with a glass coverslip. Tissue was then washed three times in cold PBS with vigorous shaking before 30 minute 4 °C incubation in 2mM EDTA to release epithelial crypts, which were washed in PBS and filtered through a 70 μm strainer. Pelleted crypts were resuspended in Matrigel and plated at 400-500 crypts per well in a prewarmed plate, incubated at 37°C for 5

minutes to allow for Matrigel solidification, and complete organoid media added. Organoid media was composed of DMEM/F12 supplemented with 2mM glutamine, 100 U/mL penicillin, 100mg/mL streptomycin, 100ug/mL Normacin (InvivoGen), 10mM HEPES, 1X N2 supplement (Life Technologies), 1X B27 supplement (Life Technologies), 500mM N-acetylcysteine, 50μg/ml mEGF, and replacing recombinant R-spondin with supernatants from R-spondin expressing L-cells and replacing recombinant Noggin with supernatants from Noggin expressing cells. Crypts were harvested from distal (last 10cm) small intestine of naive mice and plated on day 0. On day 3 and day 5, media was replaced. Organoids were treated with 2.5 ng/ml recombinant IL-13 on day 1, 3 and 5. On day 7 organoids were harvested for passage or analysis. Organoids were passaged by washing in room temperature PBS to remove Matrigel. Next, organoids were sheared with a 28G insulin syringe, washed and resuspended in fresh Matrigel. Generally, organoids were passaged at 1 well to 3-5 well ratio depending on number of organoids present.

For flow cytometry, organoids were resuspended in 1X TrypLE (Gibco). Organoids were sheared with a 28G insulin syringe, incubated for 10min at room temperature, cells washed, and then stained for flow cytometry as described below. Tuft cells were identified as $CD45^{-}$ $EpCAM^{+}$ $CD24^{+}$ $DCLK1^{+}$. For qPCR, organoids were incubated in Cell Recovery Solution (Corning) for 30 min at 4°C to remove Matrigel. Organoids were washed 2 times with PBS, pelleted and resuspended in RLT Plus buffer. RNA was isolated using the Mini Plus RNeasy kit (Qiagen) following manufacture's protocol.

**Flow cytometry and cell sorting**

Single cell suspensions from tissues or organoids were prepared as described above. For flow cytometry, samples were stained with Zombie Violet (BioLegend) in PBS for live/dead exclusion and stained in PBS + 3% FBS with antibodies to surface markers. Next, cells were fixed and permeabilized using the eBioscience™ Foxp3 / Transcription Factor Staining Buffer Set, following manufacturer's instructions for staining either cytosolic proteins (DCLK1) or nuclear proteins (GATA3 and Ki67). When cell counts were needed, counting beads (Invitrogen) were added prior to running flow cytometry. Samples were run on a Canto RUO or Symphony A3 (BD Biosciences) and analyzed with FlowJo 10 (Tree Star). Samples were FSC-A/SSC-A gated to exclude debris, FSC-A/FSC-H gated to select single cells and gated to exclude dead cells.

For cell sorting of ILC2s or tuft cells, single cell suspensions were prepared as described above. Cells were stained in PBS + 3% FBS with antibodies to surface markers and stained with DAPI for live/dead exclusion. Samples were sorted on an Aria II (BD Biosciences). Samples were FSC-A/SSC-A gated to exclude debris, FSC-A/FSC-H gated to select single cells and gated to exclude dead cells.

**ILC2 Stimulation Assay**

Small intestinal lamina propria ILC2s were isolated from mice and sorted as described. Sorted cells were plated at 5000 cells per well in a 96 well plate and incubated at 37°C overnight in 10 ng/ml IL-7 (R&D Systems) and basal media composed of high glucose DMEM supplemented with non-essential amino acids, 10% FBS, 100 U/mL penicillin, 100mg/mL streptomycin, 10mM HEPES, 1mM sodium pyruvate, 100μM 2-mercaptoethanol, and 2mM L-glutamine. The next

morning, media was replaced with fresh media and 10 ng/ml IL-7, and cells were stimulated with the indicated agonist. After a six-hour stimulation at 37°C, supernatant was collected and analyzed by cytokine bead array as described below. Cells were resuspended in fresh basal media with 10ng/ml IL-7 and incubated for an additional 48 hrs. Cells were washed, stained for intracellular Ki67 as described above. Cytokine levels in supernatants collected from cultured ILC2s were measured using Enhanced Sensitivity Flex Sets (BD Biosciences) for mouse IL-5 and IL-13 according to the manufacturer's protocol. Data was collected on a LSR II (BD Biosciences).

**Quantitative RT-PCR**

Crypts from distal small intestine were isolated as described in the organoid culture methods. After filtering crypt suspension with 70 um filter, crypts were washed in PBS two times, pelleted and resuspended in RLT Buffer. RNA was isolated using the Mini Plus RNeasy kit (Qiagen) according to manufacturer's instructions and reverse transcribed using SuperScript II (Thermo) following manufactures' protocol. cDNA was used as template for quantitative PCR with PowerUP SYBR Green (Thermo) on a Via7 cycler (Applied Biosystems). Transcripts were normalized to *Rps17* (40S ribosomal protein S17) expression. Primer sequences listed in Table 2.

**RNA Sequencing and Analysis**

150 tuft cells were sorted as $CD45^{lo}$ $EpCAM^{+}SigF^{+}CD24^{+}$ directly into lysis buffer from the SMART-Seq v4 Ultra Low Input RNA Kit (Takara) and cDNA was generated following manufacturer's instructions. Four biological replicates were collected for each genotype. Each biological replicate represents one mouse. Next-generation sequencing was performed by the

Benaroya Research Institute Genomics Core. Sequencing libraries were generated using the Nextera XT library preparation kit with multiplexing primers, according to manufacturer's protocol (Illumina), and library quality was assessed using the Tapestation (Agilent). High throughput sequencing was performed on NextSeq 2000 (Illumina), sequencing dual-indexed and paired-end 59 base pair reads. All samples were in the same run with target depth of 5 million reads to reach adequate depth of coverage.

Processing and analysis of the raw sequencing reads was performed using the DIY.Transcriptomics (diytranscriptomics.com) pipeline, with experiment-specific modifications. Raw reads were mapped to the mouse reference transcriptome using Kallisto, version 0.46.2. The quality of raw reads, as well as the results of Kallisto mapping were analyzed using fastqc and multiqc. Kallisto outputs were read into an r environment and annotated using Biomart. Samples were filtered to exclude genes with counts per million = 0 in 4 or more samples and genes annotated as pseudogenes. Finally, samples were normalized to each other. To identify differentially expressed genes, precision weights were first applied to each gene based on its mean-variance relationship using VOOM, then data was normalized using the TMM method in EdgeR. Linear modeling and bayesian stats were employed via Limma to find genes that were up- or down-regulated by 2-fold or more, with a false-discovery rate (FDR) of 0.05. The code and results for this analysis are included as Data File S2.

**5’ rapid amplification of cDNA ends**

RNA isolated from distal SI crypts was obtained as described above. For 5’ rapid amplification of cDNA ends assay, the SMARTer RACE 5’/3’ Kit (Takara) was used following manufacturer’s protocol and using the following primer:

*5’*-GATTACGCCAAGCTTGGTGGGCGGTAGTCTCCATAGGGCTCAGC-*3’.*

**Quantification and Statistical Analysis**

All experiments were performed using randomly assigned mice without investigator blinding. All data points and “n” values reflect biological replicates (i.e. mice). No data were excluded. Statistical analysis was performed as noted in figure legends using Prism 7 (GraphPad) software. Graphs show mean +/- SEM.

**3.5 Acknowledgements**

We thank all members of the von Moltke lab for helpful discussion and input on this manuscript. We thank D. Hailey and the Garvey Cell Imaging Lab in the Institute for Stem Cell & Regenerative Medicine for microscopy support; the mouse husbandry staff in the UW SLU vivarium; V. Gersuk, K. O'Brien and the Benaroya Research Institute Genomics Core for help with RNA sequencing; and M. F. Fontana for helpful comments on the manuscript. Flow cytometry data was acquired through the University of Washington, Cell Analysis Facility Shared Resource Lab, with NIH award 1S10OD024979-01A1 funding for the Symphony A3. M.S.N. was supported by a University of Washington Immunology Training Grant T32 AI106677 and by the UW Immunology Department Titus Fellowship. Work at Columbia University was supported by NIH R35GM143051, Sloan Foundation Fellowship, Klingenstein-Simons Fellowship (all to A.B.). A.B. and J.v.M. are Searle Scholars J.v.M. is a Burroughs Wellcome Investigator in the Pathogenesis of Infectious Disease. Work at Washington University was supported by R01AI139314 (MTB) and F31AI167499 (EAK). Work at the University of Washington was supported by NIH DP2OD024087 and R01AI167923.

**Author contributions**

MSN designed and performed experiments, analyzed data, and wrote the paper with JVM. LMW and DLJ assisted with experiments at the University of Washington. NN performed Tn5-tagmented whole-genome sequencing, genotype imputation for congenic strain generation and assisted with QTL analysis, with supervision by AB. EAK performed murine norovirus experiments and data analysis with supervision and funding provided by MTB. AB acquired

funding and provided resources for Tn5-sequencing. JVM conceived of and supervised the study, performed experiments, analyzed data, and wrote the paper with MSN.

## 3.6 Figures

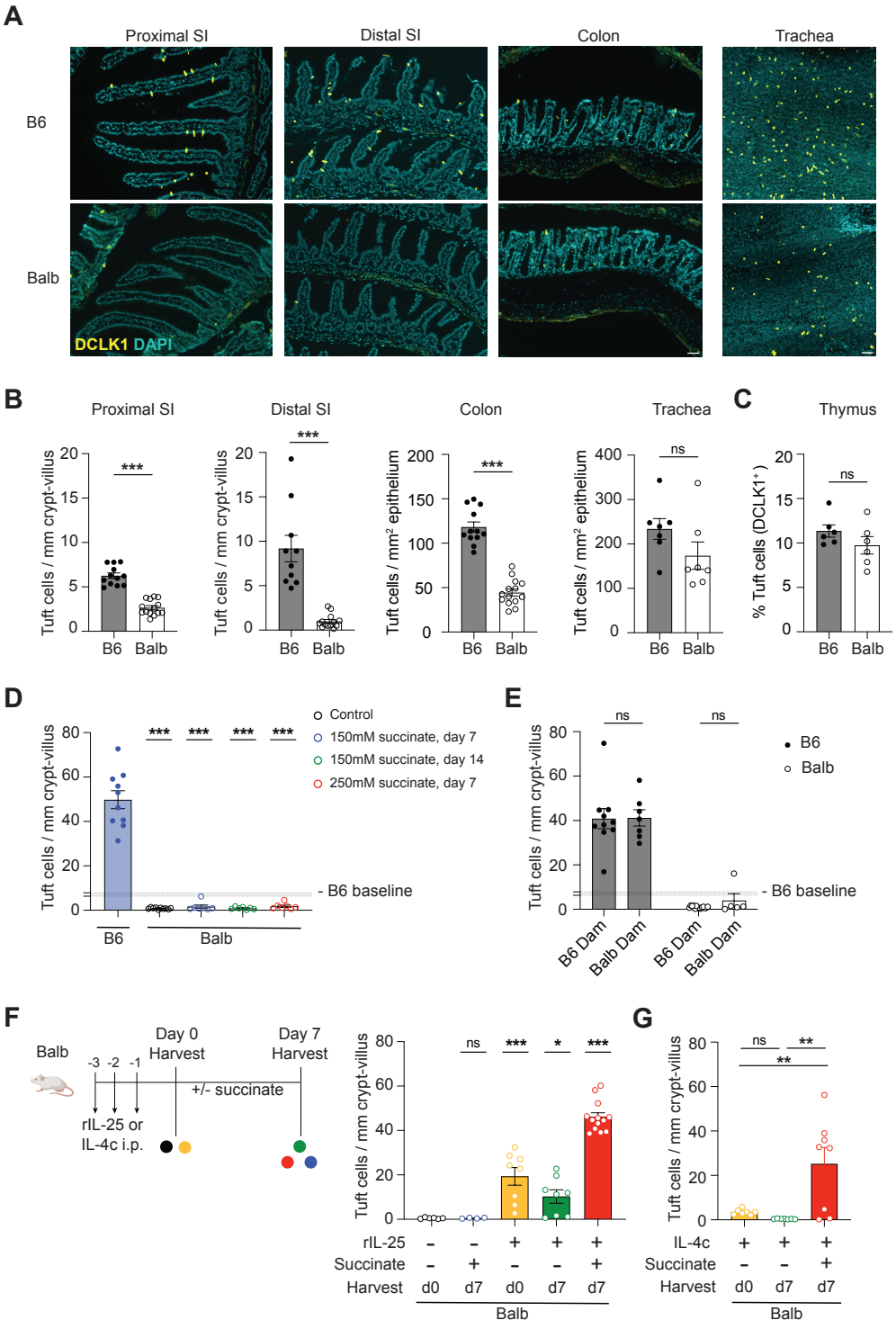
A
Proximal SI
Distal SI
Colon
Trachea
B6
Balb
DCLK1 DAPI
B
Proximal SI
Distal SI
Colon
Trachea
Tuft cells / mm crypt-villus
Tuft cells / mm² epithelium
B6
Balb
***
ns
C
Thymus
% Tuft cells (DCLK1⁺)
D
Control
150mM succinate, day 7
150mM succinate, day 14
250mM succinate, day 7
- B6 baseline
E
B6
Balb
B6 Dam
Balb Dam
F
Balb
Day 0 Harvest
Day 7 Harvest
-3 -2 -1
+/- succinate
rIL-25 or IL-4c i.p.
rIL-25
Succinate
Harvest
d0
d7
G
IL-4c

**Figure 1. Balb mice have fewer tuft cells at baseline and do not develop succinate induced hyperplasia unless primed.**

(**A** and **B**) (A) Representative images and (B) tuft cell (DCLK1+) quantification by immunofluorescence from indicated tissues and indicated mice. (**C**) Thymic tuft cell quantification by flow cytometry. (**D**) Tuft cell quantification in the distal SI of Balb mice at indicated succinate concentrations and time points. (**E**) Tuft cell quantification in the distal SI of adult B6 and Balb mice raised by dams of indicated genotype and given 150mM succinate for 7 days. (**F-G**) Experimental schematic and tuft cell quantification in the distal SI of Balb mice treated with either (F) rIL-25 or (G) IL-4c as indicated. In the graphs, each symbol represents an individual mouse from three or more pooled experiments. In (D and E), shaded area indicates the 95% confidence interval of the mean for distal SI tuft cell quantification calculated from a large cohort of control B6 mice. *$p < 0.05$, **$p < 0.01$, ***$p < 0.001$ by Mann-Whitney (B and C), by one way ANOVA with comparison to B6 (D) or Balb untreated (G) or multiple comparisons (H), and by multiple t tests (E). n.s., not significant. Graphs depict mean +/- SEM. Also see Figure S1.

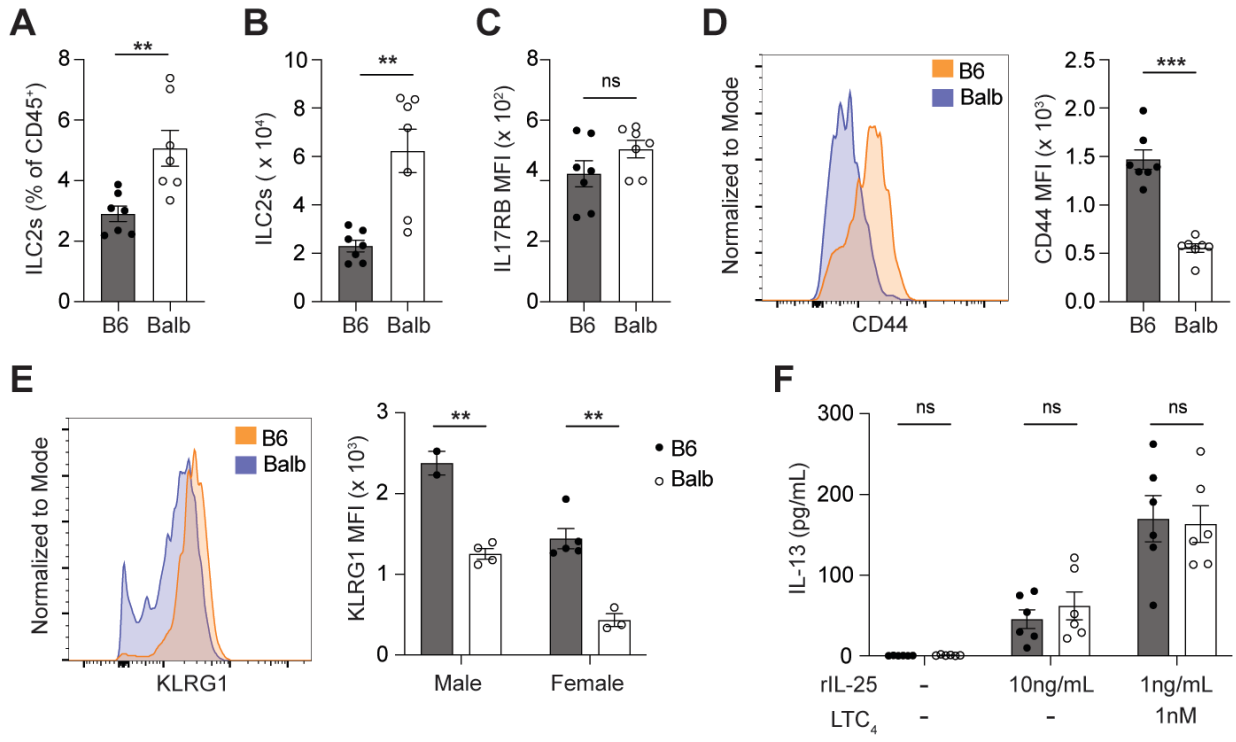


**Figure 2. Balb ILC2s are equally responsive to IL-25 but less activated at baseline compared to B6 ILC2s.**

(**A** and **B**) Quantification of ILC2s ($CD45^+$ $Lin^-$ $GATA3^+$) by (A) percentage and (B) absolute number in the SILP. (**C**, **D** and **E**) Quantification of (C) IL17RB MFI (D) CD44 MFI and (E) KLRG1 MFI on ILC2s. (**F**) IL-13 concentration in the supernatant following 6-h *in vitro* culture of SI ILC2s with the indicated concentrations of rIL-25 and $LTC_4$. In the graphs, each symbol represents an individual mouse from two pooled experiments. *$p < 0.05$, **$p < 0.01$, ***$p < 0.001$ by Mann-Whitney (A – D) or by multiple t tests (E and F). n.s., not significant. Graphs depict mean +/- SEM. Also see Figure S2.

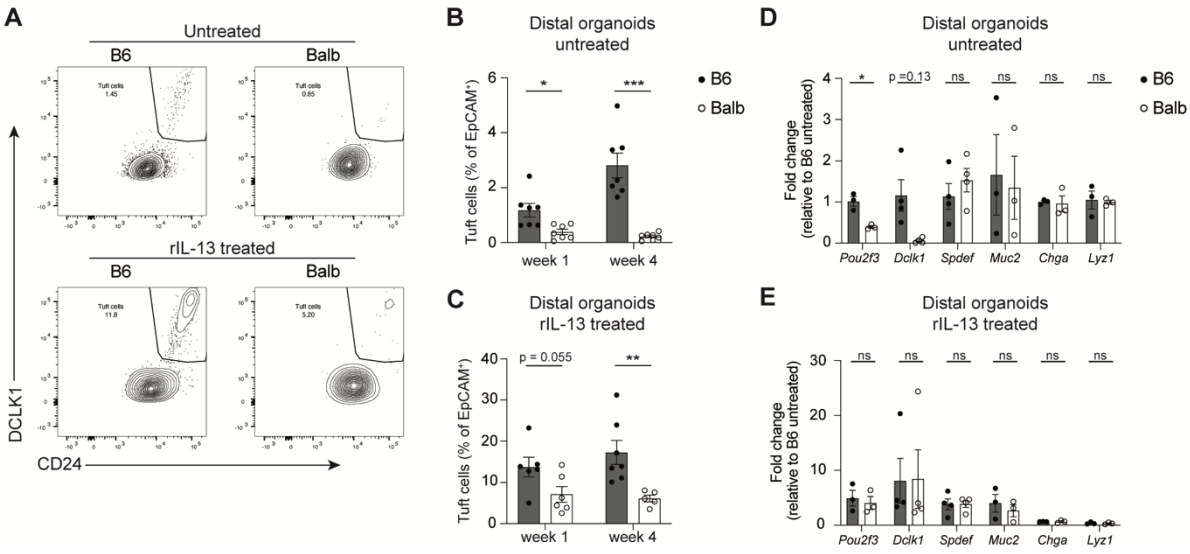


**Figure 3. Balb tuft cell defect is epithelium intrinsic and tuft cell specific.**

(**A**) Representative flow cytometry plots of tuft cell quantification from B6 or Balb distal SI organoids cultured *in vitro* for one week, either untreated or rIL-13 treated (2.5 ng/ml). (**B** and **C**) Quantification of tuft cells from (A) (**D** and **E**) Real-time PCR quantification of indicated genes normalized to B6 untreated condition, all relative to *Rps17* expression from (D) control or (E) rIL-13 treated distal SI organoids cultured for 2 weeks *in vitro*. In the graphs, each symbol represents a biological replicate based on the average of 2 to 3 technical replicates, from three to six pooled experiments. *$p < 0.05$, **$p < 0.01$, ***$p < 0.001$ by multiple t tests (B - E). n.s., not significant. Graphs depict mean +/- SEM. Also see Figure S3.

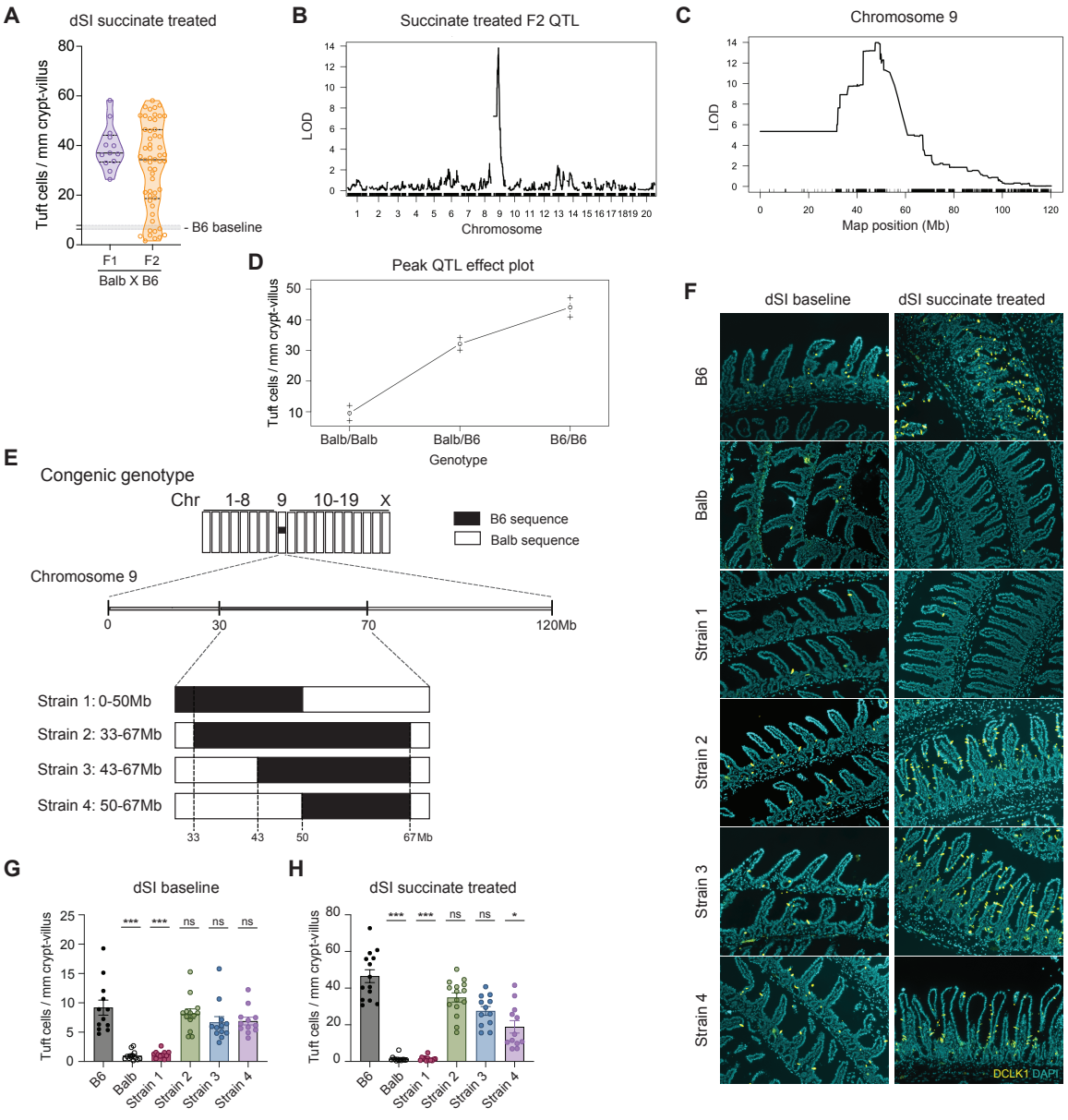


**Figure 4. A single locus on chromosome 9 regulates baseline tuft cell frequency and succinate responsiveness.**

(**A**) Quantification of tuft cells from distal SI of succinate treated female mice. (**B** and **C**) QTL mapping of succinate induced tuft cell hyperplasia in Balb X B6 F2 cross (B) whole genome and

(C) zoomed in on Chr9. (**D**) Effect plot of tuft cell phenotype based on genotype at the peak QTL (Chr9:50857809) (**E**) Schematic of genotype for congenic Strain 1-4 mice. (**F - H**) (F) Representative images and quantification of tuft cells from distal SI at (G) baseline or (H) after 150mM succinate treatment. Some B6 and Balb data points shown in (G) and (H) are also included as controls in Figure 1B and 1D. In (A), shaded area indicates the 95% confidence interval of the mean for distal SI tuft cell quantification calculated from a large cohort of control B6 mice. In the graphs, each symbol represents an individual mouse from three or more pooled experiments. *$p < 0.05$, **$p < 0.01$, ***$p < 0.001$ by one-way ANOVA (G and H) with comparison to B6. n.s., not significant. Graphs depict mean +/- SEM. Also see Figure S4.

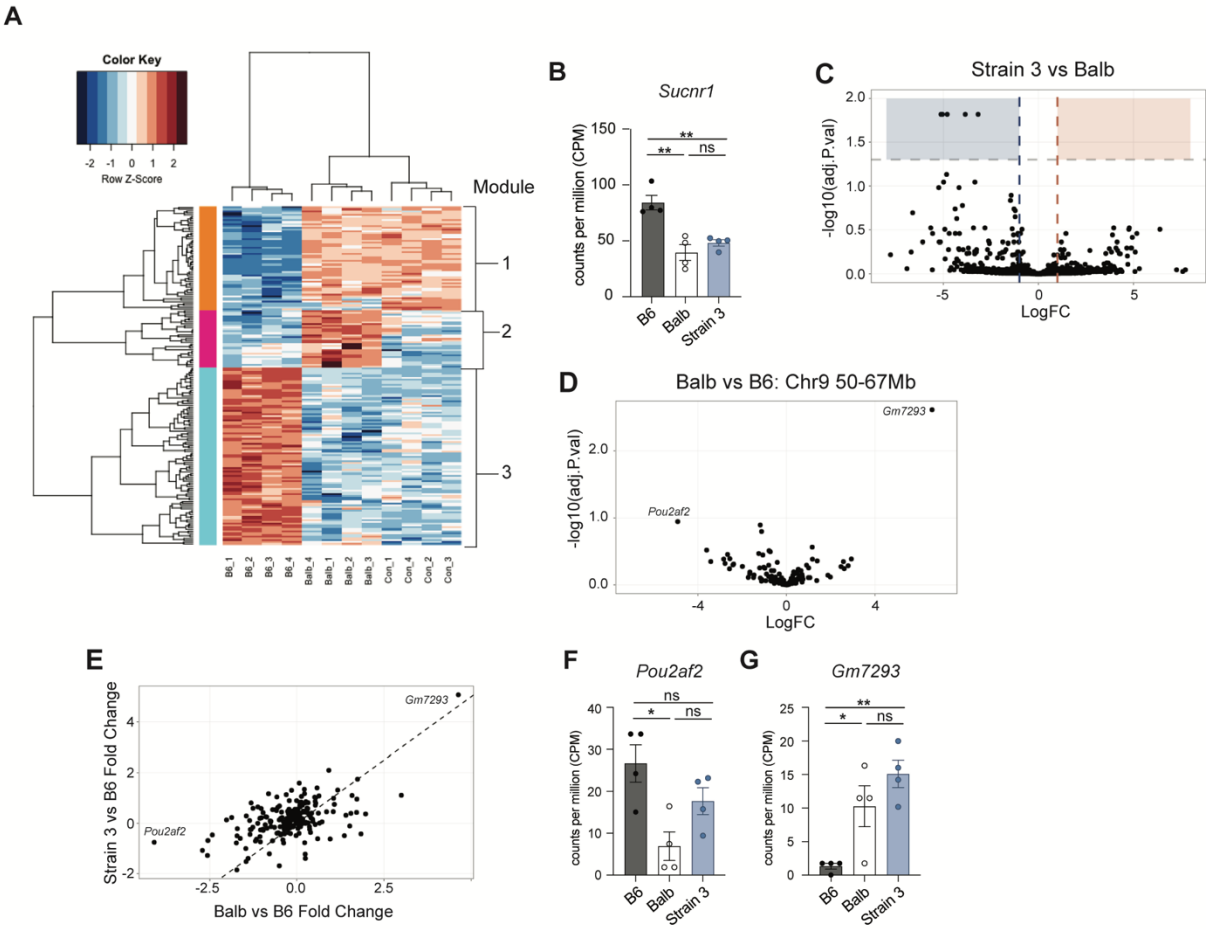


**Figure 5. mRNA sequencing of mature tuft cells from B6, Balb and Strain 3 mice.**

(**A**) Hierarchical clustering of differentially expressed genes. (**B**) Normalized read count of *Sucnr1*. (**C**) Volcano plots depicting DEGs from Strain 3 vs Balb. (**D**) Volcano plots depicting DEGs for genes found in the Chr9 50-67Mb region, from Balb vs B6. (**E**) Plot of fold change of DEGs from Strain 3 vs B6 compared to fold change from Balb vs B6. (**F** and **G**) Normalized read count of (F) *Pou2af2* and (G) *Gm7293*. *p < 0.05, **p < 0.01, ***p < 0.001 by one-way ANOVA (B, F and G). n.s., not significant. Graphs depict mean +/- SEM. Also see Figure S5.

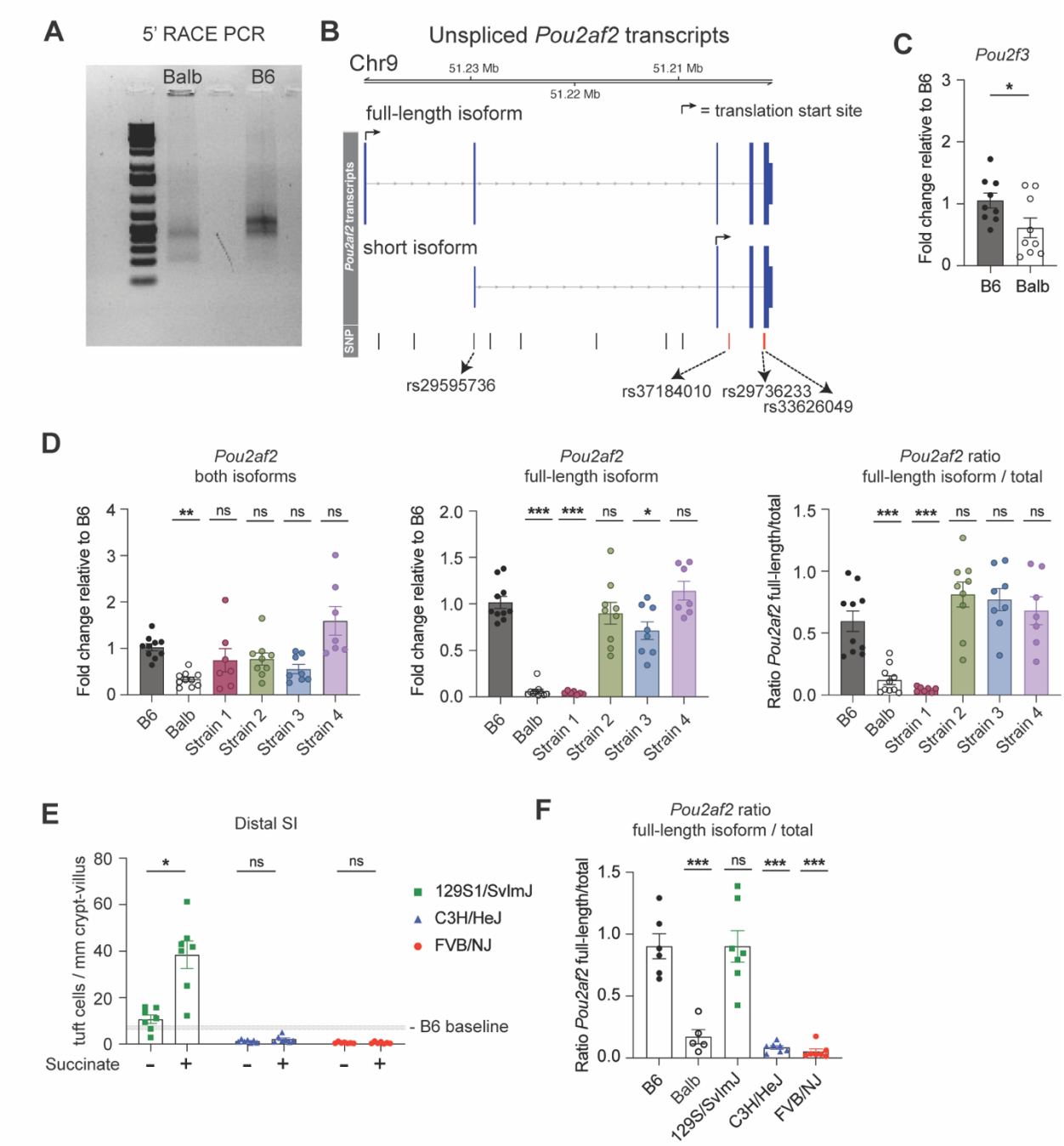


**Figure 6. *Pou2af2* isoform expression is modulated by genotype**.

(**A**) Agarose gel of 5' Rapid amplification of cDNA ends products from distal SI crypts. (**B**) Schematic of *Pou2af2* isoforms expressed in distal SI crypts with annotated SNPs (vertical bars) that differ between B6 and Balb. SNPs that also match phenotypes of other inbred strains are

highlighted in red. (**C)** Real-time PCR quantification of *Pou2f3*. (**D**) Real-time PCR quantification of indicated *Pou2af2* isoform and *Pou2af2* isoform ratio. (**E**) Tuft cell quantification in the distal SI and (**F**) *Pou2af2* isoform ratio calculated from real-time PCR quantification from distal SI crypts of indicated strains. In the graphs, each symbol represents an individual mouse three or more pooled experiments. *$p < 0.05$, **$p < 0.01$, ***$p < 0.001$ by Mann-Whitney (C), by one-way ANOVA (D and F) with comparison to B6 and by multiple t-tests (E). n.s., not significant. Graphs depict mean +/- SEM. Also see Figure S6.

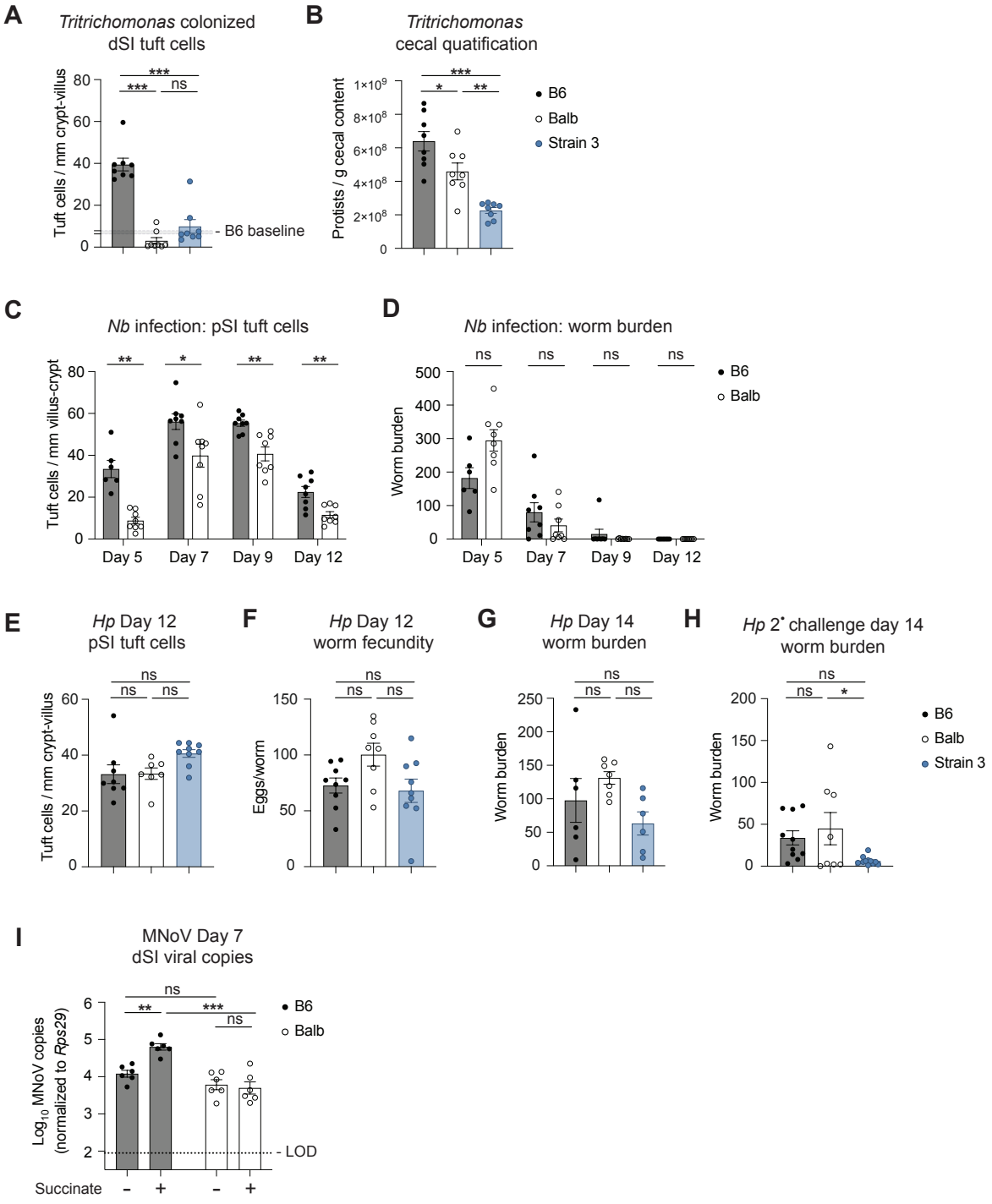
A
Tritrichomonas colonized dSI tuft cells
Tuft cells / mm crypt-villus
B6 baseline
B
Tritrichomonas cecal quatification
Protists / g cecal content
B6
Balb
Strain 3
C
Nb infection: pSI tuft cells
Tuft cells / mm villus-crypt
Day 5
Day 7
Day 9
Day 12
D
Nb infection: worm burden
Worm burden
E
Hp Day 12 pSI tuft cells
F
Hp Day 12 worm fecundity
Eggs/worm
G
Hp Day 14 worm burden
H
Hp 2˚ challenge day 14 worm burden
I
MNoV Day 7 dSI viral copies
Log10 MNoV copies (normalized to Rps29)
LOD
Succinate

**Figure 7. Tuft cell frequency at baseline tunes the kinetics and sensitivity of the tuft-ILC2 circuit.**

(**A**) Tuft cell quantification in the distal SI and (**B**) protist quantification in the cecal content of Tritrichomonas colonized mice. (**C**) Tuft cell quantification in the proximal SI and (**D**) worm burden in total intestine at the indicated time points post Nb infection. (**E**) Tuft cell quantification in the proximal SI on day 12 post Hp infection. (**F**) Overnight egg production by worms isolated from the proximal SI of mice 12 days post Hp infection. (**G** and **H**) Intestinal worm burden on day 14 of (**G**) primary or (**H**) secondary Hp infection 28 days after drug-cleared primary infection. (**I**) Mice were pretreated with 150mM sodium succinate or 300mM sodium chloride for 1 week prior to oral infection with murine norovirus (MNoV) CR6. Viral genome copies detected in the distal SI 7 days after CR6 infection. Dotted line represents limit of detection (LOD). In (**A**), shaded area indicates the 95% confidence interval of the mean for distal SI tuft cell quantification calculated from a large cohort of control B6 mice. In the graphs, each symbol represents an individual mouse from two or three pooled experiments. *$p < 0.05$, **$p < 0.01$, ***$p < 0.001$ by multiple t tests (**C** and **D**), by one-way ANOVA (**A** and **B**, **E** to **H**) or by two way ANOVA (**I**). n.s., not significant. Graphs depict mean +/- SEM. Also see Figure S7.

### 3.7 Supplemental Figures

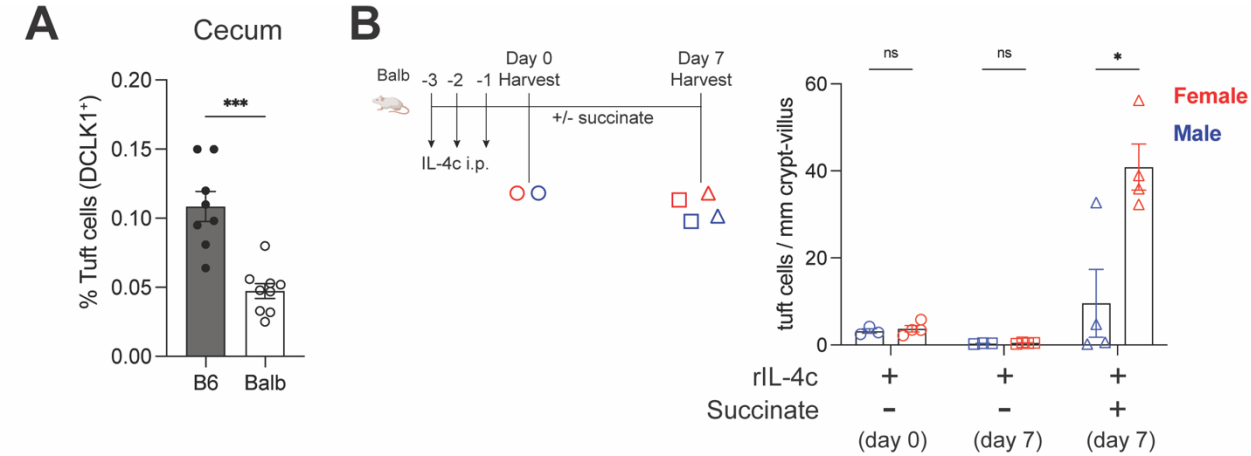


**Supplemental Figure 1. Balb mice have fewer tuft cells at baseline and rIL-4c priming leads to sex specific activation of the tuft-ILC2 circuit. Related to Figure 1.**

**(A)** Quantification of cecal tuft cells by flow cytometry. (**B**) Data from Figure 1G separated by sex. In the graphs, each symbol represents an individual mouse from two or three pooled experiments. *p < 0.05, **p < 0.01, ***p < 0.001 by Mann-Whitney (A) or multiple t tests (B). n.s., not significant. Graphs depict mean +/- SEM.

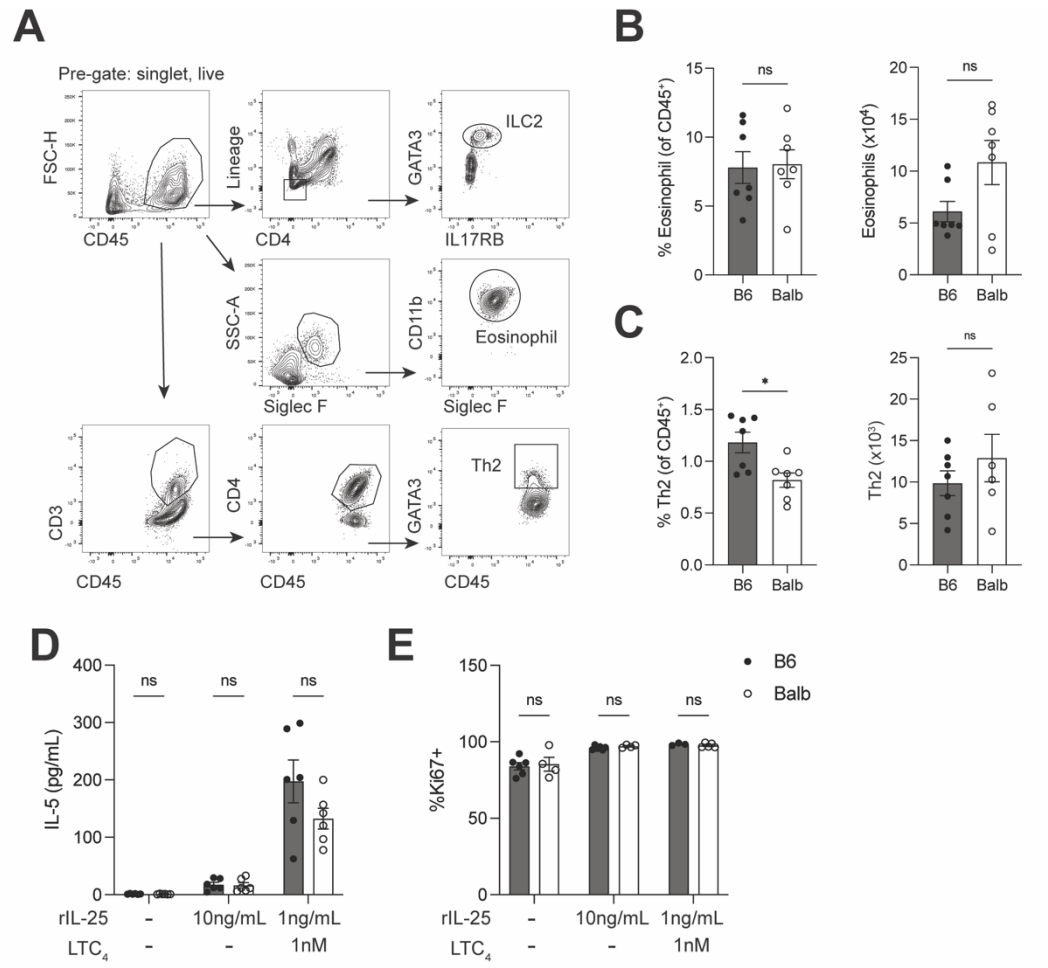


**Supplemental Figure 2. Equivalent numbers and responses of small intestinal type 2 immune cells in Balb and B6 mice. Related to Figure 2.**

(**A**) Gating strategy for identification of ILC2s, eosinophils and GATA3$^{+}$ Th2s from SI lamina propria of naive mice. (**B** and **C**) Percentage and absolute number of (B) eosinophils and (C) Th2 cells. (**D**) IL-5 concentration in the supernatant following 6-h *in vitro* culture of SI ILC2s with the indicated concentrations of rIL-25 and $LTC_4$ and (**E**) Ki67 expression 2 days after stimulation. In the graphs, each symbol represents an individual mouse from two pooled experiments. *p < 0.05, **p < 0.01, ***p < 0.001 by Mann-Whitney (B and C) or by multiple t tests (D and E). n.s., not significant. Graphs depict mean +/- SEM.

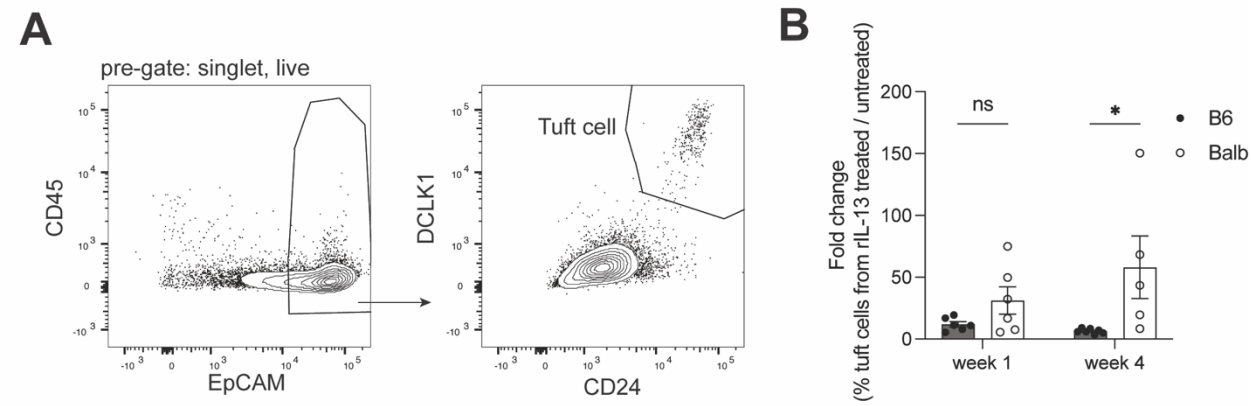


**Supplemental Figure 3. Organoid analysis. Related to Figure 3.**

(**A**) Gating strategy for identification of tuft cells from SI organoids. (**B**) Fold change in % tuft cells from rIL-13 treated over untreated organoids derived from the same biological replicate. In the graphs, each symbol represents a biological replicate based on the average of 2 to 3 technical replicates, from three to six pooled experiments. *p < 0.05, **p < 0.01, ***p < 0.001 by multiple t tests (B). n.s., not significant. Graphs depict mean +/- SEM.

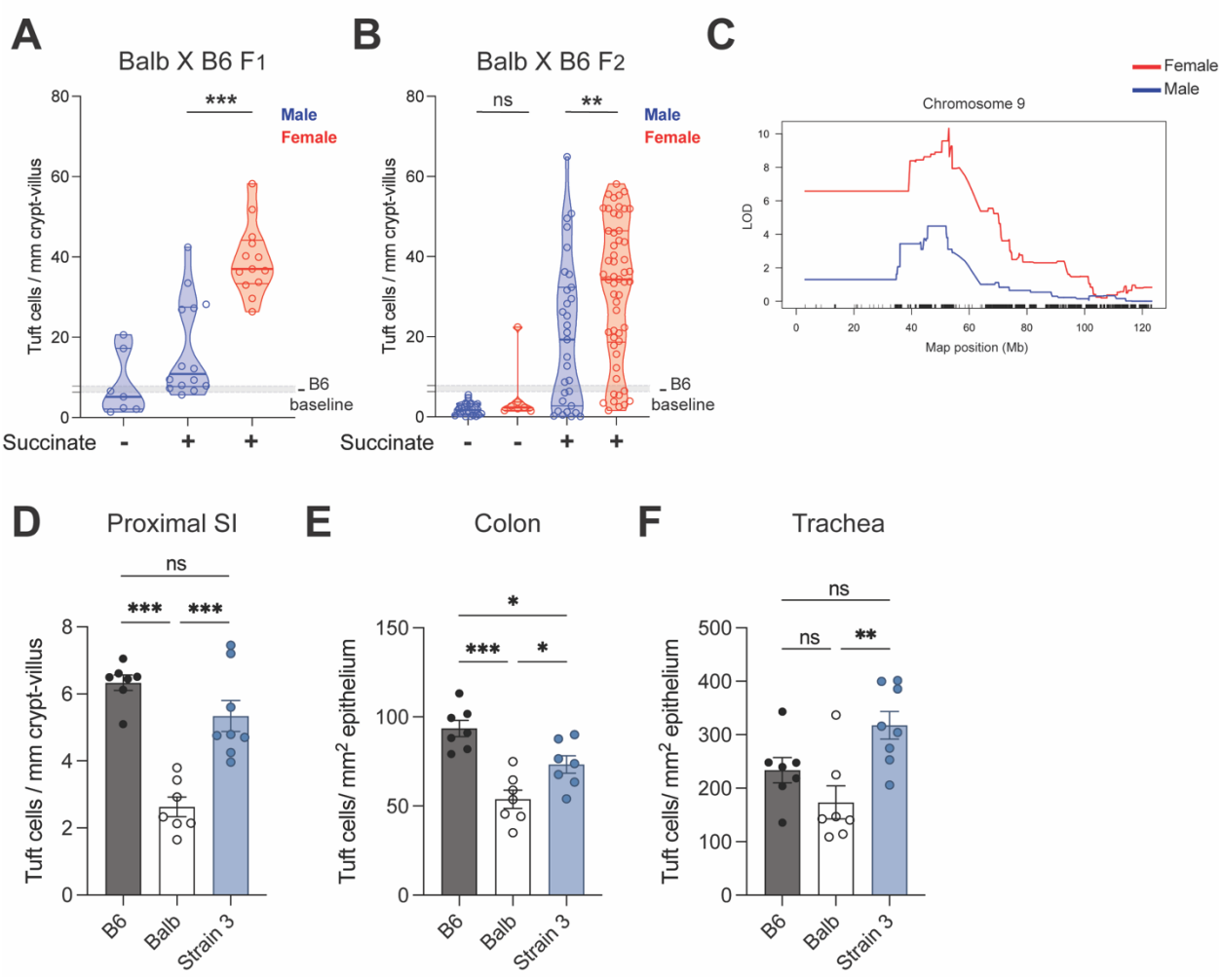


**Supplemental Figure 4. Sex effect in Balb x B6 F1 and F2 mice and recovery of tuft cell abundance in Strain 3 congenic. Related to Figure 4.**

(**A** and **B**) Tuft cell quantification in dSI of Balb X B6 (A) F1 and (B) F2 mice by sex. (**C**) Chromosome 9 QTL mapping of succinate induced tuft cell hyperplasia in Balb X B6 F2 by sex. (**D**, **E** and **F**) Tuft cell quantification in the (D) proximal SI, (E) colon and (F) trachea by immunofluorescence. B6 and Balb data in (F) are also represented in Figure 1B. In the graphs, each symbol represents an individual mouse from three or more pooled experiments. *p < 0.05, **p < 0.01, ***p < 0.001 by multiple t tests (A and B) and by one-way ANOVA (D, E and F). n.s., not significant. Graphs depict mean +/- SEM.

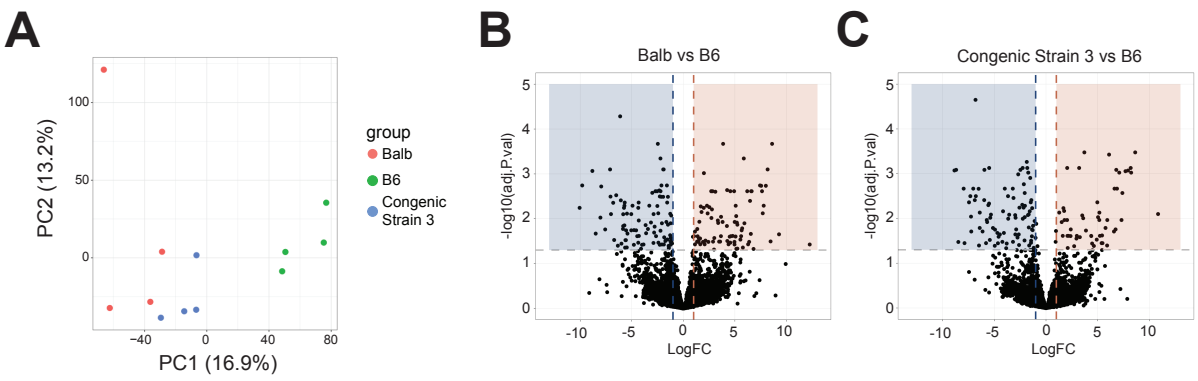


**Supplemental Figure 5. mRNA sequencing of mature tuft cells from B6, Balb and Strain 3 mice. Related to Figure 5.**

(**A**) Unsupervised PCA of gene expression. (**B** and **C**) Volcano plots of (B) Balb vs B6 and (C) Congenic vs B6. The samples in this figure were all analyzed in one sequencing run.

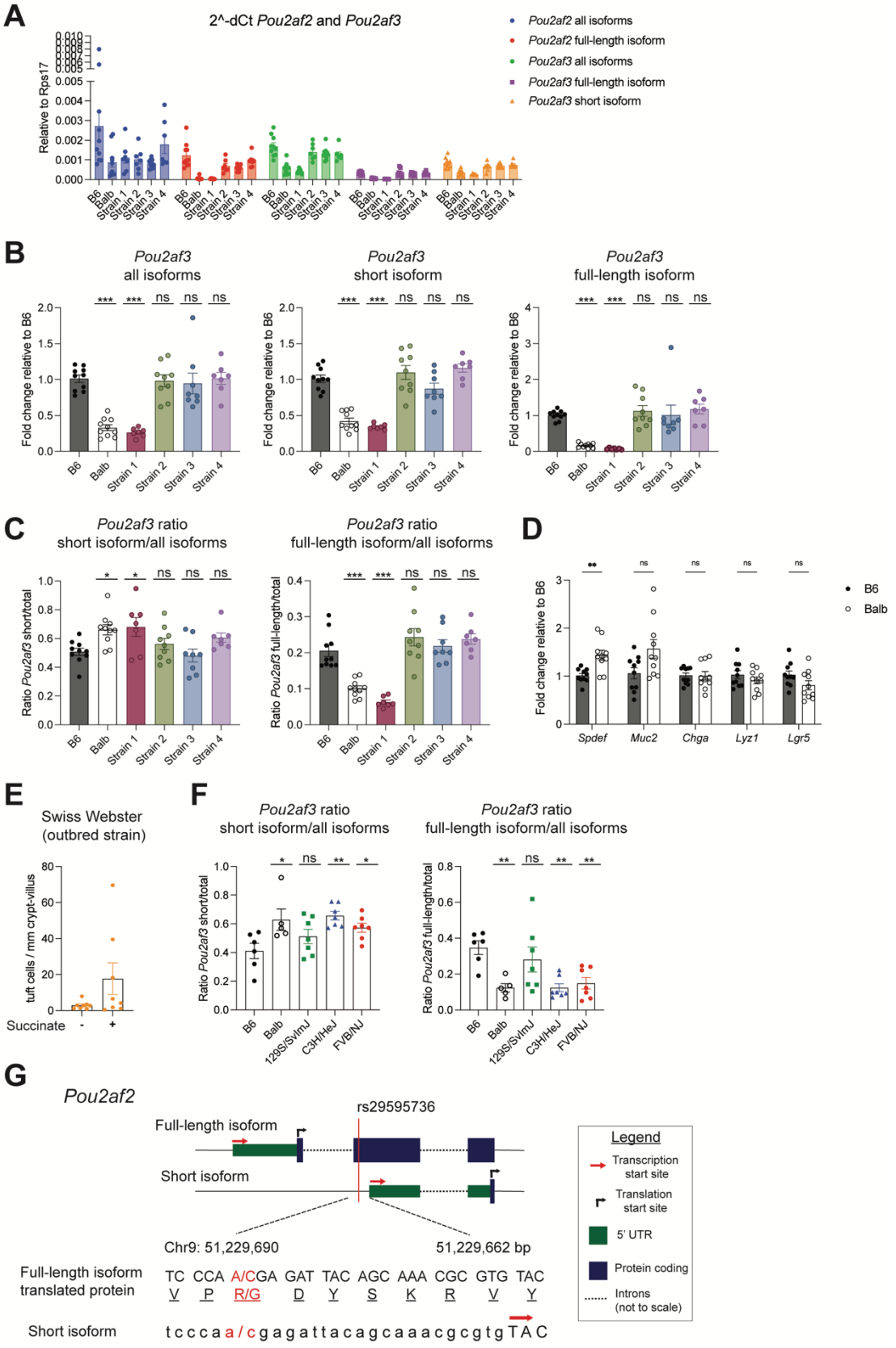
A
2^-dCt Pou2af2 and Pou2af3
Relative to Rps17
Pou2af2 all isoforms
Pou2af2 full-length isoform
Pou2af3 all isoforms
Pou2af3 full-length isoform
Pou2af3 short isoform
B
Pou2af3 all isoforms
Pou2af3 short isoform
Pou2af3 full-length isoform
Fold change relative to B6
C
Pou2af3 ratio short isoform/all isoforms
Pou2af3 ratio full-length isoform/all isoforms
Ratio Pou2af3 short/total
Ratio Pou2af3 full-length/total
D
Fold change relative to B6
Spdef
Muc2
Chga
Lyz1
Lgr5
B6
Balb
E
Swiss Webster (outbred strain)
tuft cells / mm crypt-villus
Succinate
F
Pou2af3 ratio short isoform/all isoforms
Pou2af3 ratio full-length isoform/all isoforms
129S/SvImJ
C3H/HeJ
FVB/NJ
G
Pou2af2
rs29595736
Full-length isoform
Short isoform
Chr9: 51,229,690
51,229,662 bp
Full-length isoform translated protein
TC CCA A/CGA GAT TAC AGC AAA CGC GTG TAC
V P R/G D Y S K R V Y
Short isoform
tcccaa/cgagattacagcaaacgcgtgTAC
Legend
Transcription start site
Translation start site
5' UTR
Protein coding
Introns (not to scale)

**Supplemental Figure 6. *Pou2af3* isoform expression follows similar pattern as *Pou2af2*.**

**Related to Figure 6.**

(**A**) Real-time PCR quantification of indicated genes/isoforms normalized to *Rps17* (housekeeping gene) from distal SI crypts. (**B**) *Pou2af3* isoform expression normalized to B6 and (**C**) *Pou2af3* isoform ratios. (**D**) Real-time PCR quantification of indicated genes normalized to B6. (**E**) Tuft cell quantification in dSI of Swiss Webster mice. (**F**) *Pou2af3* isoform ratios from indicated strains. (**G**) Depiction of SNP rs29595736 in *Pou2af2* isoforms and translated protein. In the graphs, each symbol represents an individual mouse from two or three pooled experiments. *$p < 0.05$, **$p < 0.01$, ***$p < 0.001$ by one-way ANOVA (B, C and F) with comparison to B6 and by multiple t tests (D). Graphs depict mean +/- SEM.

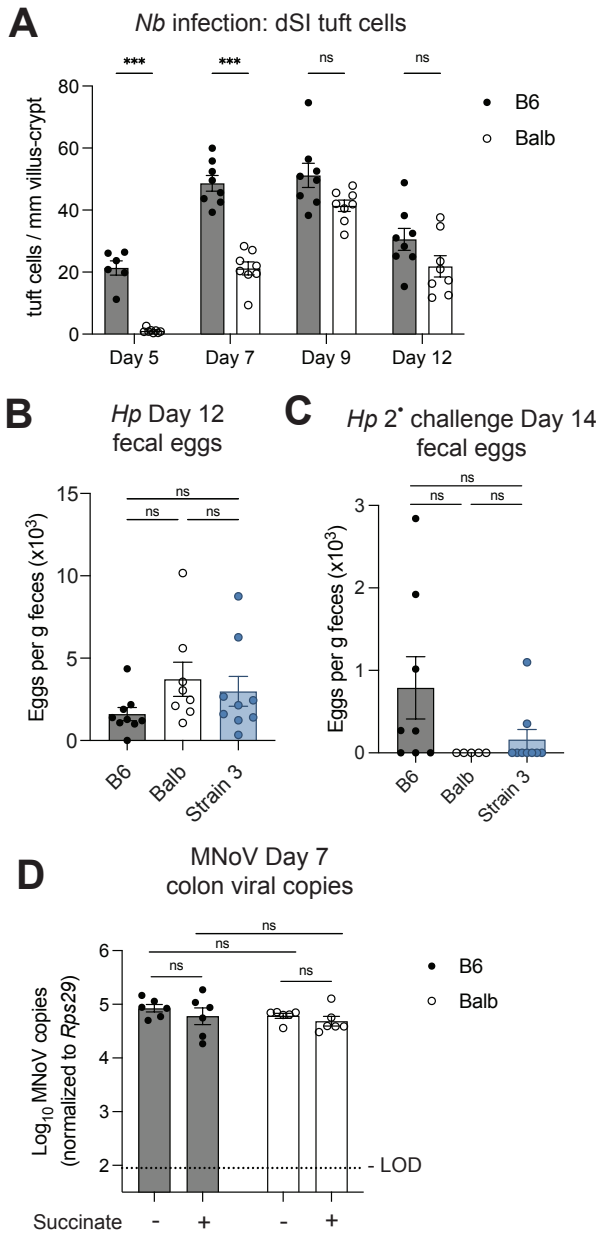


**Supplemental Figure 7. Tuft cell frequency at baseline tunes the kinetics and sensitivity of the tuft-ILC2 circuit. Related to Figure 7.**

(**A**)Tuft cell quantification in the distal SI at the indicated time points post *Nb* infection. (**B and C**) Eggs per gram feces quantified from mice (B) 12 days post primary *Hp* infection or (C) 14 days

post challenge *Hp* infection. (**D**) Mice were pretreated with 150mM sodium succinate or 300mM sodium chloride for 1 week prior to oral infection with murine norovirus (MNoV) CR6. Viral genome copies detected in the colon 7 days after CR6 infection. Dotted line represents limit of detection (LOD). In the graphs, each symbol represents an individual mouse from two pooled experiments. *$p < 0.05$, **$p < 0.01$, ***$p < 0.001$ by multiple t tests (A), by one-way ANOVA (B-C) and by two-way ANOVA (D). n.s., not significant. Graphs depict mean +/- SEM.

## 3.8 Tables

| Module 1 | Module 2 | Module 3 | |
|---|---|---|---|
| *1500011B03Rik* | *1700056N10Rik* | *1700011H14Rik* | *Kpna2* |
| *9230105E05Rik* | *Ascl2* | *1700081H04Rik* | *Krtap3-1* |
| *A930015D03Rik* | *B630005N14Rik* | *2010005H15Rik* | *Lect2* |
| *Aadac* | *Bhlha15* | *9030624J02Rik* | *Ly6a* |
| *Acaa1b* | *Bhlhe41* | *AA467197* | *Ly96* |
| *Adi1* | *Ceacam10* | *Acta1* | *Mlip* |
| *AK157302* | *Chst4* | *Ago1* | *mt-Nd3* |
| *Alad* | *Defa-rs1* | *Ahcy* | *Myadm* |
| *Baiap2l1* | *Defa-rs7* | *Arhgap9* | *Olfm1* |
| *BC064078* | *Defa17* | *B3gnt3* | *Otp* |
| *Cap1* | *Defa20* | *Btnl5-ps* | *Pde4d* |
| *Cd44* | *Defa22* | *C2cd4b* | *Pnp2* |
| *Cela2a* | *Defa24* | *Calhm3* | *Psmb5* |
| *Cyp3a41a* | *Defa3* | *Ccdc23* | *Rnaset2b* |
| *Dynlt1b* | *Dnah5* | *Ccdc28b* | *Rpl21* |
| *Fah* | *Dock10* | *Ccdc73* | *Rpl26* |
| *Gm10093* | *Gcg* | *Ccl27a* | *Rpl29* |
| *Gm10184* | *Gm15284* | *Cd38* | *Rpl30* |
| *Gm10260* | *Gm15299* | *Cd74* | *Rplp0* |
| *Gm10282* | *Gm15308* | *Cep85* | *Rps2* |
| *Gm12166* | *Ifitm3* | *Cpne8* | *Rtn4ip1* |
| *Gm21915* | *Lyz1* | *Cst6* | *Sc5d* |
| *Gm29084* | *mt-Atp8* | *Defa21* | *Sprr2a1* |
| *Gm3106* | *mt-Co3* | *Dio1* | *Sprr2a2* |
| *Gm4737* | *mt-Cytb* | *Dynlt1a* | *Sqrdl* |
| *Gm5575* | *Nupr1* | *E030030I06Rik* | *St3gal4* |
| *Gm5900* | *Rnase4* | *Eno1* | *Stk25* |
| *Gm6472* | *Slc12a2* | *Fam177a* | *Sucnr1* |
| *Gm7293* | *Ssh2* | *Fam20a* | *Suco* |
| *Gm8730* | *Them7* | *Fbxl21* | *Tbcb* |
| *Gm9825* | *Zfp934* | *Fgl1* | *Tek* |
| *Gstm2* | | *Gapdh* | *Tmem245* |
| *Hddc3* | | *Gas7* | *Tmem254a* |
| *Hebp1* | | *Gchfr* | *Tmem27* |
| *Hist1h2aa* | | *Gcnt1* | *Tpm3* |
| *Hist1h2al* | | *Gm14306* | *Trim12a* |
| *Hmga1-rs1* | | *Gm14308* | *Ubc* |
| *Iqcc* | | *Gm14851* | *Ube2m* |
| *Nudcd1* | | *Gm26782* | *Zfp251* |
| *Ocel1* | | *Gm4631* | *Zfp738* |
| *Pan2* | | *Gm4724* | |
| *Rab3gap1* | | *Gm4952* | |
| *Rbm45* | | *Gm7861* | |
| *Riok1* | | *Gm8923* | |
| *RP24-82E11.1* | | *Gmpr* | |
| *Rps18-ps3* | | *Gusb* | |
| *Rps2-ps10* | | *Gvin1* | |
| *Rtfdc1* | | *H2-Ab1* | |
| *Sephs2* | | *H2-K1* | |
| *Serpina3f* | | *Hivep3* | |
| *Sgip1* | | *Hsbp1l1* | |
| *Slc38a6* | | *Hspa12a* | |
| *Slc41a1* | | *Hyi* | |
| *Tfam* | | *Intu* | |
| *Tmem242* | | *Itih5* | |
| *Tpm3-rs7* | | *Iyd* | |

**Table 1. DEGs that overlap with the SI tuft cell signature (Related to Figure 5A)**

| Primer | Sequence (5' to 3') | Source |
|---|---|---|
| Spdef_F | TCCTCTCTGCTCACTCTGAA | Lo et al, 2017 (doi: 10.1016/j.jcmgh.2016.10.001) |
| Spdef_R | AGAGCTCATGTGTATCCCTAGA | Lo et al, 2017 (doi: 10.1016/j.jcmgh.2016.10.001) |
| DCLK1_F: | CAAGCCAGCCATGTCGTTC | von Moltke et al, 2016 (doi: 10.1038/nature16161) |
| DCLK1_R: | TTCCTTTGAAGTAGCGGTCAC | von Moltke et al, 2016 (doi: 10.1038/nature16161) |
| Pou2f3_F: | CAGAGACGCATTAAGCTAGGC | Primerbank 119226248c3 |
| Pou2f3_R: | GCGAGATGGTAGTCTGGCT | Primerbank 119226248c4 |
| Chga_F: | ATCCTCTCTATCCTGCGACAC | von Moltke et al, 2016 (doi: 10.1038/nature16161) |
| Chga_R: | GGGCTCTGGTTCTCAAACACT | von Moltke et al, 2016 (doi: 10.1038/nature16161) |
| Lyz1_F: | GAGACCGAAGCACCGACTATG | von Moltke et al, 2016 (doi: 10.1038/nature16161) |
| Lyz1_R: | CGGTTTTGACATTGTGTTCGA | von Moltke et al, 2016 (doi: 10.1038/nature16161) |
| Muc2_F: | ATGCCCACCTCCTCAAAGAC | von Moltke et al, 2016 (doi: 10.1038/nature16161) |
| Muc2_R: | GTAGTTTCCGTTGGAACAGTGAA | von Moltke et al, 2016 (doi: 10.1038/nature16161) |
| Lgr5_F: | CCTACTCGAAGACTTACCCAG | Howitt et al, 2020 (10.4049/immunohorizons.1900099) |
| Lgr5_R: | GCATTGGGGTGAATGATAGCA | Howitt et al, 2020 (10.4049/immunohorizons.1900099) |
| Rsp17_F: | CGCCATTATCCCCAGCAAG | von Moltke et al, 2016 (doi: 10.1038/nature16161) |
| Rsp17_R: | TGTCGGGATCCACCTCAATG | von Moltke et al, 2016 (doi: 10.1038/nature16161) |
| Pou2af2_long_isoform_F: | GCTTCCTTCACACAGGACCAGGC | Designed for this study |
| Pou2af2_ long_isoform_R: | ACTGGCGATCCTGGCATCTGGA | Designed for this study |
| Pou2af2_all_isoforms_F: | TCCTCCCAGCCTCCGTTCATCC | Designed for this study |
| Pou2af2_all_isoforms_F: | CAAAGGGCTTGCTCATGCCGGA | Designed for this study |
| Pou2af3_all_isoforms_F: | GGCGTCCGTGTGAAGATGACCG | Designed for this study |
| Pou2af3_all_isoforms_R: | GAAGGTGGAGACCGCTGCTTCC | Designed for this study |
| Pou2af3_ long_isoform _F: | GCTGCAGCATCCAGTCTCCAGC | Designed for this study |
| Pou2af3_ long_isoform _F: | CGGTCATCTTCACACGGACGCC | Designed for this study |
| Pou2af3_short_isoform_F: | AGAGGGAGGAAGGGGGTGAGGA | Designed for this study |
| Pou2af3_ short_isoform _R: | CGGTCATCTTCACACGGACGCC | Designed for this study |

**Table 2. qPCR primers**

# Chapter 4

Summary and future directions

## 4.1 Summary

### Succinate is a ligand of intestinal tuft cells

In Chapter 2 we identify succinate as a ligand of intestinal tuft cells that is sufficient to initiate a robust innate type 2 immune response. We demonstrate that through the receptor, SUCNR1, tuft cells sense luminal succinate to rapidly activate ILC2s in the lamina propria. Once activated, the ILC2s produce canonical type 2 cytokines, including IL-13, which signals back onto the intestinal cell stems to drive tuft cell and goblet cell hyperplasia. Besides remodeling the epithelium, ILC2 activation also promotes ILC2 proliferation and tissue eosinophilia, classic markers of type 2 immunity.

Succinate is a metabolite of many bacteria, protists and helminths, and we found that both *N. brasiliensis* and Tritrichomonads secrete succinate when cultured *in vitro*. However, succinate sensing is dispensable for tuft cell activation during anti-helminth immunity. On the other hand, we found this SUCNR1-dependent signaling is required for sensing of *Tritrichomonas* protists. Additionally, mono-colonization with *B. ovatus*, a succinate producing bacterial species, induced tuft cell hyperplasia in the distal small intestine. All together these data describe a novel paradigm where small intestinal tuft cells monitor microbial metabolism and instigate type 2 immune responses through succinate sensing.

### *Pou2af2* isoform usage regulates tuft cell differentiation and tunes intestinal innate type 2 immunity

In Chapter 3 we identify a genetic locus that regulates tuft cell differentiation and the threshold of tuft-ILC2 circuit activation between different strains of mice. This work is based on

the observation that C57BL/6J (B6) mice treated with succinate develop tuft cell hyperplasia whereas Balb/cJ (Balb) mice do not. At baseline, Balb mice have fewer tuft cells throughout the intestine. Quantitative trait loci mapping of Balb X B6 F2 mice revealed a single locus on chromosome 9 associated with variations in succinate responsiveness. Congenic Balb mice carrying the B6 chromosome 9 locus have elevated baseline numbers of tuft cells and develop tuft cell hyperplasia when treated with succinate.

Within this Chr9 locus is *Pou2af2*, which encodes a transcriptional cofactor essential for tuft cell development *(54)*. We identify two isoforms of *Pou2af2* expressed in intestinal crypts, of which only the long isoform encodes a functional protein. The ratio of long isoform to total *Pou2af2* transcript is significantly decreased in Balb tuft cell progenitors but is restored to B6 levels in the congenic Balb.Chr9$^{B6/B6}$ mice. Finally, we find Balb mice maintain effective activation of the tuft-ILC2 circuit when challenged with helminths but do not activate the circuit when colonized with innocuous *Tritrichomonas* protists. Responses to these stimuli are restored to C57BL/6J levels in Balb.Chr9$^{B6/B6}$ mice. In sum, we demonstrate differential *Pou2af2* isoform usage accounts for the lower frequency of tuft cells at baseline and tunes the tuft-ILC2 response in different strains of mice.

**4.2 Future directions**

Combined, these data expand our understanding of tuft cell differentiation and reveal nuances in how intestinal tuft cells initiate immune response to different commensal or pathogenic triggers. In B6 mice, the threshold of activation is more sensitive and the tuft-ILC2 circuit is easily triggered by succinate sensing. In Balb mice however, this threshold is higher and succinate fluctuations can be ignored by the immune system. Our work demonstrates that at least one component of how this threshold is determined is at the level of tuft cell differentiation. Importantly, in both strains of mice anti-helminth immunity is rapid and highly effective.

Of intestinal tuft cell activators, helminths pose the biggest threat to the health of the host. Correspondingly, it seems there are many layers of protection that ensure the tuft-ILC2 circuit and downstream immune response will occur upon helminth infection. First, in response to helminths, tuft cells produce IL-25 as well as cysteinyl leukotrienes, which together activate ILC2s more potently than IL-25 alone*(19, 53)*. Furthermore, there is probable redundancy in how tuft cells sense helminths. In our work we demonstrated that although *N. brasiliensis* produces succinate and propionate as metabolites, *Sucnr1*$^{-/-}$*;Ffar3*$^{-/-}$ mice still mount a robust type 2 response upon infection. Further work is needed to identify exactly how tuft cells sense helminth infection, but likely it will be a combination of several sensors as to provide optimal protection to the host.

In contrast to helminth infection, it is yet unclear why tuft cells initiate type 2 immune responses to protist colonization or bacterial dysbiosis*(20, 66)*. In these scenarios, tuft cells do not produce cysteinyl leukotrienes and the resulting type 2 immune responses are not quite so

robust as during helminth infection. Nonetheless, initiation of the tuft-ILC2 circuit and accompanying epithelial remodeling takes energy and resources, from increased mucus production to intestine lengthening to accommodate for the higher ratio of secretory verses absorptive cells*(67)*. While protist colonization activates this type 2 response in B6 mice, mice that do not or cannot sense the protists are not negatively affected. This all raises the question of why sense succinate in the first place? While much more work is needed to understand the significance of succinate sensing responses, it is important to consider that all the work presented here and done on this topic thus far was performed with mice in specific pathogen free conditions. In the wild, humans and animals encounter a much more complex set of pathogens, often simultaneously or chronically. In these contexts, it may be beneficial to have multiple sensing modalities, tuned for a variety of cues that could all alert the immune system of possible threats or keep the immune system poised to respond better when a more serious threat is encountered. We can begin to model these complexities even in laboratory mice. For example, we found that B6 mice treated with succinate were able to clear helminth infection more quickly*(29)*. Far more work is needed to fully understand how these initiation circuits behave in more complicated contexts.

One concept highlighted by our work is that tuft cells are adapted to their specific tissue location. For instance, tuft cells express more *Sucnr1* transcript in the distal small intestine as compared to the proximal small intestine*(67)*. Correspondingly, bacteria and protists colonize the distal small intestine more so than the proximal small intestine. On the other hand, helminths primarily infect the proximal small intestine and anti-helminth tuft cell hyperplasia is most robust there as well. Furthermore, colonic tuft cells do not express high levels of *Sucnr1*,

perhaps because sensing succinate, which may be abundantly available from the colonic microbiome, would not prove beneficial for host immunity*(29)*. The tissue-specific transcriptional programs of tuft cells, which encompass the activating receptors they express, can provide valuable insight into the ligands and roles of tuft cells within each of these tissues.

Building on this, it will be important to continue exploring how tuft cell differentiation is regulated, both within the small intestine, but also in other tissues. Our work demonstrated that one mechanisms for regulating tuft cell differentiation is through manipulation of *Pou2af2* isoform expression in the intestinal crypt where tuft cell progenitors arise. While this adds to our understanding of tuft cell differentiation, there is much left to be discovered. For instance, an interesting observation that arose from the analysis of the congenic strains is that while homeostatic tuft cell numbers were restored to B6 levels in Strain 2, 3 and 4, there was a step-wise increase in succinate induced tuft cells. Specifically, Strain 2 developed the most robust tuft cell hyperplasia while Strain 4 did not. This raises the possibility that homeostatic tuft cell differentiation could rely on different genetic regions compared to STAT6 induced tuft cell hyperplasia. Perhaps there is a combinatorial effect of one genetic locus 50Mb or above on Chr9 that regulates *Pou2af2* isoform expression at homeostasis and another locus between 45 and 50Mbs on Chr9 that regulates IL-13 dependent tuft cell differentiation. A more nuanced understanding of intestinal tuft cell differentiation is needed to fully explore these questions and these congenic strains might prove useful in doing so.

Our understanding of how tuft cells differentiate and whether tuft cell hyperplasia occurs is even more limited in tissues other than the small intestine. The requirement of the transcription factor POU2F3 for tuft cell differentiation in all tissues has been well

established*(21, 25–27)*. Most recently, Wu et al. identified *Pou2af2* and *Pou2af3*, the genes that encode OCA-T1 and OCA-T2, as essential POU2F3 co-factors, and described the tissue-specific roles of *Pou2af2(54)*. Their work revealed that tuft cells in the thymus and stomach are *Pou2af2* independent, whereas intestinal and trachea tuft cells require *Pou2af2*. Our work adds an additional layer of nuance with genetic differences driving meaningful changes in tuft cell differentiation not only in the small intestine, but in the trachea as well through *Pou2af2* isoform expression. In our analysis of small intestinal crypts, we also noted that *Pou2af3* isoform expression ratios follow the same pattern as *Pou2af2* suggesting that similar genetic regulator mechanism may affect both genes. How these gene networks affect tuft cell frequency in other organs remains to be determined. New roles of tuft cells in various immune capacities are emerging often. The better we understand tuft cell differentiation in each tissue, the better equipped we will be to answer fundamental questions about the function of tuft cells and to possibly create novel therapeutic approaches for human disease by manipulating these functions.

Finally, a large gap in knowledge is our understanding of how well murine tuft cells reflect the roles of tuft cells in humans and human disease. The vast majority of tuft cells studies have been performed in mice. However, it is important to understand how well this biology is recapitulated in human tuft cells. While most of the work presented here has focused on the role of tuft cells in type 2 immune responses, the data we do have about human tuft cells mostly comes from biopsies from healthy individuals, cancer patients or patients with inflammatory bowel disease*(120–126)*. From these studies we know that tuft cells can be found in human small intestine, colon, thymus and several other tissues in line with findings in mice.

Furthermore, human tuft cells express many of the same genes as mouse tuft cells including TRPM5, CHAT, COX1, ALOX5*(53, 121, 124)*. Importantly, the requirement of POU2F3 and OCA-T1 seem to be consistent between human and mouse, at least in tuft cell-like variants of small cell lung cancer*(54)*. All the human data published thus far supports the conclusion that there are many similarities between human and mouse tuft cells, encouraging our work on murine tuft cells and fueling our hope that the more we understand tuft cell biology, the better we will be able to inform the development of future therapies for people infected with helminths, and afflicted by allergic diseases.

## REFERENCES


1. Soil-transmitted helminth infections*World Heal. Organ.* (available at http://www.who.int/news-room/fact-sheets/detail/soil-transmitted-helminth-infections).

2. B. J. H. Dierick, T. van der Molen, B. M. J. Flokstra-de Blok, A. Muraro, M. J. Postma, J. W. H. Kocks, J. F. M. van Boven, Burden and socioeconomics of asthma, allergic rhinitis, atopic dermatitis and food allergy. *Expert Rev. Pharmacoecon. Outcomes Res.* **20**, 437–453 (2020).

3. J. E. Allen, R. M. Maizels, Diversity and dialogue in immunity to helminths. *Nat. Rev. Immunol. 2011 116* **11**, 375–388 (2011).

4. S. J. Galli, M. Tsai, A. M. Piliponsky, The development of allergic inflammation. *Nat. 2008 4547203* **454**, 445–454 (2008).

5. C. A. Janeway, R. Medzhitov, Innate Immune Recognition. *https://doi.org/10.1146/annurev.immunol.20.083001.084359* **20**, 197–216 (2003).

6. O. Takeuchi, S. Akira, Pattern Recognition Receptors and Inflammation. *Cell* **140**, 805–820 (2010).

7. N. N. Patel, M. A. Kohanski, I. W. Maina, A. D. Workman, D. R. Herbert, N. A. Cohen, Sentinels at the wall: epithelial-derived cytokines serve as triggers of upper airway type 2 inflammation. *Int. Forum Allergy Rhinol.* **9**, 93–99 (2019).

8. T. Hasegawa, T. Oka, S. Demehri, Alarmin Cytokines as Central Regulators of Cutaneous Immunity. *Front. Immunol.* **13**, 1378 (2022).

9. R. Divekar, H. Kita, Recent advances in epithelium-derived cytokines (IL-33, IL-25, and thymic stromal lymphopoietin) and allergic inflammation. *Curr. Opin. Allergy Clin. Immunol.* **15**, 98–103 (2015).

10. K. Moro, T. Yamada, M. Tanabe, T. Takeuchi, T. Ikawa, H. Kawamoto, J.-I. Furusawa, M. Ohtani, H. Fujii, S. Koyasu, Innate production of T H 2 cytokines by adipose tissue-associated c-Kit 1 Sca-1 1 lymphoid cells. (2010), doi:10.1038/nature08636.

11. D. R. Neill, S. H. Wong, A. Bellosi, R. J. Flynn, M. Daly, T. K. A. Langford, C. Bucks, C. M. Kane, P. G. Fallon, R. Pannell, H. E. Jolin, A. N. J. McKenzie, Nuocytes represent a new innate effector leukocyte that mediates type-2 immunity. *Nat. 2010 4647293* **464**, 1367–1370 (2010).

12. A. E. Price, H. E. Liang, B. M. Sullivan, R. L. Reinhardt, C. J. Eisley, D. J. Erle, R. M. Locksley, Systemically dispersed innate IL-13-expressing cells in type 2 immunity. *Proc. Natl. Acad. Sci. U. S. A.* **107**, 11489–11494 (2010).

13. J. W. McGinty, J. von Moltke, A three course menu for ILC and bystander T cell activation. *Curr. Opin. Immunol.* **62**, 15–21 (2020).

14. C. S. N. Klose, T. Mahlakõiv, J. B. Moeller, L. C. Rankin, A.-L. Flamar, H. Kabata, L. A. Monticelli, S. Moriyama, G. Garbès Putzel, N. Rakhilin, X. Shen, E. Kostenis, G. M. König, T. Senda, D. Carpenter, D. L. Farber, D. Artis, The neuropeptide neuromedin U stimulates innate lymphoid cells and type 2 inflammation. *Nat. Publ. Gr.* **549** (2017), doi:10.1038/nature23676.

15. A. Wallrapp, samantha J. Riesenfeld, P. Burkett, R. Abdulnour, J. Nyman, D. Dionne, M. Hofree, M. Cuoco, C. Rodman, D. Farouq, brian J. Haas, timothy L. Tickle, J. J. Trombetta, P. Baral, christoph N. Klose, T. Mahlakõiv, D. Artis, O. Rozenblatt-rosen, I. Chiu, bruce D. Levy, M. Kowalczyk, A. Regev, V. K. Kuchroo, The neuropeptide NMU amplifies ILC2-driven allergic lung inflammation. *Nat. Publ. Gr.* (2017), doi:10.1038/nature24029.

16. J. von Moltke, C. E. O'Leary, N. A. Barrett, Y. Kanaoka, K. F. Austen, R. M. Locksley, Leukotrienes provide an NFAT-dependent signal that synergizes with IL-33 to activate ILC2s. *J.*

*Exp. Med.* **214**, 27–37 (2017).

17. R. R. Ricardo-Gonzalez, S. J. Van Dyken, C. Schneider, J. Lee, J. C. Nussbaum, H. E. Liang, D. Vaka, W. L. Eckalbar, A. B. Molofsky, D. J. Erle, R. M. Locksley, Tissue signals imprint ILC2 identity with anticipatory function. *Nat. Immunol.* **19**, 1093–1099 (2018).

18. P. G. Fallon, S. J. Ballantyne, N. E. Mangan, J. L. Barlow, A. Dasvarma, D. R. Hewett, A. McIlgorm, H. E. Jolin, A. N. J. McKenzie, Identification of an interleukin (IL)-25-dependent cell population that provides IL-4, IL-5, and IL-13 at the onset of helminth expulsion. *J. Exp. Med.* **203**, 1105–1116 (2006).

19. J. von Moltke, M. Ji, H.-E. Liang, R. M. Locksley, Tuft-cell-derived IL-25 regulates an intestinal ILC2–epithelial response circuit. *Nature* **529**, 221–225 (2016).

20. M. R. Howitt, S. Lavoie, M. Michaud, A. M. Blum, S. V Tran, J. V Weinstock, C. A. Gallini, K. Redding, R. F. Margolskee, L. C. Osborne, D. Artis, W. S. Garrett, Tuft cells, taste-chemosensory cells, orchestrate parasite type 2 immunity in the gut. *Science (80-. ).* **351**, 1329–1333 (2016).

21. F. Gerbe, E. Sidot, D. J. Smyth, M. Ohmoto, I. Matsumoto, V. Dardalhon, P. Cesses, L. Garnier, M. Pouzolles, B. Brulin, M. Bruschi, Y. Harcus, V. S. Zimmermann, N. Taylor, R. M. Maizels, P. Jay, Intestinal epithelial tuft cells initiate type 2 mucosal immunity to helminth parasites. *Nature* **529**, 226–230 (2016).

22. C. E. O'Leary, C. Schneider, R. M. Locksley, Tuft Cells-Systemically Dispersed Sensory Epithelia Integrating Immune and Neural Circuitry. *Annu. Rev. Immunol.* **37**, 47–72 (2019).

23. C. N. Miller, I. Proekt, J. von Moltke, K. L. Wells, A. R. Rajpurkar, H. Wang, K. Rattay, I. S. Khan, T. C. Metzger, J. L. Pollack, A. C. Fries, W. W. Lwin, E. J. Wigton, A. V. Parent, B. Kyewski, D. J. Erle, K. A. Hogquist, L. M. Steinmetz, R. M. Locksley, M. S. Anderson, Thymic tuft cells

promote an IL-4-enriched medulla and shape thymocyte development. *Nature* **559**, 627–631 (2018).

24. C. Bornstein, S. Nevo, A. Giladi, N. Kadouri, M. Pouzolles, F. Gerbe, E. David, A. Machado, A. Chuprin, B. Tóth, O. Goldberg, S. Itzkovitz, N. Taylor, P. Jay, V. S. Zimmermann, J. Abramson, I. Amit, Single-cell mapping of the thymic stroma identifies IL-25-producing tuft epithelial cells. *Nat. 2018 5597715* **559**, 622–626 (2018).

25. T. Yamaguchi, J. Yamashita, M. Ohmoto, I. Aoudé, T. Ogura, W. Luo, A. A. Bachmanov, W. Lin, I. Matsumoto, J. Hirota, Skn-1a/Pou2f3 is required for the generation of Trpm5-expressing microvillous cells in the mouse main olfactory epithelium. *BMC Neurosci.* **15**, 13 (2014).

26. M. Ohmoto, T. Yamaguchi, J. Yamashita, A. A. Bachmanov, J. Hirota, I. Matsumoto, Pou2f3/Skn-1a is necessary for the generation or differentiation of solitary chemosensory cells in the anterior nasal cavity. *Biosci. Biotechnol. Biochem.* **77**, 2154–2156 (2013).

27. J. Yamashita, M. Ohmoto, T. Yamaguchi, I. Matsumoto, J. Hirota, Y. Ishimaru, Ed. Skn-1a/Pou2f3 functions as a master regulator to generate Trpm5-expressing chemosensory cells in mice. *PLoS One* **12**, e0189340 (2017).

28. C. Bezençon, A. Fürholz, F. Raymond, R. Mansourian, S. Métairon, J. Le Coutre, S. Damak, Murine intestinal cells expressing Trpm5 are mostly brush cells and express markers of neuronal and inflammatory cells. *J. Comp. Neurol.* **509**, 514–525 (2008).

29. M. S. Nadjsombati, J. W. McGinty, M. R. Lyons-Cohen, J. B. Jaffe, L. DiPeso, C. Schneider, C. N. Miller, J. L. Pollack, G. A. Nagana Gowda, M. F. Fontana, D. J. Erle, M. S. Anderson, R. M. Locksley, D. Raftery, J. von Moltke, Detection of Succinate by Intestinal Tuft Cells Triggers a Type 2 Innate Immune Circuit. *Immunity* **49**, 33-41.e7 (2018).

30. N. Barker, Adult intestinal stem cells: Critical drivers of epithelial homeostasis and regeneration*Nat. Rev. Mol. Cell Biol.* **15**, 19–33 (2014).

31. H. Gehart, H. Clevers, Tales from the crypt: new insights into intestinal stem cells. *Nat. Rev. Gastroenterol. Hepatol.* , doi:10.1038/s41575-018-0081-y.

32. F. Gerbe, J. H. Van Es, L. Makrini, B. Brulin, G. Mellitzer, S. Robine, B. Romagnolo, N. F. Shroyer, J. F. Bourgaux, C. Pignodel, H. Clevers, P. Jay, Distinct ATOH1 and Neurog3 requirements define tuft cells as a new secretory cell type in the intestinal epithelium. *J. Cell Biol.* **192**, 767–780 (2011).

33. M. Bjerknes, C. Khandanpour, T. Möröy, T. Fujiyama, M. Hoshino, T. J. Klisch, Q. Ding, L. Gan, J. Wang, M. G. Martín, H. Cheng, Origin of the brush cell lineage in the mouse intestinal epithelium. *Dev. Biol.* **362**, 194–218 (2012).

34. C. A. Herring, A. Banerjee, E. T. McKinley, A. J. Simmons, J. Ping, J. T. Roland, J. L. Franklin, Q. Liu, M. J. Gerdes, R. J. Coffey, K. S. Lau, Unsupervised Trajectory Analysis of Single-Cell RNA-Seq and Imaging Data Reveals Alternative Tuft Cell Origins in the Gut. *Cell Syst.* **6**, 37-51.e9 (2018).

35. A. Banerjee, C. A. Herring, B. Chen, H. Kim, A. J. Simmons, A. N. Southard-Smith, M. M. Allaman, J. R. White, M. C. Macedonia, E. T. Mckinley, M. A. Ramirez Solano, E. A. Scoville, Q. Liu, K. T. Wilson, R. J. Coffey, M. K. Washington, J. A. Goettel, K. S. Lau, Succinate Produced by Intestinal Microbes Promotes Specification of Tuft Cells to Suppress Ileal Inflammation. *Gastroenterology* **0** (2020), doi:10.1053/j.gastro.2020.08.029.

36. C. Schubart, B. Krljanac, M. Otte, C. Symowski, E. Martini, C. Günther, C. Becker, C. Daniel, D. Voehringer, Selective expression of constitutively activated STAT6 in intestinal epithelial cells promotes differentiation of secretory cells and protection against helminths. *Mucosal Immunol.*

*2018 122* **12**, 413–424 (2018).

37. A. D. Gracz, L. A. Samsa, M. J. Fordham, D. C. Trotier, B. Zwarycz, Y. H. Lo, K. Bao, J. Starmer, J. R. Raab, N. F. Shroyer, R. L. Reinhardt, S. T. Magness, Sox4 Promotes Atoh1-Independent Intestinal Secretory Differentiation Toward Tuft and Enteroendocrine Fates. *Gastroenterology* **155**, 1508-1523.e10 (2018).

38. M. A. Kohanski, A. D. Workman, N. N. Patel, L. Y. Hung, J. P. Shtraks, B. Chen, M. Blasetti, L. Doghramji, D. W. Kennedy, N. D. Adappa, J. N. Palmer, D. R. Herbert, N. A. Cohen, Solitary chemosensory cells are a primary epithelial source of IL-25 in patients with chronic rhinosinusitis with nasal polyps. *J. Allergy Clin. Immunol.* **142**, 460-469.e7 (2018).

39. Y. H. Huang, O. Klingbeil, X. Y. He, X. S. Wu, G. Arun, B. Lu, T. D. D. Somerville, J. P. Milazzo, J. E. Wilkinson, O. E. Demerdash, D. L. Spector, M. Egeblad, J. Shi, C. R. Vakoc, POU2F3 is a master regulator of a tuft cell-like variant of small cell lung cancer. *Genes Dev.* **32**, 915–928 (2018).

40. N. Goto, A. Fukuda, Y. Yamaga, T. Yoshikawa, T. Maruno, H. Maekawa, S. Inamoto, K. Kawada, Y. Sakai, H. Miyoshi, M. M. Taketo, T. Chiba, H. Seno, Lineage tracing and targeting of IL17RB+ tuft cell-like human colorectal cancer stem cells. *Proc. Natl. Acad. Sci. U. S. A.* **116**, 12996–13005 (2019).

41. L. G. Bankova, D. F. Dwyer, E. Yoshimoto, S. Ualiyeva, J. W. McGinty, H. Raff, J. von Moltke, Y. Kanaoka, K. Frank Austen, N. A. Barrett, The cysteinyl leukotriene 3 receptor regulates expansion of IL-25–producing airway brush cells leading to type 2 inflammation. *Sci. Immunol.* **3**, 9453 (2018).

42. C. K. Rane, S. R. Jackson, C. F. Pastore, G. Zhao, A. I. Weiner, N. N. Patel, D. R. Herbert, N. A. Cohen, A. E. Vaughan, Development of solitary chemosensory cells in the distal lung after

severe influenza injury. *Am. J. Physiol. - Lung Cell. Mol. Physiol.* **316**, L1141–L1149 (2019).

43. D. Höfer, B. Püschel, D. Drenckhahn, Taste receptor-like cells in the rat gut identified by expression of alpha-gustducin. *Proc. Natl. Acad. Sci. U. S. A.* **93**, 6631–4 (1996).

44. R. Dando, S. D. Roper, Acetylcholine is released from taste cells, enhancing taste signalling. *J. Physiol.* **590**, 3009–3017 (2012).

45. C. Schneider, C. E. O'Leary, R. M. Locksley, Regulation of immune responses by tuft cells. *Nat. Rev. Immunol.* **19**, 584 (2019).

46. C. J. Saunders, M. Christensen, T. E. Finger, M. Tizzano, Cholinergic neurotransmission links solitary chemosensory cells to nasal inflammation. *Proc. Natl. Acad. Sci. U. S. A.* **111**, 6075–6080 (2014).

47. R. J. Lee, B. M. Hariri, D. B. McMahon, B. Chen, L. Doghramji, N. D. Adappa, J. N. Palmer, D. W. Kennedy, P. Jiang, R. F. Margolskee, N. A. Cohen, Bacterial D-amino acids suppress sinonasal innate immunity through sweet taste receptors in solitary chemosensory cells. *Sci. Signal.* **10** (2017), doi:10.1126/scisignal.aam7703.

48. M. Tizzano, B. D. Gulbransen, A. Vandenbeuch, T. R. Clapp, J. P. Herman, H. M. Sibhatu, M. E. A. Churchill, W. L. Silver, S. C. Kinnamon, T. E. Finger, Nasal chemosensory cells use bitter taste signaling to detect irritants and bacterial signals. *Proc. Natl. Acad. Sci. U. S. A.* **107**, 3210–3215 (2010).

49. G. Krasteva, B. J. Canning, P. Hartmann, T. Z. Veres, T. Papadakis, C. Mühlfeld, K. Schliecker, Y. N. Tallini, A. Braun, H. Hackstein, N. Baal, E. Weihe, B. Schütz, M. Kotlikoff, I. Ibanez-Tallon, W. Kummer, Cholinergic chemosensory cells in the trachea regulate breathing. *Proc. Natl. Acad. Sci. U. S. A.* **108**, 9478–9483 (2011).

50. K. Deckmann, K. Filipski, G. Krasteva-Christ, M. Fronius, M. Althaus, A. Rafiq, T. Papadakis, L. Renno, I. Jurastow, L. Wessels, M. Wolff, B. Schütz, E. Weihe, V. Chubanov, T. Gudermann, J. Klein, T. Bschleipfer, W. Kummer, Bitter triggers acetylcholine release from polymodal urethral chemosensory cells and bladder reflexes. *Proc. Natl. Acad. Sci. U. S. A.* **111**, 8287–8292 (2014).

51. M. Keshavarz, S. F. Tabrizi, A.-L. Ruppert, U. Pfeil, Y. Schreiber, J. Klein, I. Brandenburger, G. Lochnit, S. Bhushan, A. Perniss, K. Deckmann, P. Hartmann, M. Meiners, P. Mermer, A. Rafiq, S. Winterberg, T. Papadakis, D. Thomas, C. Angioni, J. Oberwinkler, V. Chubanov, T. Gudermann, U. Gärtner, S. Offermanns, B. Schütz, W. Kummer, Cysteinyl leukotrienes and acetylcholine are biliary tuft cell cotransmitters. *Sci. Immunol.* **7**, 6734 (2022).

52. C. E. O'Leary, J. Sbierski-Kind, M. E. Kotas, J. C. Wagner, H.-E. Liang, A. W. Schroeder, J. C. de Tenorio, J. von Moltke, R. R. Ricardo-Gonzalez, W. L. Eckalbar, A. B. Molofsky, C. Schneider, R. M. Locksley, Bile acid–sensitive tuft cells regulate biliary neutrophil influx. *Sci. Immunol.* **7**, 1080 (2022).

53. J. W. McGinty, H. A. Ting, T. E. Billipp, M. S. Nadjsombati, D. M. Khan, N. A. Barrett, H. E. Liang, I. Matsumoto, J. von Moltke, Tuft-Cell-Derived Leukotrienes Drive Rapid Anti-helminth Immunity in the Small Intestine but Are Dispensable for Anti-protist Immunity. *Immunity* **52**, 528-541.e7 (2020).

54. X. S. Wu, X. Y. He, J. J. Ipsaro, Y. H. Huang, J. B. Preall, D. Ng, Y. T. Shue, J. Sage, M. Egeblad, L. Joshua-Tor, C. R. Vakoc, OCA-T1 and OCA-T2 are coactivators of POU2F3 in the tuft cell lineage. *Nature* **607**, 169–175 (2022).

55. A. Chudnovskiy, A. Mortha, V. Kana, A. Kennard, J. D. Ramirez, A. Rahman, R. Remark, I. Mogno, R. Ng, S. Gnjatic, E. ad D. Amir, A. Solovyov, B. Greenbaum, J. Clemente, J. Faith, Y.

Belkaid, M. E. Grigg, M. Merad, Host-Protozoan Interactions Protect from Mucosal Infections through Activation of the Inflammasome. *Cell* **167**, 444-456.e14 (2016).

56. N. K. Escalante, P. Lemire, M. Cruz Tleugabulova, D. Prescott, A. Mortha, C. J. Streutker, S. E. Girardin, D. J. Philpott, T. Mallevaey, The common mouse protozoa Tritrichomonas muris alters mucosal T cell homeostasis and colitis susceptibility. *J. Exp. Med.* **213**, 2841–2850 (2016).

57. A. C. Ariza, P. M. T. Deen, J. H. Robben, The succinate receptor as a novel therapeutic target for oxidative and metabolic stress-related conditions*Front. Endocrinol. (Lausanne).* **3**, 285–296 (2012).

58. A. Trompette, E. S. Gollwitzer, K. Yadava, A. K. Sichelstiel, N. Sprenger, C. Ngom-Bru, C. Blanchard, T. Junt, L. P. Nicod, N. L. Harris, B. J. Marsland, Gut microbiota metabolism of dietary fiber influences allergic airway disease and hematopoiesis. *Nat. Med.* **20**, 159–166 (2014).

59. A. C. Ariza, P. M. T. Deen, J. H. Robben, The succinate receptor as a novel therapeutic target for oxidative and metabolic stress-related conditions*Front. Endocrinol. (Lausanne).* **3**, 22 (2012).

60. J. A. Ferreyra, K. J. Wu, A. J. Hryckowian, D. M. Bouley, B. C. Weimer, J. L. Sonnenburg, Gut Microbiota-Produced Succinate Promotes C. difficile Infection after Antibiotic Treatment or Motility Disturbance. *Cell Host Microbe* **16**, 770–777 (2014).

61. F. De Vadder, P. Kovatcheva-Datchary, C. Zitoun, A. Duchampt, F. Bä, G. Mithieux, Microbiota-Produced Succinate Improves Glucose Homeostasis via Intestinal Gluconeogenesis Cell Metabolism Microbiota-Produced Succinate Improves Glucose Homeostasis via Intestinal Gluconeogenesis. *Cell Metab.* **24**, 151–157 (2016).

62. M. Muller, M. Mentel, J. J. van Hellemond, K. Henze, C. Woehle, S. B. Gould, R.-Y. Yu, M. van der Giezen, A. G. M. Tielens, W. F. Martin, Biochemistry and Evolution of Anaerobic Energy

Metabolism in Eukaryotes. *Microbiol. Mol. Biol. Rev.* **76**, 444–495 (2012).

63. A. G. M. Tielens, Energy generation in parasitic helminths*Parasitol. Today* **10**, 346–352 (1994).

64. D. K. Saz, T. P. Bonner, M. Karlin, H. J. Saz, Biochemical observations on adult Nippostrongylus brasiliensis. *J. Parasitol.* **57**, 1159–1162 (1971).

65. P. Rajkumar, B. Cha, J. Yin, L. J. Arend, T. G. P˘ Aunescu, Y. Hirabayashi, M. Donowitz, J. L. Pluznick, Identifying the localization and exploring a functional role for Gprc5c in the kidney. , doi:10.1096/fj.201700610RR.

66. W. Lei, W. Ren, M. Ohmoto, J. F. Urban, I. Matsumoto, R. F. Margolskee, P. Jiang, Activation of intestinal tuft cell-expressed Sucnr1 triggers type 2 immunity in the mouse small intestine. *Proc. Natl. Acad. Sci. U. S. A.* **115**, 5552–5557 (2018).

67. C. Schneider, C. E. O'Leary, J. von Moltke, H.-E. Liang, Q. Y. Ang, P. J. Turnbaugh, S. Radhakrishnan, M. Pellizzon, A. Ma, R. M. Locksley, A Metabolite-Triggered Tuft Cell-ILC2 Circuit Drives Small Intestinal Remodeling. *Cell* **174**, 271-284.e14 (2018).

68. T. Rubic, G. Lametschwandtner, S. Jost, S. Hinteregger, J. Kund, N. Carballido-Perrig, C. Schwärzler, T. Junt, H. Voshol, J. G. Meingassner, X. Mao, G. Werner, A. Rot, J. M. Carballido, Triggering the succinate receptor GPR91 on dendritic cells enhances immunity. *Nat. Immunol.* **9**, 1261–1269 (2008).

69. T. Rubić-Schneider, N. Carballido-Perrig, C. Regairaz, L. Raad, S. Jost, C. Rauld, B. Christen, G. Wieczorek, R. Kreutzer, J. Dawson, G. Lametschwandner, A. Littlewood-Evans, J. M. Carballido, GPR91 deficiency exacerbates allergic contact dermatitis while reducing arthritic disease in mice. *Allergy Eur. J. Allergy Clin. Immunol.* **72**, 444–452 (2017).

70. A. Littlewood-Evans, S. Sarret, V. Apfel, P. Loesle, J. Dawson, J. Zhang, A. Muller, B. Tigani, R. Kneuer, S. Patel, S. Valeaux, N. Gommermann, T. Rubic-Schneider, T. Junt, J. M. Carballido, GPR91 senses extracellular succinate released from inflammatory macrophages and exacerbates rheumatoid arthritis. *J. Exp. Med.* **213**, 1655–1662 (2016).

71. G. M. Tannahill, A. M. Curtis, J. Adamik, E. M. Palsson-Mcdermott, A. F. McGettrick, G. Goel, C. Frezza, N. J. Bernard, B. Kelly, N. H. Foley, L. Zheng, A. Gardet, Z. Tong, S. S. Jany, S. C. Corr, M. Haneklaus, B. E. Caffrey, K. Pierce, S. Walmsley, F. C. Beasley, E. Cummins, V. Nizet, M. Whyte, C. T. Taylor, H. Lin, S. L. Masters, E. Gottlieb, V. P. Kelly, C. Clish, P. E. Auron, R. J. Xavier, L. A. J. O'Neill, Succinate is an inflammatory signal that induces IL-1β through HIF-1α. *Nature* **496**, 238–242 (2013).

72. S. Wolffram, M. Badertscher, E. Scharrer, Carrier-mediated transport is involved in mucosal succinate uptake by rat large intestine. *Exp. Physiol.* **79**, 215–226 (1994).

73. H. E. Liang, R. L. Reinhardt, J. K. Bando, B. M. Sullivan, I. C. Ho, R. M. Locksley, Divergent expression patterns of IL-4 and IL-13 define unique functions in allergic immunity. *Nat. Immunol.* **13**, 58–66 (2012).

74. F. Mohrs, M., Ledermann, B., Kohler, G., Dorfmueller, A., Gessner, A., and Brombacher, Differences between IL-4- and IL-4 receptor alpha- deficient mice in chronic leishmaniasis reveal a protective role for IL-13 receptor signaling. *J. Immunol.* **162**, 7302–7308 (1999).

75. J. Paik, O. Pershutkina, S. Meeker, J. J. Yi, S. Dowling, C. Hsu, A. M. Hajjar, L. Maggio-Price, D. A. C. Beck, Potential for using a hermetically-sealed, positive-pressured isocage system for studies involving germ-free mice outside a flexible-film isolator. *Gut Microbes* **6**, 255–265 (2015).

76. H. Sokol, B. Pigneur, L. Watterlot, O. Lakhdari, L. G. Bermúdez-Humarán, J. J. Gratadoux, S. Blugeon, C. Bridonneau, J. P. Furet, G. Corthier, C. Grangette, N. Vasquez, P. Pochart, G. Trugnan, G. Thomas, H. M. Blottière, J. Doré, P. Marteau, P. Seksik, P. Langella, Faecalibacterium prausnitzii is an anti-inflammatory commensal bacterium identified by gut microbiota analysis of Crohn disease patients. *Proc. Natl. Acad. Sci. U. S. A.* **105**, 16731–16736 (2008).

77. E. E. Gray, D. Winship, J. M. Snyder, S. J. Child, A. P. Geballe, D. B. Stetson, The AIM2-like Receptors Are Dispensable for the Interferon Response to Intracellular DNA. *Immunity* **45**, 255–266 (2016).

78. D. W. Huang, B. T. Sherman, R. A. Lempicki, Systematic and integrative analysis of large gene lists using DAVID bioinformatics resources. *Nat. Protoc.* **4**, 44–57 (2009).

79. D. W. Huang, B. T. Sherman, R. A. Lempicki, Bioinformatics enrichment tools: Paths toward the comprehensive functional analysis of large gene lists. *Nucleic Acids Res.* **37**, 1–13 (2009).

80. H. Saeki, M. Togo, S. Imai, T. Ishii, A new method for the serial cultivation of Tritrichomonas muris. *Nippon juigaku zasshi. Japanese J. Vet. Sci.* **45**, 151–156 (1983).

81. T. Sato, H. Clevers, Primary mouse small intestinal epithelial cell cultures. *Methods Mol. Biol.* **945**, 319–328 (2013).

82. M. Camberis, G. Le Gros, J. Urban, Animal Model of Nippostrongylus brasiliensis and Heligmosomoides polygyrus. *Curr. Protoc. Immunol.* **55**, 19.12.1-19.12.27 (2003).

83. F. P. Heinzel, M. D. Sadick, B. J. Holaday, R. L. Coffman, R. M. Locksley, Reciprocal expression of interferon γ or interleukin 4 during the resolution or progression of murine leishmaniasis. Evidence for expansion of distinct helper T cell subsets. *J. Exp. Med.* **169**, 59–72 (1989).

84. R. M. Locksley, P. Scott, Helper T-cell subsets in mouse leishmaniasis: induction, expansion and effector function. *Immunol. Today* **12**, A58–A61 (1991).

85. W. Hartmann, B. Blankenhaus, M. L. Brunn, J. Meiners, M. Breloer, Elucidating different pattern of immunoregulation in BALB/c and C57BL/6 mice and their F1 progeny. *Sci. Rep.* **11**, 1–14 (2021).

86. K. J. Filbey, J. R. Grainger, K. A. Smith, L. Boon, N. Van Rooijen, Y. Harcus, S. Jenkins, J. P. Hewitson, R. M. Maizels, Innate and adaptive type 2 immune cell responses in genetically controlled resistance to intestinal helminth infection. *Immunol. Cell Biol.* **92**, 436–448 (2014).

87. L. A. Reynolds, K. A. Smith, K. J. Filbey, Y. Harcus, J. P. Hewitson, S. A. Redpath, Y. Valdez, M. J. Yebra, B. Brett Finlay, R. M. Maizels, Commensal-pathogen interactions in the intestinal tract lactobacilli promote infection with, and are promoted by, helminth parasites. *Gut Microbes* **5**, 522–532 (2014).

88. J. M. Behnke, F. A. Iraqi, J. M. Mugambi, S. Clifford, S. Nagda, D. Wakelin, S. J. Kemp, R. L. Baker, J. P. Gibson, High resolution mapping of chromosomal regions controlling resistance to gastrointestinal nematode infections in an advanced intercross line of mice. *Mamm. Genome* **17**, 584–597 (2006).

89. J. D. Gorham, M. L. Güler, R. G. Steen, A. J. Mackey, M. J. Daly, K. Frederick, W. F. Dietrich, K. M. Murphy, Genetic mapping of a marine locus controlling development of T helper 1/T helper 2 type responses. *Proc. Natl. Acad. Sci. U. S. A.* **93**, 12467–12472 (1996).

90. C. S. Hsieh, S. E. Macatonia, A. O'Garra, K. M. Murphy, T cell genetic background determines default t helper phenotype development in vitro. *J. Exp. Med.* **181**, 713–721 (1995).

91. M. R. Howitt, Y. G. Cao, M. B. Gologorsky, J. A. Li, A. L. Haber, M. Biton, J. Lang, M. Michaud,

A. Regev, W. S. Garrett, The Taste Receptor TAS1R3 Regulates Small Intestinal Tuft Cell Homeostasis. *ImmunoHorizons* **4**, 23–32 (2020).

92. S. Laffont, E. Blanquart, M. Savignac, C. Cénac, G. Laverny, D. Metzger, J. P. Girard, G. T. Belz, L. Pelletier, C. Seillet, J. C. Guéry, Androgen signaling negatively controls group 2 innate lymphoid cells. *J. Exp. Med.* **214**, 1581–1592 (2017).

93. L. Mathä, H. Shim, C. A. Steer, Y. H. Yin, I. Martinez, G. Fumio Takei, Female and male mouse lung group 2 innate lymphoid cells differ in gene expression profiles and cytokine production. *PLoS One* **14** (2019), doi:10.1371/journal.pone.0214286.

94. J. Y. Cephus, M. T. Stier, H. Fuseini, J. A. Yung, S. Toki, M. H. Bloodworth, W. Zhou, K. Goleniewska, J. Zhang, S. L. Garon, R. G. Hamilton, V. V. Poloshukin, K. L. Boyd, R. S. Peebles, D. C. Newcomb, Testosterone Attenuates Group 2 Innate Lymphoid Cell-Mediated Airway Inflammation. *Cell Rep.* **21**, 2487–2499 (2017).

95. C. Wang, Z. Bin Xu, Y. Q. Peng, H. Y. Zhang, Q. N. Yu, Y. B. Guo, W. P. Tan, Y. L. Liu, X. C. Meng, S. Bin Fang, D. Chen, Q. L. Fu, Sex differences in group 2 innate lymphoid cell-dominant allergic airway inflammation. *Mol. Immunol.* **128**, 89–97 (2020).

96. S. Kadel, E. Ainsua-Enrich, I. Hatipoglu, S. Turner, S. Singh, S. Khan, S. Kovats, A Major Population of Functional KLRG1 – ILC2s in Female Lungs Contributes to a Sex Bias in ILC2 Numbers. *ImmunoHorizons* **2**, 74–86 (2018).

97. S. Picelli, Å. K. Björklund, B. Reinius, S. Sagasser, G. Winberg, R. Sandberg, Tn5 transposase and tagmentation procedures for massively scaled sequencing projects. *Genome Res.* **24**, 2033–2040 (2014).

98. D. B. Schubart, A. Rolink, M. H. Kosco-Vilbois, F. Botteri, P. Matthias, B-cell-specif ic

coactivator OBF-1/OCA-B/Bob1 required for immune response and germinal centre formation. *Nature* **383**, 538–542 (1996).

99. D. Chasman, K. Cepek, P. A. Sharp, C. O. Pabo, Crystal structure of an OCA-B peptide bound to an Oct-1 POU domain/octamer DNA complex: specific recognition of a protein-DNA interface. (1999) (available at www.genesdev.org).

100. J. M. Behnke, J. M. Mugambi, S. Clifford, F. A. Iraqi, R. L. Baker, J. P. Gibson, D. Wakelin, Genetic variation in resistance to repeated infections with Heligmosomoides polygyrus bakeri, in inbred mouse strains selected for the mouse genome project. *Parasite Immunol.* **28**, 85–94 (2006).

101. W. Wojciechowski, D. P. Harris, F. Sprague, B. Mousseau, M. Makris, K. Kusser, T. Honjo, K. Mohrs, M. Mohrs, T. Randall, F. E. Lund, Cytokine-Producing Effector B Cells Regulate Type 2 Immunity to H. polygyrus. *Immunity* **30**, 421–433 (2009).

102. R. M. Anthony, J. F. Urban, F. Alem, H. A. Hamed, C. T. Rozo, J. L. Boucher, N. Van Rooijen, W. C. Gause, Memory TH2 cells induce alternatively activated macrophages to mediate protection against nematode parasites. *Nat. Med. 2006 128* **12**, 955–960 (2006).

103. C. B. Wilen, S. Lee, L. L. Hsieh, R. C. Orchard, C. Desai, B. L. Hykes, M. R. McAllaster, D. R. Balce, T. Feehley, J. R. Brestoff, C. A. Hickey, C. C. Yokoyama, Y.-T. Wang, D. A. MacDuff, D. Kreamalmayer, M. R. Howitt, J. A. Neil, K. Cadwell, P. M. Allen, S. A. Handley, M. van Lookeren Campagne, M. T. Baldridge, H. W. Virgin, Tropism for tuft cells determines immune promotion of norovirus pathogenesis. *Science* **360**, 204–208 (2018).

104. A. Tenesa, S. M. Farrington, J. G. D. Prendergast, M. E. Porteous, M. Walker, N. Haq, R. A. Barnetson, E. Theodoratou, R. Cetnarskyj, N. Cartwright, C. Semple, A. J. Clark, F. J. L. Reid, L. A.

Smith, K. Kavoussanakis, T. Koessler, P. D. P. Pharoah, S. Buch, C. Schafmayer, J. Tepel, S. Schreiber, H. Völzke, C. O. Schmidt, J. Hampe, J. Chang-Claude, M. Hoffmeister, H. Brenner, S. Wilkening, F. Canzian, G. Capella, V. Moreno, I. J. Deary, J. M. Starr, I. P. M. Tomlinson, Z. Kemp, K. Howarth, L. Carvajal-Carmona, E. Webb, P. Broderick, J. Vijayakrishnan, R. S. Houlston, G. Rennert, D. Ballinger, L. Rozek, S. B. Gruber, K. Matsuda, T. Kidokoro, Y. Nakamura, B. W. Zanke, C. M. T. Greenwood, J. Rangrej, R. Kustra, A. Montpetit, T. J. Hudson, S. Gallinger, H. Campbell, M. G. Dunlop, Genome-wide association scan identifies a colorectal cancer susceptibility locus on 11q23 and replicates risk loci at 8q24 and 18q21. *Nat. Genet.* **40**, 631 (2008).

105. B. T. Harris, V. Rajasekaran, J. P. Blackmur, A. O'Callaghan, K. Donnelly, M. Timofeeva, P. G. Vaughan-Shaw, F. V. N. Din, M. G. Dunlop, S. M. Farrington, Transcriptional dynamics of colorectal cancer risk associated variation at 11q23.1 correlate with tuft cell abundance and marker expression in silico. *Sci. Reports 2022 121* **12**, 1–13 (2022).

106. P. Desai, H. Janova, J. P. White, T. S. Stappenbeck, L. B. Thackray, M. S. Diamond Correspondence, G. V Reynoso, H. D. Hickman, M. T. Baldridge, J. F. Urban, M. S. Diamond, Enteric helminth coinfection enhances host susceptibility to neurotropic flaviviruses via a tuft cell-IL-4 receptor signaling axis. *Cell* **184** (2021), doi:10.1016/j.cell.2021.01.051.

107. A. Perniss, S. Liu, B. Boonen, M. Keshavarz, A. L. Ruppert, T. Timm, U. Pfeil, A. Soultanova, S. Kusumakshi, L. Delventhal, Ö. Aydin, M. Pyrski, K. Deckmann, T. Hain, N. Schmidt, C. Ewers, A. Günther, G. Lochnit, V. Chubanov, T. Gudermann, J. Oberwinkler, J. Klein, K. Mikoshiba, T. Leinders-Zufall, S. Offermanns, B. Schütz, U. Boehm, F. Zufall, B. Bufe, W. Kummer, Chemosensory Cell-Derived Acetylcholine Drives Tracheal Mucociliary Clearance in Response to Virulence-Associated Formyl Peptides. *Immunity* **52**, 683-699.e11 (2020).

108. M. I. Hollenhorst, I. Jurastow, R. Nandigama, S. Appenzeller, L. Li, J. Vogel, S. Wiederhold, M. Althaus, M. Empting, J. Altmüller, A. K. H. Hirsch, V. Flockerzi, B. J. Canning, A. E. Saliba, G. Krasteva-Christ, Tracheal brush cells release acetylcholine in response to bitter tastants for paracrine and autocrine signaling. *FASEB J.* **34**, 316–332 (2020).

109. A. M. Bolger, M. Lohse, B. Usadel, Trimmomatic: a flexible trimmer for Illumina sequence data. *Bioinformatics* **30**, 2114–2120 (2014).

110. D. J. Adams, A. G. Doran, J. Lilue, T. M. Keane, The Mouse Genomes Project: a repository of inbred laboratory mouse strain genomes. *Mamm. Genome* **26**, 403–412 (2015).

111. R. Corbett-Detig, R. Nielsen, A Hidden Markov Model Approach for Simultaneously Estimating Local Ancestry and Admixture Time Using Next Generation Sequence Data in Samples of Arbitrary Ploidy. *PLoS Genet.* **13** (2017), doi:10.1371/journal.pgen.1006529.

112. C. J. C. Johnston, E. Robertson, Y. Harcus, J. R. Grainger, G. Coakley, D. J. Smyth, H. J. Mcsorley, R. Maizels, C. : Johnston, C. J. Robertson, J. R. Coakley, G. Smyth, D. J. Mcsorley, Cultivation of Heligmosomoides Polygyrus: An Immunomodulatory Nematode Parasite and its Secreted Products. *J. Vis. Exp* , 52412 (2015).

113. D. Voehringer, T. A. Reese, X. Huang, K. Shinkai, R. M. Locksley, Type 2 immunity is controlled by IL-4/IL-13 expression in hematopoietic non-eosinophil cells of the innate immune system. *J. Exp. Med.* **203**, 1435–1446 (2006).

114. S. Steinfelder, S. Rausch, D. Michael, A. A. Kühl, S. Hartmann, Immunity to infection Intestinal helminth infection induces highly functional resident memory CD4 + T cells in mice. *Eur. J. Immunol* **47**, 353–363 (2017).

115. D. W. Strong, L. B. Thackray, T. J. Smith, H. W. Virgin, Protruding Domain of Capsid Protein

Is Necessary and Sufficient To Determine Murine Norovirus Replication and Pathogenesis In Vivo. *J. Virol.* **86**, 2950–2958 (2012).

116. K. A. Chachu, A. D. LoBue, D. W. Strong, R. S. Baric, H. W. Virgin, Immune mechanisms responsible for vaccination against and clearance of mucosal and lymphatic norovirus infection. *PLoS Pathog.* **4**, e1000236 (2008).

117. M. T. Baldridge, S. Lee, J. J. Brown, N. McAllister, K. Urbanek, T. S. Dermody, T. J. Nice, H. W. Virgin, Expression of Ifnlr1 on Intestinal Epithelial Cells Is Critical to the Antiviral Effects of Interferon Lambda against Norovirus and Reovirus. *J. Virol.* **91**, 2079–2095 (2017).

118. L. Baert, C. E. Wobus, E. Van Coillie, L. B. Thackray, J. Debevere, M. Uyttendaele, Detection of murine norovirus 1 by using plaque assay, transfection assay, and real-time reverse transcription-PCR before and after heat exposure. *Appl. Environ. Microbiol.* **74**, 543–546 (2008).

119. M. T. Baldridge, T. J. Nice, B. T. McCune, C. C. Yokoyama, A. Kambal, M. Wheadon, M. S. Diamond, Y. Ivanova, M. Artyomov, H. W. Virgin, Commensal microbes and interferon-λ determine persistence of enteric murine norovirus infection. *Science (80-. ).* **347**, 266–269 (2015).

120. H. P. Barham, S. E. Cooper, C. B. Anderson, M. Tizzano, T. T. Kingdom, T. E. Finger, S. C. Kinnamon, V. R. Ramakrishnan, Solitary chemosensory cells and bitter taste receptor signaling in human sinonasal mucosa. *Int. Forum Allergy Rhinol.* **3**, 450–457 (2013).

121. B. Schütz, A. L. Ruppert, O. Strobel, M. Lazarus, Y. Urade, M. W. Büchler, E. Weihe, Distribution pattern and molecular signature of cholinergic tuft cells in human gastro-intestinal and pancreatic-biliary tract. *Sci. Rep.* **9**, 1–13 (2019).

122. R. Elmentaite, N. Kumasaka, K. Roberts, A. Fleming, E. Dann, H. W. King, V. Kleshchevnikov,

M. Dabrowska, S. Pritchard, L. Bolt, S. F. Vieira, L. Mamanova, N. Huang, F. Perrone, I. Goh Kai'En, S. N. Lisgo, M. Katan, S. Leonard, T. R. W. Oliver, C. E. Hook, K. Nayak, L. S. Campos, C. Domínguez Conde, E. Stephenson, J. Engelbert, R. A. Botting, K. Polanski, S. van Dongen, M. Patel, M. D. Morgan, J. C. Marioni, O. A. Bayraktar, K. B. Meyer, X. He, R. A. Barker, H. H. Uhlig, K. T. Mahbubani, K. Saeb-Parsy, M. Zilbauer, M. R. Clatworthy, M. Haniffa, K. R. James, S. A. Teichmann, Cells of the human intestinal tract mapped across space and time. *Nat. 2021 5977875* **597**, 250–255 (2021).

123. N. Miyata, L. L. Morris, Q. Chen, C. Thorne, A. Singla, W. Zhu, M. Winter, S. D. Melton, H. Li, L. Sifuentes-Dominguez, E. Llano, K. Huff-Hardy, P. Starokadomskyy, A. Lopez, T. A. Reese, E. Turer, D. D. Billadeau, S. E. Winter, E. Burstein, Microbial Sensing by Intestinal Myeloid Cells Controls Carcinogenesis and Epithelial Differentiation. *Cell Rep.* **24**, 2342–2355 (2018).

124. J. Burclaff, R. J. Bliton, K. A. Breau, M. T. Ok, I. Gomez-Martinez, J. S. Ranek, A. P. Bhatt, J. E. Purvis, J. T. Woosley, S. T. Magness, A Proximal-to-Distal Survey of Healthy Adult Human Small Intestine and Colon Epithelium by Single-Cell Transcriptomics. *CMGH* **13**, 1554–1589 (2022).

125. W. J. Huh, J. Te Roland, M. Asai, I. Kaji, Distribution of duodenal tuft cells is altered in pediatric patients with acute and chronic enteropathy. *Biomed. Res.* **41**, 113–118 (2020).

126. Y. Yamada, K. Simon-Keller, D. Belharazem-Vitacolonnna, H. Bohnenberger, M. Kriegsmann, K. Kriegsmann, G. Hamilton, T. Graeter, G. Preissler, G. Ott, E. D. Roessner, I. Dahmen, R. K. Thomas, P. Ströbel, A. Marx, A Tuft Cell–Like Signature Is Highly Prevalent in Thymic Squamous Cell Carcinoma and Delineates New Molecular Subsets Among the Major Lung Cancer Histotypes. *J. Thorac. Oncol.* **16**, 1003–1016 (2021).